Defense Threat Reduction Agency
8725 John J. Kingman Road, MS-6201
Fort Belvoir, VA 22060-6201

DTRA-TR-14-031

TECHNICAL REPORT

Mathematical Models of Human Hematopoiesis Following Acute Radiation Exposure

DISTRIBUTION A. Approved for public release: distribution is unlimited.

April 2014

DTRA01-03-D-0014; 0038

Jacqueline Wentz
Darren Oldson
Daniela Stricklin

Prepared by:

Applied Research Associates, Inc.
801 N. Quincy Street
Suite 700
Arlington, VA 22203

This page intentionally left blank.

REPORT DOCUMENTATION PAGE

Form Approved
OMB No. 0704-0188

The public reporting burden for this collection of information is estimated to average 1 hour per response, including the time for reviewing instructions, searching existing data sources, gathering and maintaining the data needed, and completing and reviewing the collection of information. Send comments regarding this burden estimate or any other aspect of this collection of information, including suggestions for reducing the burden, to Department of Defense, Washington Headquarters Services, Directorate for Information Operations and Reports (0704-0188), 1215 Jefferson Davis Highway, Suite 1204, Arlington, VA 22202-4302. Respondents should be aware that notwithstanding any other provision of law, no person shall be subject to any penalty for failing to comply with a collection of information if it does not display a currently valid OMB control number.
PLEASE DO NOT RETURN YOUR FORM TO THE ABOVE ADDRESS.

1. REPORT DATE DD-MM-YYYY)	2. REPORT TYPE	3. DATES COVERED From - To)
April 25, 2014	Technical Report	

4. TITLE AND SUBTITLE	5a. CONTRACT NUMBER
Mathematical Models of Human Hematopoiesis following Acute Radiation Exposure	DTRA-01-03-D-0014
	5b. GRANT NUMBER
	5c. PROGRAM ELEMENT NUMBER
6. AUTHOR(S)	5d. PROJECT NUMBER
Jacqueline Wentz Darren Oldson Daniela Stricklin	5e. TASK NUMBER 0038
	5f. WORK UNIT NUMBER

7. PERFORMING ORGANIZATION NAME(S) AND ADDRESS(ES)	8. PERFORMING ORGANIZATION REPORT NUMBER
Applied Research Associates, Inc. 801 N. Quincy Street, Suite 700 Arlington, VA 22203	
9. SPONSORING/MONITORING AGENCY NAME(S) AND ADDRESS(ES)	10. SPONSOR/MONITOR'S ACRONYM(S)
Nuclear Technologies Directorate Defense Threat Reduction Agency 8725 John J. Kingman Road, Mail Stop 6201 Fort Belvoir, VA 22060-6201	DTRA J9
	11. SPONSOR/MONITOR'S REPORT NUMBER(S)

12. DISTRIBUTION/AVAILABILITY STATEMENT

Approved for public release; distribution is unlimited.

13. SUPPLEMENTARY NOTES

14. ABSTRACT

This report details the development of mathematical models that describe the effects of acute radiation exposure on hematopoiesis. The models were developed from an existing structure and modified so that they could be integrated with effects on hematopoiesis from other injuries, such as thermal burns. Experimental data provided insight on many model parameters; other parameters were fit to case study data. The final models were validated against additional case study data. The outcome of our work are models that describe the dose response of circulating platelets, granulocytes, and lymphocytes as a function of time after irradiation. The information provided is valuable in understanding the physiological effects of radiation exposure and the time course of these effects.

15. SUBJECT TERMS

hematopoiesis, acute radiation sickness, modeling, radiation effects, granulocytes, platelets, and thrombocytes

16. SECURITY CLASSIFICATION OF:			17. LIMITATION OF ABSTRACT	18. NUMBER OF PAGES	19a. NAME OF RESPONSIBLE PERSON
a. REPORT	b. ABSTRACT	c. THIS PAGE			Dr. Paul Blake
U	U	U	UU	132	19b. TELEPHONE NUMBER (Include area code) 703-767-3433

Standard Form 298 (Rev. 8/98)
Prescribed by ANSI Std. Z39.18

UNIT CONVERSION TABLE

U.S. customary units to and from international units of measurement*

U.S. Customary Units	Multiply by → / ← Divide by†		International Units
Length/Area/Volume			
inch (in)	2.54	$\times 10^{-2}$	meter (m)
foot (ft)	3.048	$\times 10^{-1}$	meter (m)
yard (yd)	9.144	$\times 10^{-1}$	meter (m)
mile (mi, international)	1.609 344	$\times 10^{3}$	meter (m)
mile (nmi, nautical, U.S.)	1.852	$\times 10^{3}$	meter (m)
barn (b)	1	$\times 10^{-28}$	square meter (m^2)
gallon (gal, U.S. liquid)	3.785 412	$\times 10^{-3}$	cubic meter (m^3)
cubic foot (ft^3)	2.831 685	$\times 10^{-2}$	cubic meter (m^3)
Mass/Density			
pound (lb)	4.535 924	$\times 10^{-1}$	kilogram (kg)
atomic mass unit (AMU)	1.660 539	$\times 10^{-27}$	kilogram (kg)
pound-mass per cubic foot (lb ft^{-3})	1.601 846	$\times 10^{1}$	kilogram per cubic meter (kg m^{-3})
Pound-force (lbf avoirdupois)	4.448 222		Newton (N)
Energy/Work/Power			
electronvolt (eV)	1.602 177	$\times 10^{-19}$	joule (J)
erg	1	$\times 10^{-7}$	joule (J)
kiloton (kT) (TNT equivalent)	4.184	$\times 10^{12}$	joule (J)
British thermal unit (Btu) (thermochemical)	1.054 350	$\times 10^{3}$	joule (J)
foot-pound-force (ft lbf)	1.355 818		joule (J)
calorie (cal) (thermochemical)	4.184		joule (J)
Pressure			
atmosphere (atm)	1.013 250	$\times 10^{5}$	pascal (Pa)
pound force per square inch (psi)	6.984 757	$\times 10^{3}$	pascal (Pa)
Temperature			
degree Fahrenheit (^oF)	[T(^oF) − 32]/1.8		degree Celsius (^oC)
degree Fahrenheit (^oF)	[T(^oF) + 459.67]/1.8		kelvin (K)
Radiation			
activity of radionuclides [curie (Ci)]	3.7	$\times 10^{10}$	per second (s^{-1}‡)
air exposure [roentgen (R)]	2.579 760	$\times 10^{-4}$	coulomb per kilogram (C kg^{-1})
absorbed dose (rad)	1	$\times 10^{-2}$	joule per kilogram (J kg^{-1}§)
equivalent and effective dose (rem)	1	$\times 10^{-2}$	joule per kilogram (J kg^{-1}**)

*Specific details regarding the implementation of SI units may be viewed at http://www.bipm.org/en/si/.

†Multiply the U.S. customary unit by the factor to get the international unit. Divide the international unit by the factor to get the U.S. customary unit.

‡The special name for the SI unit of the activity of a radionuclide is the becquerel (Bq). (1 Bq = 1 s^{-1}).

§The special name for the SI unit of absorbed dose is the gray (Gy). (1 Gy = 1 J kg^{-1}).

**The special name for the SI unit of equivalent and effective dose is the sievert (Sv). (1 Sv = 1 J kg^{-1}).

Table of Contents

Table of Contents i

List of Figures iv

List of Tables v

Acknowledgements vii

Executive Summary 1

1 Introduction 3
- 1.1 Background . . . 3
- 1.2 Purpose . . . 3

2 Methods 5
- 2.1 Existing Mathematical Models . . . 5
- 2.2 Model Development . . . 5
- 2.3 Parameter Estimation and Confidence Interval Calculations . . . 6

3 Overview of Hematopoietic Models 9
- 3.1 Model Structure . . . 9
- 3.2 Stimulatory Hematopoiesis Mediator . . . 9
- 3.3 Cell Survival Curves and Damaged Compartments . . . 10

4 Thrombopoiesis Model 13
- 4.1 Conceptual Model . . . 13
  - 4.1.1 Radiation damage . . . 13
  - 4.1.2 Feedback mechanisms . . . 14
- 4.2 Mathematical Model . . . 16
- 4.3 Radiation Model Parameter Sources . . . 18
  - 4.3.1 Maximum mitotic repopulation rate (α) . . . 18
  - 4.3.2 Platelet transit rate (ψ) . . . 18
  - 4.3.3 MK subcompartment number (n) . . . 18
  - 4.3.4 Platelet subcompartment number (m) . . . 18
  - 4.3.5 Ratio of receptor concentrations (θ_3) . . . 19
  - 4.3.6 Maximum and minimum rates of MK maturation (δ_{min}, δ_{max}) . . . 19
  - 4.3.7 Number of platelets produced per MK (σ) . . . 19
  - 4.3.8 Radiosensitivity of mitotic progenitor cells (D_1^0, n_1) . . . 20
  - 4.3.9 Number of targets per MK (n_2) . . . 20
  - 4.3.10 Effect of damaged states on mediator levels (μ) . . . 20
- 4.4 Optimization Data . . . 20
- 4.5 Results: Optimization and MCMC Analysis . . . 20
- 4.6 Validation . . . 21

4.6.1 Relative compartment sizes . . . 22

5 Granulopoiesis Model **29**
5.1 Conceptual Model . . . 29
5.1.1 Radiation damage . . . 29
5.1.2 Feedback mechanisms . . . 30
5.2 Mathematical Model . . . 30
5.3 Radiation Model Parameter Sources . . . 32
5.3.1 Maximum mitotic repopulation rate (α) . . . 32
5.3.2 Compartment transition rates (δ, m, l, κ, γ) . . . 33
5.3.3 Receptor concentration ratios (θ_2, θ_3, θ_4) . . . 33
5.3.4 Granulocyte radiosensitivity (D_3^0, D_4^0) . . . 33
5.3.5 Time of abortive rise Δt_{ae} (τ, v) . . . 33
5.3.6 Targets per cell (n_1, n_2, n_3, n_4) . . . 34
5.3.7 Effect of damaged states on mediator levels (μ) . . . 34
5.4 Optimization Data . . . 34
5.5 Results: Optimization and MCMC Analysis . . . 34
5.6 Validation . . . 34
5.6.1 Relative compartment sizes . . . 35

6 Lymphopoiesis Model **41**
6.1 Conceptual Model . . . 41
6.1.1 Radiation damage . . . 41
6.1.2 Feedback loops . . . 41
6.2 Mathematical Model . . . 42
6.3 Radiation Model Parameter Sources . . . 43
6.3.1 Maximum mitotic repopulation rate (α) . . . 43
6.3.2 Rate of post-mitotic progenitor maturation (δ) . . . 43
6.3.3 Rate of lymphocyte clearance from blood (ψ) . . . 44
6.3.4 Effect of damaged states on mediator levels (μ) . . . 44
6.3.5 Radiosensitivity of post-mitotic precursors (D_2^0) . . . 44
6.3.6 Radiosensitivity of lymphocytes (D_3^0, n_3) . . . 44
6.3.7 Targets per progenitor (n_1, n_2) . . . 44
6.3.8 Parameter dependencies (θ_3) . . . 44
6.4 Optimization Data . . . 45
6.5 Results: Optimization and MCMC Analysis . . . 46
6.6 Validation . . . 47

7 Discussion **51**
7.1 Thrombopoiesis . . . 52
7.2 Granulopoiesis . . . 54
7.3 Lymphopoiesis . . . 57
7.4 Comparison with Expert Predictions . . . 58
7.5 Treatment Effects . . . 59
7.6 Partial Body Effects . . . 63

7.7 Current and Future Effort 63

8 Conclusion **67**

9 References **69**

Appendices **75**

Appendix A Human Case Study Data **75**
A.1 General Considerations and Criteria 75
A.2 Case Study Descriptions 76
A.2.1 Criticality accidents 76
A.2.2 Radiation therapy 78
A.2.3 Industrial irradiator accidents 79
A.2.4 Miscellaneous 80
A.3 Summary and Conclusions 81

Appendix B Supplemental Model Comparisons **87**
B.1 Optimization Data Comparisons 87
B.2 Other Model Validations and Comparisons 96

Appendix C Markov Chain Monte Carlo and Identifiability Analysis **115**

Abbreviations, Acronyms, and Symbols **119**

List of Figures

4.1 Thrombopoiesis model diagram . . . 14
4.2 Feedback effect of platelets on MK transit time . . . 15
4.3 Thrombopoiesis model compared to select optimization data . . . 24
4.4 Thrombopoiesis model compared to select validation data . . . 25
4.5 Thrombopoiesis model overlaid on thrombopheresis data . . . 26
5.1 Granulopoiesis model diagram . . . 29
5.2 Granulopoiesis model compared to select optimization data . . . 39
5.3 Granulopoiesis model compared to select validation data . . . 40
6.1 Lymphopoiesis model diagram . . . 41
6.2 Lymphopoiesis model compared to select optimization data . . . 48
6.3 Lymphopoiesis model compared to select validation data . . . 49
7.1 Thrombopoiesis simulations . . . 53
7.2 Thrombopoiesis case study comparisons . . . 54
7.3 Granulopoiesis simulations . . . 55
7.4 Granulopoiesis case study comparisons . . . 56
7.5 Lymphopoiesis simulations . . . 57
7.6 Lymphopoiesis case study comparisons . . . 58
7.7 Comparison of hematopoietic model outputs to METREPOL . . . 60
7.8 Comparison of hematopoietic model outputs to 1988 UNSCEAR report . . . 61
7.9 Hematopoietic dynamics following radiation and treatment . . . 62
7.10 Hematopoietic dynamics following partial body exposure . . . 64
B.1 Thrombopoiesis model compared to optimization data . . . 87
B.2 Granulopoiesis model compared to optimization data . . . 90
B.3 Lymphopoiesis model compared to optimization data . . . 93
B.4 Thrombopoiesis model compared to validation data . . . 96
B.5 Granulopoiesis model compared to validation data . . . 99
B.6 Lymphopoiesis model compared to validation data . . . 101
B.7 Mean hematopoietic response of 11 subjects from Chernobyl 1986 . . . 104
B.8 Chernobyl case studies: Platelet data . . . 105
B.9 Chernobyl case studies: Granulocyte data . . . 106
B.10 Chernobyl case studies: Lymphocyte data . . . 107
B.11 Example of variability between the hematopoietic response of two radiation victim . . . 108
B.12 Effects of treatment: 4.0 Gy case study . . . 109
B.13 Effects of treatment: 11.0 Gy case study . . . 110
B.14 Effects of non-uniform exposure: 5.8 Gy (2.8-10 Gy) case study . . . 111
B.15 Effects of non-uniform exposure: 17 Gy (13-20 Gy) case study . . . 112
C.1 Thrombopoiesis MCMC analysis . . . 116
C.2 Granulopoiesis MCMC analysis . . . 117
C.3 Lymphopoiesis MCMC analysis . . . 118

List of Tables

4.1 Cell concentrations in each compartment of the thrombopoiesis model 17
4.2 Optimization data summary for thrombopoiesis model 21
4.3 Thrombopoiesis optimized parameters and confidence intervals. 22
4.4 Biological parameter values for thrombopoiesis 23
5.1 Cell concentrations in each compartment of the granulopoiesis model 31
5.2 Optimization data summary for granulopoiesis model 35
5.3 Granulopoiesis optimized parameter values and confidence intervals. 36
5.4 Biological parameter values for granulopoiesis 38
6.1 Cell concentrations in each compartment of the lymphopoiesis model 42
6.2 Optimization data summary for lymphopoiesis model 45
6.3 Biological parameter values for lymphopoiesis 46
6.4 Lymphopoiesis optimized parameters and confidence intervals 47
A.1 Case studies used in optimization 82
A.2 Case studies for potential use in validation and future work 84

This page intentionally left blank.

Acknowledgements

The authors gratefully acknowledge the support provided by:

- Dr. Paul Blake of DTRA/J9 for programmatic support.
- Dr. Glen Reeves for critical review of this report.
- Neumedicines and Dr. Vladimir Vainstein whose interactions during a separate project analyzing the effect of IL-12 in non-human primates and humans provided invaluable insight into the modeling presented in this work.
- Dr. Olga Smirnova and Shaowen Hu whose previous modeling efforts provided valuable starting points in our work.

This page intentionally left blank.

Executive Summary

This report details the development of mathematical models that describe the effects of acute radiation exposure on hematopoiesis. The models were developed from an existing structure and modified so that they could be integrated with effects on hematopoiesis from other injuries, such as thermal burns. Experimental data provided insight on many model parameters; other parameters were fit to case study data. The final models were validated against additional case study data. Challenges were encountered in using case study data for model optimization and validation due to individual variability, uncertainty in radiation dose estimates in human accident data, and potential impact of treatment. However, models were developed that capture the major trends in circulating platelets, granulocytes, and lymphocytes after radiation exposure. The thrombocyte model demonstrates a dose-dependent decline in platelets and subsequent recovery. Likewise, the granulocyte model illustrates an initial decline in granulocyte count, a dose-dependent abortive rise, and subsequent recovery. Lymphocyte model predicts dose-dependent lymphocyte decline and slow recovery. The outcome of our work is models that describe the dose response of circulating platelets, granulocytes, and lymphocytes as a function of time after irradiation. The information provided is valuable in understanding the physiological effects of radiation exposure and the time course of these effects. In addition to combined injury model development, future work could include the integration of parameters for treatment, partial body effects, and population variability. These modeling efforts support more realistic radiological and nuclear scenario analyses in large diverse populations, thereby, facilitating preparedness and medical resource planning.

This page intentionally left blank.

1 Introduction

1.1 Background

Applied Research Associates, Inc. (ARA) has been tasked by Defense Threat Reduction Agency (DTRA) to support their mission to safeguard against weapons of mass destruction (WMD). ARA is supporting this effort by developing state-of-the-art mathematical models that predict medical and performance consequences from radiation and combined injuries, thereby enhancing our understanding of the potential impact of a nuclear detonation. This work will improve current casualty estimation capabilities through an interdisciplinary approach that integrates experimental data with mechanistic mathematical modeling.

The hematopoietic models presented in this work describe hematopoiesis after acute radiation exposure without treatment. The main intent in developing these models was to merge them with analogous models of acute injury, such as burn, to better understand the impact of combined injury on pathophysiology and thereby improve mortality estimates of combined injury by accounting for mechanistic interactions. Hematopoietic model parameters for thermal injury have also been developed; however, details on the models for burn and combined injury will be presented subsequently. In addition to the insight gained from combined injury modeling, the models of hematopoiesis and radiation alone provide clinically relevant outputs that afford insight on the time–dependent evolution of casualties and hence medical resource requirements as a function of time.

The hematopoietic models developed in our current work will complement the Radiation-Induced Performance Decrement (RIPD) model, which is a physiologically-based mechanistic model of acute radiation sickness (ARS) developed in the 1990s (Matheson et al. 1998). RIPD was integrated into a software tool used for planning and scenario predictions for nuclear detonations, has since been updated, and will be included in our broader software platform Health Effects from Nuclear and Radiation Environments (HENRE). HENRE will house all new models developed for prompt injury, combined injury, and other relevant models as they are developed.

1.2 Purpose

Physiologically-based mechanistic models of the human response to irradiation can yield valuable information for use in nuclear disaster preparedness planning. Understanding how biological systems change after radiation exposure provides insight on the pathophysiological processes leading to mortality as well as the evolution of these processes over time. Models that describe these processes can be used to correlate biological endpoints with time–dependent clinical manifestations and probabilities of mortality. Information on clinical endpoints can help medical planners determine when and under what circumstances medical resources might be needed. For example, the time at which platelet counts decrease below a critical threshold can suggest when platelet transfusions will be needed, and when analyzed on a population level, how many transfusions for a particular scenario might be required.

This report presents our work on models describing hematopoiesis after acute radiation exposure. Hematopoiesis is the process by which blood cells are generated from hematopoi-

etic stem cells (HSCs) in the bone marrow. The cellular components of blood play essential roles in nourishing, protecting, and healing the human body. Due to their fast proliferation rate, bone marrow hematopoietic progenitors are highly radiosensitive. Thus, the hematopoietic system shows a marked response to irradiation. The hematopoietic syndrome of ARS has been well-documented and characterized (Fliedner, Friesecke, et al. 2001). The hematopoietic response after radiation has been used to estimate radiation dose after accidental over-exposures, develop prognoses, and guide treatment decisions.

Our work on physiologically-based mechanistic models describing the effects of radiation exposure in humans on thrombopoiesis, granulopoiesis, and lymphopoiesis is detailed in this report. Thrombopoiesis, granulopoiesis, and lymphopoiesis correspond to the processes of formation of platelets (also known as thrombocytes), granulocytes, and lymphocytes, respectively. Granulocytes and lymphocytes are both white blood cells which are highly involved in the immune response. Platelets, which have a less well understood role in immunity, are also involved in hemostasis and help with coagulation, or blood clot formation. These models describe hematopoietic cell sensitivity to irradiation, i.e. radiation dose-dependent rate of cell damage and death, and the impact of the perturbed state on cell proliferation and differentiation rates. The methodologies used for model development, parameterization, computational algorithms, optimization, and validation are described in this report.

2 Methods

2.1 Existing Mathematical Models

A number of mathematical models of hematopoiesis have been developed previously for understanding blood cell dynamics in general and following different insults and/or treatment. These include models of radiation exposure (Gräßle 2000; Akushevich et al. 2011), granulocyte colony stimulating factor treatment (Vainstein et al. 2005), and chemotherapy (Scholz et al. 2010). Russian scientist, Olga A. Smirnova, developed a series of mathematical models that describe cellular dynamics after acute and protracted radiation exposures (Smirnova 2011). These models are based on several decades of radiobiological experiments and human case study data. Dr. Smirnova's series of hematopoietic models include murine thrombopoiesis, granulopoiesis, and lymphopoiesis and human thrombopoiesis and granulopoiesis (Smirnova 2011; Smirnova 2012). NASA has also developed radiation models based off of Smirnova's work including models for lymphopoiesis in humans (Hu, Smirnova, et al. 2012) and granulopoiesis in rodents, canines, primates, and humans (Hu and Cucinotta 2011). Since these models describe the impact of radiation on blood cell kinetics, they served as excellent starting points for our model development. However, data and details on how some parameters were derived were lacking or embedded in Russian literature. An attempt was made to reconstruct as much of Smirnova's original work as possible, including obtaining and translating Russian literature that was accessible. Nevertheless, many details remained unclear. Because Smirnova's models were designed for simulating both acute and protracted radiation effects, some parameter values were likely determined so that protracted effects could be accurately predicted. The current work is focused on predicting the hematopoietic response to acute (single, high dose rate) radiation exposures; we have not endeavored to address protracted doses at this point.

2.2 Model Development

In this work parameter values were tuned to match acute effects as accurately as possible. The human model development was guided by work done on establishing non-human primate (NHP) hematopoietic models for a separate project (Wentz et al. 2014). For the NHP model development, a significant amount of hematological data from experimental work with rhesus monkeys was made available to us from a clinical partner. This data was supplemented with published data on rhesus hematopoietic kinetics after different irradiation doses. Key features of the hematopoietic response and required structure of the models could be delineated from work with the NHP data since these studies involved precise experimental conditions. Modern literature was reviewed and experimental data collected for as many of the hematopoietic model parameters as possible. Based on the NHP work, availability of experimental data, and published parameter values (for example, compartment sizes or transition rates), the model structure was altered as needed and new model parameters were developed.

To develop human model parameters, optimize their values, and validate model outputs, clinical data on human blood cell kinetics after radiation exposure was required. Therefore, published data on radiation accidents and radiation therapy was collected. Details on the

case studies reviewed and selected are described in more detail in Appendix A. Briefly, data available on acute, whole body gamma exposures that had little or no treatment was prioritized. Since very little data is available for strictly "acute, whole body gamma exposures with no treatment", a number of other studies were used with careful consideration placed on assigning relevant doses in cases involving different quality radiations, inhomogeneous exposures, protracted exposures, and treatment.

2.3 Parameter Estimation and Confidence Interval Calculations

The statistical computing environment R (v3.0.0, R Core Team 2013) was used to generate numerical solutions of ordinary differential equations (ODEs), estimate model parameters, and provide confidence intervals for parameters. Specifically, ODEs were solved using the "ode" function from the deSolve package (Soetaert, Petzoldt, and Setzer 2010), and parameter estimation was performed using the modCost and modFit tools from the FME package (Soetaert and Petzoldt 2010). ModFit performs constrained fitting of a model to data using input including (1) a function to be minimized, (2) initial parameter values, (3) the lower and upper bounds to be used for each parameter, and (4) the optimization method.

Parameter estimation can be formulated as a nonlinear least squares optimization problem, and the structure of the least squares objective function can be leveraged to create alternatives to Newton's method, such as the Levenberg–Marquardt Method (Moré 1978; Heath 1997). The Levenberg–Marquardt Method can be viewed as a combination of the Gauss–Newton Method and the Steepest Descent Method, and it can provide a robust and efficient way to locate optimum parameter values. The modFit function's Levenberg–Marquardt option was thus used as part of our parameter estimation methodology.

The objective function f we provided to modFit() maps a given parameter vector $\vec{\xi}_k$ to a residual. This mapping includes the following steps:

1. The ODE simulation is performed at each radiation dose level.
2. The output of each ODE simulation and the observed data is used as input for modCost which calculates and returns the residuals.
3. The residuals from each simulation are combined across doses and returned.

modFit then uses $f(\vec{\xi}_k)$ and the Levenberg–Marquardt Method to generate the next approximate parameter vector $\vec{\xi}_{k+1}$. These steps are then repeated to generate additional approximate solutions $\vec{\xi}_{k+2}$, $\vec{\xi}_{k+3}, \ldots$ until a convergence test is passed. Finally, we note that the optimizations were performed on normalized data in which each data value was divided by a baseline value. This allows for comparison of residuals between datasets without inadvertently weighting one dataset more than another.

To calculate parameter confidence intervals, the Markov Chain Monte Carlo (MCMC) method with the adaptive Metropolis algorithm was used (Laine 2008; Haario et al. 2001). Given an initial parameter vector $\vec{\xi}_j$, an estimate for the parameter covariance matrix, and the same function f as described above, the parameter space was randomly sampled to generate a new parameter vector $\vec{\xi}_{j+1}$. The likelihood L of the new parameter vector $\vec{\xi}_{j+1}$ was determined, and if $L(\vec{\xi}_{j+1}) \geq L(\vec{\xi}_j)$, $\vec{\xi}_{j+1}$ was chosen. If $L(\vec{\xi}_{j+1}) < L(\vec{\xi}_j)$, $\vec{\xi}_{j+1}$ was selected

with probability α, where $\alpha = P(\vec{\xi}_{j+1})/P(\vec{\xi}_j)$ and P is the probability of a given parameter vector. These calculations were performed in R, using modMCMC which is also a function in the FME library. To determine whether the models were identifiable the collinearity value was determined using the collin function from the FME package in R (see Brun et al. 2001).

This page intentionally left blank.

3 Overview of Hematopoietic Models

3.1 Model Structure

To model the complex process of hematopoiesis, several simplifications that preserve key system characteristics are adopted. Cells are grouped into compartments based on degree of maturity, differentiation, and location in the body (ex. bone marrow, tissue, or circulation). The primary cell compartments are mitotic bone marrow precursor cells (X_1), post-mitotic bone marrow precursor cells (X_2), and the fully differentiated cells (granulocytes, lymphocytes, or platelets) in the blood (X_3). The granulopoiesis model includes an additional compartment (X_4) that represents granulocytes in the tissue.

Ordinary differential equations are used to describe the transition between the developmental stages:

$$\dot{x_1} = Bx_1 - Cx_1 \tag{1}$$
$$\dot{x_2} = Cx_1 - Fx_2 \tag{2}$$
$$\dot{x_3} = Fx_2 - Ex_3 \tag{3}$$

where $\dot{x}_i$ represents the change in cell i ($i = 1, 2, 3$) concentration with time. x_1 cells reproduce at rate B, which is dependent on the concentration of the mediator in the system (see Section 3.2). C and F are rates of transition between states. These rates can be dependent on the state variables, and thus describe feedback mechanisms. E is the rate of normal x_3 cell death or clearance from the circulation.

3.2 Stimulatory Hematopoiesis Mediator

All the models include a generic mediator I as part of a negative feedback system to regulate the production of HSCs. In Smirnova's models, this mediator is considered to be inhibitory. That is, increased mediator concentration directly reduces the x_1 repopulation rate, and as the number of cells in the model increases, more of the mediator is produced. However, we have changed the biological interpretation of the mediator from inhibitory to stimulatory in order to relate the mediator to the action of known hematopoietic stimulators such as thrombopoietin (TPO) and granulocyte colony-stimulating factor (G-CSF). Thus, in our version of the model, the negative feedback mechanism is less direct: as the number of hematopoietic cells increases, the stimulatory mediator decays more rapidly, leading to less stimulation and a reduced x_1 repopulation rate. However, in both versions of the model (inhibitory mediator, stimulatory mediator), the mediator is assumed to be in a quasi–steady state (i.e., $dI/dt \approx 0$); therefore, as explained below, for this particular study our change of perspective does not affect the model's predictions.

In the original model, the mediator I is described as an inhibitor of the x_1 repopulation rate. The concentration of I increases as the concentration of each cell population increases according to the following equation:

$$\frac{dI_i}{dt} = G_i(x_1 + \theta_2 x_2 + \theta_3 x_3) - H_i I_i \tag{4}$$

Here the subscript i refers to parameters in the original model that describe the inhibitory mediator (the subscript s will be used to denote parameters that describe the stimulatory representation). Equation 4 can be considered "fast" relative to the change in cell concentrations with time $(\dot{x}_1, \dot{x}_2, \dot{x}_3)$ and thus the approximation $I_i = (G_i/H_i)(x_1 + \theta_2 x_2 + \theta_3 x_3)$ is used. The rate of x_1 repopulation, B_i, is given by the following equation:

$$B_i = \frac{\alpha}{1 + I_i/K_i} = \frac{\alpha}{1 + \beta_i(x_1 + \theta_2 x_2 + \theta_3 x_3)} \tag{5}$$

where $\beta_i = \frac{G_i}{H_i K_i}$ and α is the maximum rate of repopulation.

To change the description of the mediator from inhibitory to stimulatory, the mediator's relation to the concentration of cells in the system is altered. Rather than having cell concentrations affect the rate of mediator generation, cell concentrations affect the rate of mediator decay. The following equation describes this new system:

$$\frac{dI_s}{dt} = G_s - H_s(x_1 + \theta_2 x_2 + \theta_3 x_3) I_s \tag{6}$$

Here the mediator is produced at a constant rate G_s. It is then removed from the system at a rate that is dependent on cell concentration.

The rate of x_1 repopulation is changed so that K is a stimulatory rate constant rather than an inhibitory rate constant and is given by the following equation.

$$B_s = \frac{\alpha}{1 + K_s/I_s} = \frac{\alpha}{1 + \frac{K_s H_s(x_1 + \theta_2 x_2 + \theta_3 x_3)}{G_s}} = \frac{\alpha}{1 + \beta_s(x_1 + \theta_2 x_2 + \theta_3 x_3)} \tag{7}$$

where $\beta_s = \frac{H_s K_s}{G_s}$.

The equations for B_i and B_s are the same except for the constants β_i and β_s. However, after scaling the models using their equilibrium points, the models are the same (i.e., β_i and β_s do not appear in the nondimensional form of the models). Thus, using a quasi-steady-state approximation for I, the mathematical models are identical, but the definition of the mediator action has changed. However, restructuring the model based on a stimulatory mediator affords a mechanism for integrating treatment with hematopoietic stimulators, such as G-CSF, into future radiation effects models.

3.3 Cell Survival Curves and Damaged Compartments

The radiosensitivity of a given compartment X_i depends on the cell line being modeled. In the thrombopoiesis model, cells in the X_1 and X_2 groups are sensitive to radiation; in the granulopoiesis and lymphopoiesis models, all cell groups (X_i, $1 \leq i \leq 4$ for granulopoiesis, $1 \leq i \leq 3$ for lymphopoiesis) are sensitive to radiation.

If cell group X_i is radiosensitive, cells in the group can become damaged (X_i^d compartment). Damaged cells die within days at rate μ. In addition, for granulopoiesis, cells in the X_1 group can become weakly damaged (X_1^{wd} compartment). The weakly damaged state provides a way to model the abortive rise phenomena, observed 5 to 30 days after radiation

exposure, in which a second transient increase in granulocyte cell count occurs (Bond et al. 1965). Weakly damaged cells reproduce and mature like undamaged cells for a specified time interval Δt_{ae} after exposure. After this time interval, the weakly damaged cells and their progeny die off at rate η.

In Smirnova's original model, cell damage is modeled using the one-target-one-hit theory of cell damage in which the specific rate of damage is proportional to the radiation dose (Joiner 2009). After acute radiation of dose D, the proportion of undamaged or surviving cells is

$$S = e^{-D/D_i^0} \tag{8}$$

However, this model is limited in its ability to capture the dose-response characteristics of cell survival. Therefore, we have implemented a more general cell survival model, the multi-target-single-hit model (Joiner 2009). In this model, the surviving fraction of cells after acute radiation of dose D is

$$S = 1 - (1 - e^{-D/D_i^0})^{n_i} \tag{9}$$

where n_i is the average number of hits required to damage a cell in compartment X_i and D_i^0 is the dose that results in (on average) one hit per target. As expected, when $n_i = 1$ this model simplifies to the one-target-one-hit model. Thus, for each radiosensitive cell group, there are two parameters that determine the proportion of cells that are undamaged: D_i^0 and n_i.

For the granulopoiesis cell lineage, an x_1 cell can become either fully damaged or weakly damaged. To simulate this, we define two different types of radiation hits, a full-damage hit and a weak-damage hit. In order for an x_1 cell to become fully damaged, it must receive n_1 full-damage hits, while all other cells that receive n_1 hits become weakly damaged. The fraction of damaged cells that are fully damaged following acute radiation dose D is given by $1/(1 + \vartheta)$, where

$$\vartheta = \frac{(1 - e^{-D/D_1^0})^{n_1} - (1 - e^{-D/D_1^{000}})^{n_1}}{(1 - e^{-D/D_1^{000}})^{n_1}} \tag{10}$$

and D_1^{000} is the dose that results in (on average) one full-damage hit per target. By definition $D_1^{000} > D_1^0$.

This page intentionally left blank.

4 Thrombopoiesis Model

4.1 Conceptual Model

Thrombopoiesis is the process of platelet formation. Platelets are responsible for the coagulation of blood and are a source of growth factors which regulate cell growth and division. Platelet generation is initiated by self-renewing HSCs in the bone marrow. These stem cells differentiate and through a series of mitotic divisions produce megakaryocytes (MKs), the precursors of platelets. As MKs mature, their ploidy increases through a series of endomitoses. Once mature, MKs produce platelets which enter the blood stream.

Similar to the baseline model structure, the thrombopoietic model consists of three compartments. The X_1 compartment represents mitotic precursors in the bone marrow, ranging from HSCs to megakaryoblasts. The X_2 compartment represents MKs in the bone marrow, and the X_3 compartment represents platelets in circulation. Each MK produces thousands of platelets resulting in an amplification. The number of platelets produced per MK is denoted σ.

Following radiation exposure in humans, there is a delay before the peripheral platelet counts start to decline (Bond et al. 1965). This delay is likely due to the time needed for the early progenitors affected by radiation to mature. In order to simulate this delayed effect, sub-compartments were added to the MK compartment. A cell entering the X_2 compartment travels through each of the subcompartments before producing platelets. Furthermore, the first half of the MK subcompartments are labeled as immature MKs and the second half are labeled mature MKs. The reason for this differentiation is for feedback purposes and is described in Section 4.1.2. The platelet compartment is also divided into subcompartments to generate more biologically realistic transit time distributions (Murphy and Francis 1971). Figure 4.1 illustrates the structure of the thrombopoiesis model.

4.1.1 Radiation damage

In our model, both mitotic progenitors and MKs are radiosensitive while in Smirnova's model MKs are radioresistant. MK radiosensitivity was added because at high radiation doses (5-8 Gy), the delay in platelet decline following radiation exposure does not occur, suggesting MKs are becoming damaged (Cohn and Milne 1956). Thus, we included MK radiosensitivity in our human model.

When cells become damaged, they enter into only one damaged state for each cell type (X_1^d for damaged mitotic progenitors and X_2^d for damaged MKs). In Smirnova's model cells may become moderately, heavily, or weakly damaged. This level of detail may have been required for Smirnova's protracted radiation models; however, none of the kinetic blood cell count data for acute exposures supported including a weakly damaged cell compartment, and the proportion of cells entering the moderately verses heavily damaged cell compartment did not significantly affect model output. Thus, to simplify the model and minimize parameters, the weakly damaged cell compartments have been removed, and the moderately and heavily damaged cell compartments have been merged into one damaged compartment.

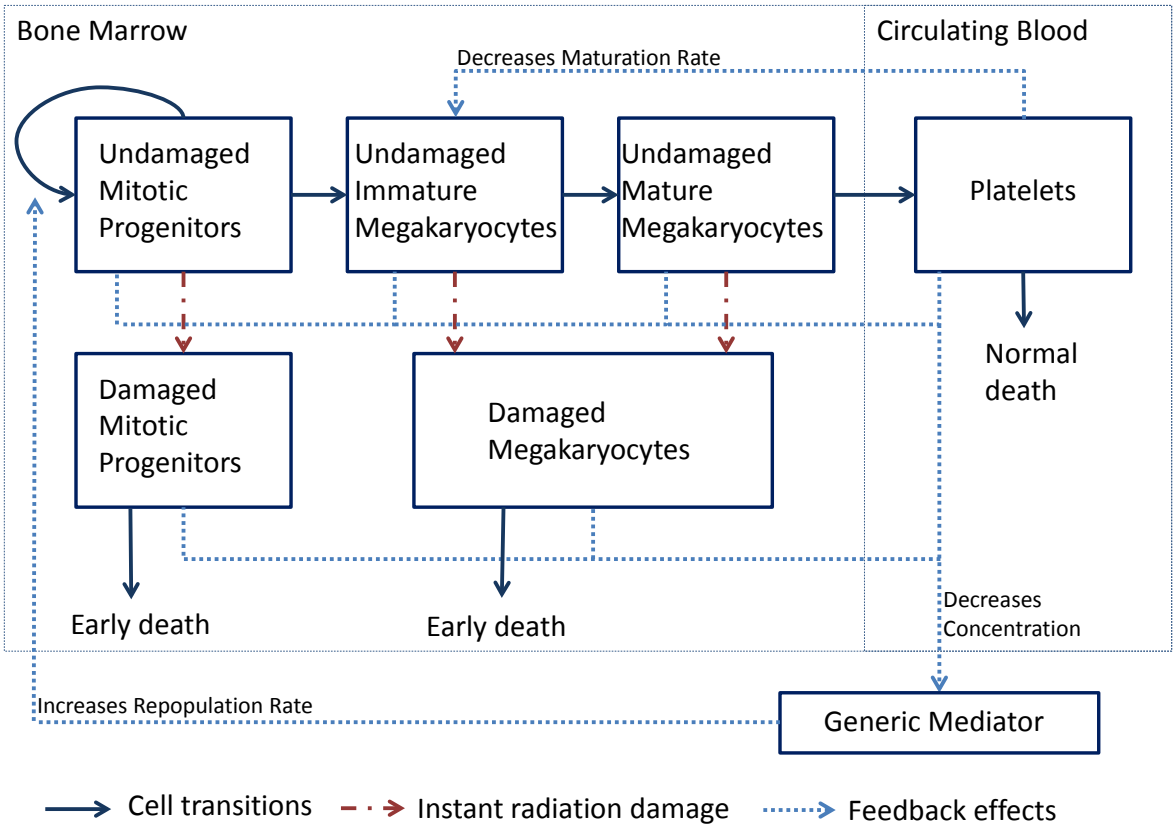

Figure 4.1: Thrombopoiesis model diagram

4.1.2 Feedback mechanisms

The model has two feedback mechanisms that are essential for maintaining and, if concentrations are perturbed, returning to equilibrium. The first mechanism involves a generic mediator, the level of which is regulated by the concentration of cells in the system. The mediator stimulates the repopulation rate of mitotic progenitors. Because the action of the mediator is fast with respect to the hematopoietic cell kinetics, the rate of repopulation (B) can be written as a function of cell concentration (see Section 3.2 for derivation).

$$B = \frac{\alpha}{1 + \beta(x_1^{ud} + x_1^d + \theta_2(x_2^{ud} + x_2^d) + \theta_3 x_3)} \tag{11}$$

Due to the significant stimulatory role of TPO in thrombopoiesis (Kaushansky 2005), it is assumed to represent a large portion of the generic mediator. Thus, known biological mechanisms involving TPO are used to justify the effects of the generic mediator in our model. TPO concentration is regulated by platelets and MKs through receptor interactions. Specifically, receptors on the membranes of platelets and MKs bind to and engulf TPO, removing it from the system.

In the second feedback mechanism, the concentration of platelets alters the maturation rate of immature MKs. Information on the impact of platelets on MK maturation can be gleaned from studies on platelet kinetics following thrombopheresis, which is the removal

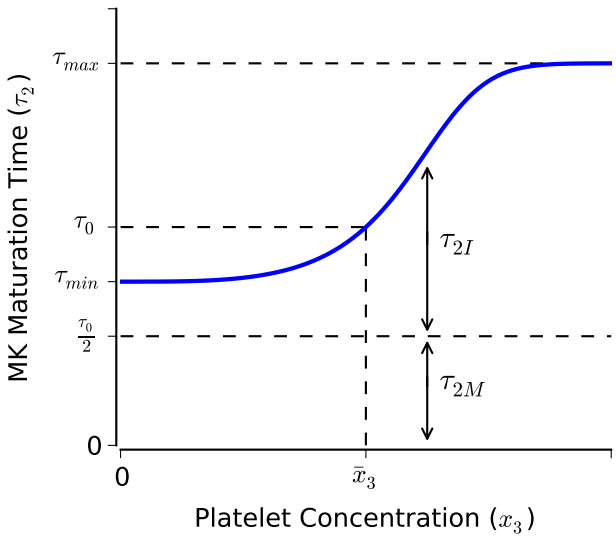

Figure 4.2: Feedback effect of platelets x_3 on MK maturation time (τ_2)

of platelets from an individual for donation (Sullivan et al. 1977). In these studies, the platelet concentration increases at the expected rate for the first 3-4 days given known platelet production rates. However, an increase in the production rate approximately 4 days after thrombopheresis suggests that the platelet concentration affects the maturation of early MKs. TPO is known to affect MK maturation as well as the early progenitor repopulation but does not affect the formation of platelets from the MK cytoplasm (Kaushansky 2005). For these reasons, a negative effect of platelet concentration was added on only immature MK maturation rather than on the entire MK compartment. To divide the X_2 compartment into immature and mature MKs, the first half of the sub-compartments were classified as immature X_{2I} while the second half of the sub-compartments were classified as mature X_{2M}. Thus, the number of MK compartments is limited to being an even integer.

To model this second feedback mechanism, we assume that the normal transit time through the entire MK compartment is τ_0, and that this transit time ranges from τ_{min} to τ_{max}. We also assume that (see Fig. 4.2)

- the transit time τ_{2M} through the mature MK compartment (X_{2M}) is fixed at $\tau_0/2$, so that the transit time τ_{2I} through the immature MK compartment (X_{2I}) ranges from $\tau_{2I,min} = \tau_{min} - \tau_0/2$ to $\tau_{2I,max} = \tau_{max} - \tau_0/2$
- $\tau_{max} > \tau_0 > \tau_{min} > \frac{\tau_0}{2}$ (τ_{min} must be greater than $\frac{\tau_0}{2}$ because $\frac{\tau_0}{2}$ is the transit time through the mature MK sub-compartments)

When the system is at equilibrium, we want $\tau_{2I} = \tau_0/2$ (so that $\tau_{2I} + \tau_{2M} = \tau_0$). Moreover, as x_3 decreases we want $\tau_{2I} \to \tau_{2I,min}$, and as x_3 increases we want $\tau_{2I} \to \tau_{2I,max}$. With these goals in mind, we define

$$\tau_{2I} = \frac{1}{Z(\frac{1}{\tau_0/2}, \frac{1}{\tau_{2I,max}}, \frac{1}{\tau_{2I,min}})} \tag{12}$$

$$= \frac{1}{Z(2\delta_0, \frac{\delta_{min}}{1-\frac{\delta_{min}}{2\delta_0}}, \frac{\delta_{max}}{1-\frac{\delta_{max}}{2\delta_0}})} \tag{13}$$

where

$$Z(x, x_{min}, x_{max}) = x_{min} + (x_{max} - x_{min})^{1-\widetilde{x}_3^{\lambda}}(x - x_{min})^{\widetilde{x}_3^{\lambda}} \tag{14}$$

$$\delta_0 = \frac{1}{\tau_0} \tag{15}$$

$$\delta_{min} = \frac{1}{\tau_{max}} \tag{16}$$

$$\delta_{max} = \frac{1}{\tau_{min}} \tag{17}$$

δ_{min} and δ_{max} are respectively the minimum and maximum possible net transition rates through the entire MK compartment. Note that the above assumption that $\tau_{max} > \tau_0 > \tau_{min} > \frac{\tau_0}{2}$ is equivalent to the assumption that $\delta_{min} < \delta_0 < \delta_{max} < 2\delta_0$.

Given this model, it is clear that when the system is at equilibrium (and thus $\widetilde{x}_3 \equiv 1$), $\tau_{2I} = \tau_0/2$, so that the total MK transit time is $\tau_{2I} + \tau_{2M} = \tau_0 = \delta_0^{-1}$. As the concentration of platelets approaches zero, τ_{2I} approaches $(1 - \delta_{max}/2\delta_0)/\delta_{max} = \tau_{2I,min}$. Thus, the total MK transit time approaches $\tau_{2I,min} + \tau_{2M} = (\tau_{min} - \tau_0/2) + \tau_0/2 = \tau_{min}$. Similarly, as the concentration of platelets increases, the total MK transit time approaches τ_{max}.

Smirnova's original model included a feedback effect of x_3 on ploidy levels. However, we found that after adding the feedback on maturation rate, an effect of x_3 on ploidy did not improve model outputs and was therefore removed from the model.

The sources for transition rates between compartments and of cell decay (γ, n, δ, δ_{min}, δ_{max}, m, ψ, μ), radiosensitivity parameters (D_1^0, n_1, D_2^0, n_2), and other parameters (α, λ, σ, θ_2, θ_3) are provided in Section 4.3.

4.2 Mathematical Model

The mathematical model of thrombopoiesis is described by a set of initial conditions and differential equations that describe the change in cell concentrations with time. A description of each cell compartment is provided in Table 4.1.

At equilibrium cell concentrations in the X_1, X_2, and X_3 compartment are equal to $\bar{x}_1^{ud}$, $\bar{x}_2^{ud}$, and $\bar{x}_3$, respectively. Following acute exposure, radiosensitive cells immediately transition into the damaged compartment. The following equations define how cell concentrations change following an acute exposure of dose D and determine initial conditions for the temporal model.

$$x_1^{ud} = \bar{x}_1^{ud}\left(1 - (1 - e^{-D/D_1^0})^{n_1}\right) \tag{18}$$

$$x_{2I,i}^{ud} = \frac{\bar{x}_2^{ud}}{n}\left(1 - (1 - e^{-D/D_2^0})^{n_2}\right) \quad (i = 1, 2, ..., n/2) \tag{19}$$

$$x_{2M,i}^{ud} = \frac{\bar{x}_2^{ud}}{n}\left(1 - (1 - e^{-D/D_2^0})^{n_2}\right) \quad (i = 1, 2, ..., n/2) \tag{20}$$

Table 4.1: Cell concentrations in each compartment of the thrombopoiesis model

Variable name	Description
x_1^{ud}	Undamaged cells in the mitotic compartment X_1
$x_{2I,i}^{ud}$	Undamaged immature MKs in the ith subcompartment of X_{2I}
$x_{2M,i}^{ud}$	Undamaged mature MKs in the ith subcompartment of X_{2M}
$x_{3,i}$	Undamaged circulating platelets in the ith subcompartment of X_3
x_1^d	Damaged cells in the mitotic compartment X_1
x_2^d	Damaged MKs in the X_2 compartment
$\bar{x}_i^{ud}$	Concentration of cells in the X_i compartment at equilibrium (i=1,2)
$\bar{x}_3$	Concentration of cells in the X_3 compartment at equilibrium

$$x_{3,i} = \frac{\bar{x}_3}{m} \quad (i = 1, 2, ..., m) \tag{21}$$

$$x_1^d = \bar{x}_1^{ud}\left(1 - e^{-D/D_1^0}\right)^{n_1} \tag{22}$$

$$x_2^d = \bar{x}_2^{ud}\left(1 - e^{-D/D_2^0}\right)^{n_2} \tag{23}$$

Once radiation exposure occurs, a series of differential equations are used to describe the compartmental transitions, repopulation and decay rates, and the feedback mechanisms shown in Figure 4.1. σ is a constant which represents the number of platelets produced per MK. The following equations describe the model where Eq. 18–23 are used to calculate initial conditions. $\dot{x}_i$ represents dx_i/dt.

$$\dot{x}_1^{ud} = Bx_1^{ud} - \gamma x_1^{ud} \tag{24}$$

$$\dot{x}_{2I,1}^{ud} = \gamma x_1^{ud} - n\delta x_{2I,1}^{ud} \tag{25}$$

$$\dot{x}_{2I,i}^{ud} = n\delta x_{2I,i-1}^{ud} - n\delta x_{2I,i}^{ud} \quad (i = 2, 3, ..., n/2) \tag{26}$$

$$\dot{x}_{2M,1}^{ud} = n\delta x_{2I,n/2}^{ud} - n\delta_0 x_{2M,1}^{ud} \tag{27}$$

$$\dot{x}_{2M,i}^{ud} = n\delta_0 x_{2M,i-1}^{ud} - n\delta_0 x_{2M,i}^{ud} \quad (i = 2, 3, ..., n/2) \tag{28}$$

$$\dot{x}_{3,1} = \sigma n\delta_0 x_{2M,n/2}^{ud} - m\psi x_{3,1} \tag{29}$$

$$\dot{x}_{3,i} = m\psi x_{3,i-1} - m\psi x_{3,i} \quad (i = 2, 3, ..., m) \tag{30}$$

$$\dot{x}_i^d = -\mu x_i^d \quad (i = 1, 2) \tag{31}$$

where

$$B = \frac{\alpha}{1 + \beta\left(\theta_1(x_1^{ud} + x_1^d) + \theta_2(x_2^{ud} + x_2^d) + \theta_3 x_3\right)} \tag{32}$$

$$x_2^{ud} = \sum_{i=1}^{n/2} x_{2I,i}^{ud} + x_{2M,i}^{ud} \tag{33}$$

$$x_3 = \sum_{i=1}^{m} x_{3,i} \tag{34}$$

$$\delta = \frac{1}{2} Z(2\delta_0, \frac{\delta_{min}}{1 - \frac{\delta_{min}}{2\delta_0}}, \frac{\delta_{max}}{1 - \frac{\delta_{max}}{2\delta_0}}) \tag{35}$$

$$Z(x, x_{min}, x_{max}) = x_{min} + (x_{max} - x_{min})^{1-\widetilde{x}_3^{\lambda}} (x - x_{min})^{\widetilde{x}_3^{\lambda}} \tag{36}$$

4.3 Radiation Model Parameter Sources

Thrombopoiesis parameters were determined either using experimental data or through optimization. The optimized parameters include γ, δ, λ, θ_2, and D_2^0. The following gives a detailed explanation of the source of all other parameters in the human thrombopoiesis model.

4.3.1 Maximum mitotic repopulation rate (α)

The maximum mitotic repopulation rate was set to 2.0 d^{-1} which results in a minimum division time of

$$T_{div} = \frac{ln(2)}{2d^{-1}} \cdot \frac{24h}{1d} = 8.3h \tag{37}$$

In adult humans, cells can divide up to about twice a day, and the DNA synthesis phase only takes approximately 8 h (Andreeff et al. 2000). Thus, a max repopulation rate of 2.0 d^{-1} is biologically reasonable.

4.3.2 Platelet transit rate (ψ)

Several studies have reported a platelet lifespan in humans of approximately 9 d (Schmitt et al. 2001; Mezzano et al. 1982; Kaushansky 2005; Finch et al. 1977). Thus, the value of ψ was set to 1/9 or 0.11 d^{-1}.

4.3.3 MK subcompartment number (n)

The number of megakaryocyte subcompartments was set to 10 ($n = 10$). Following low dose radiation exposure in humans, platelet counts remain steady for a period of time before rapidly declining. These results can be interpreted as meaning MKs have a fairly fixed maturation time with little variance, suggesting a large value for n. However, in order to decrease computational time for the optimizations, 10 subcompartments was chosen as an upper threshold. Increasing n beyond 10 only improved fits slightly but increased the amount of time it took to run simulations significantly.

4.3.4 Platelet subcompartment number (m)

Fitting human platelet data to gamma functions has led to m values between 7 and 11 (Dowling et al. 2010). Here m was set to the midpoint of this range, 9. A second biomathematical

model of thrombopoiesis used 7 platelet subcompartments (Scholz et al. 2010), reinforcing the notion that 9 is a feasible number.

4.3.5 Ratio of receptor concentrations (θ_3)

The relative feedback effect of x_2 and x_3 on the x_1 repopulation rate is determined by the TPO receptor concentration on the surface of MKs and platelets. The ratio of platelet TPO receptors to MK TPO receptors gives an approximate value of the ratio θ_3/θ_2. In humans, the calculated number of TPO receptors on MKs in the peripheral and umbilical cord blood is 1933 ± 772 (n=3) and 184 ± 48 (n=4) sites per cell, respectively (Kuwaki et al. 1998). The average value of the peripheral and umbilical cord blood MK receptor count is 934 receptors per MK. The number of TPO receptors in healthy humans, using data from 5 experiments, was 30 ± 4 (Broudy et al. 1997). Thus, the ratio of θ_3 to θ_2 is 30/934 and $\theta_3 = 0.03 \cdot \theta_2$.

4.3.6 Maximum and minimum rates of MK maturation (δ_{min}, δ_{max})

The maximum and minimum rates of MK maturation were determined by allowing the immature MK maturation time to decrease or increase by up to 50%. Thus, if the immature MK maturation time is $1/2\delta_0$, the maximum maturation time is $3/4\delta_0$ and the minimum maturation time is $1/4\delta_0$. This leads to minimum and maximum total MK maturation times of:

$$\tau_{max} = \frac{3}{4\delta_0} + \frac{1}{2\delta_0} = \frac{5}{4\delta_0} \tag{38}$$

$$\tau_{min} = \frac{1}{4\delta_0} + \frac{1}{2\delta_0} = \frac{3}{4\delta_0} \tag{39}$$

Thus,

$$\delta_{min} = \frac{4\delta_0}{5} \tag{40}$$

$$\delta_{max} = \frac{4\delta_0}{3} \tag{41}$$

$$\tag{42}$$

When 92% of platelets were removed from the circulation of rats, the MK maturation time decreased to 62-85% of control values (Ebbe et al. 1968). This provides some validation for setting τ_{min} equal to 75% of normal.

4.3.7 Number of platelets produced per MK (σ)

The number of platelets produced per MK (3000 platelets/MK) was assumed to be the same as in Smirnova's murine and human models (Smirnova 2011). This value is in agreement with other studies in humans (Deutsch and Tomer 2013).

4.3.8 Radiosensitivity of mitotic progenitor cells (D_1^0, n_1)

In humans, the D_0 and n values for MK colony-forming units (CFU-MKs) when stimulated with only TPO were 0.79 Gy and 1.0, respectively (Kashiwakura et al. 2000). These values correspond with the variables for mitotic progenitor radiosensitivity. Thus, D_1^0=0.79 Gy and n_1=1.0 for humans.

4.3.9 Number of targets per MK (n_2)

The number of hits required to kill a MK was set to 4 ($n_2 = 4$). This variable was originally included in the optimization procedure, but there was a large collinearity between n_2 and D_2^0 making it not possible to optimize these two parameters together. Thus, rather than optimize n_2, the value was systematically increased until a decline was seen in the early plateau phase at a dose level supported by experimental data.

4.3.10 Effect of damaged states on mediator levels (μ)

The death rate of damaged cells was set to 1.0 d^{-1}. In Smirnova's original model, the moderately and heavily damaged compartments had death rates of 0.5 d^{-1} and 6.0 d^{-1} to simulate mitotic and interphase death, respectively (Smirnova 2011). Here, the damaged compartment contains both cells that die during mitosis and interphase. Thus, the value of 1.0 d^{-1} provides an approximate average lifespan of 1.0 d.

4.4 Optimization Data

For the radiation model optimization, data was collected from multiple sources. Table 4.2 provides a summary of the radiation data used in optimizing the human thrombopoiesis model. Information on the data reference, dose, and baseline values is given for all case studies. Data from 17 case studies were used in the optimization, 11 of which contained data points up to and beyond 30 days post-radiation exposure. The subjects received doses ranging from 0.12 to 12.5 Gy.

4.5 Results: Optimization and MCMC Analysis

The optimized parameter values and corresponding 95% confidence intervals are given in Table 4.3. Also provided are the initialization value, the lower bound, and the upper bound placed on each parameter prior to running the optimization. Table 4.4 gives a complete list of parameter values, descriptions, and bases. Figure 4.3 shows the optimized model compared to select data used for the optimization. Each dataset comes from the specified case study/patient. The remainder of the optimization data is compared to the model output in Appendix B.1. For details on the MCMC results and identifiability analysis see Appendix C.

Table 4.2: Optimization data summary for thrombopoiesis model

Incident/Subject	Reference	Dose (Gy)	Baseline ($10^3 \mu L^{-1}$)
Los Alamos 1945–2	Hempelmann et al. 1952	0.12	819.26[a]
UT CARL 1971	Andrews et al. 1961*	2.6	350.63[a]
Argonne 1952–I	Bond et al. 1965	1.5	111.23[a]
Y-12 1958–B	Andrews et al. 1961*	2.97	161.25[a]
Y-12 1958–C	Andrews et al. 1961*	3.73	181.25[a]
Y-12 1958–A	Bond et al. 1965	4.02	289.56[a]
Vinca 1958–B	Jammet et al. 1959	3.51	210.31[a]
Vinca 1958–H	Jammet et al. 1959	4.37	233.73[a]
Vinca 1958–M	Jammet et al. 1959	5.74	219.88[a]
Vinca 1958–G	Jammet et al. 1959	5.35	250.00[b]
Vinca 1958–D	Jammet et al. 1959	5.40	250.00[b]
Vinca 1958–V	Jammet et al. 1959	6.11	221.29[a]
Yarmonenko 1988–Z	Yarmonenko 1988	9.8	140.21[a]
Nesvizh 1991	Baranov et al. 1994	12.5	106.75[a]
Cancer patients 1958-mean of 18	Miller et al. 1958	1.0	197.25[c]
Cancer patients 1958-mean of 12	Miller et al. 1958	1.5	234.25[c]
Cancer patients 1958-mean of 30	Miller et al. 1958	2.0	155.75[c]

[a]Mean of up to four data points collected within 3 days of radiation exposure
[b]Mean platelet concentration observed in humans (Valentin 2002)
[c]Mean of pre-radiation data points
*Data provided by Ron Goans
Additional details on the human case studies provided in Appendix A.

4.6 Validation

To validate the human thrombopoiesis model, the model outputs were compared to data on platelet count following radiation in humans that were not included in the optimization (Hempelmann et al. 1952; Bond et al. 1965; Hirama et al. 2003; Stavem et al. 1985; Mettler et al. 2001; Mettler 2001). Select validation results are shown in Figure 4.4. The remainder of the validation results are presented in Appendix B.2.

Validation was also performed by comparing model output to kinetic platelet data from patients following thrombopheresis (Lasky et al. 1981; Weisbach et al. 1999; Sullivan et al. 1977). In thrombopheresis a certain percentage of platelets are removed from the blood stream. We can initialize the value of x_3 in our model using this percentage, where we

Table 4.3: Thrombopoiesis optimized parameters and confidence intervals

Parameter	Optimized Value	2.5%[a]	97.5%[b]	Initial Value (Lower,Upper)[c]
γ (d^{-1})	0.2556	0.2254	0.2819	0.2647 (0.01, 1.99)
δ (d^{-1})	0.0589	0.0503	0.0683	0.0586 (0.05, 0.2)
θ_2	0.0063	0.0041	0.0109	0.0049 (0.0039, 20)
λ	3.51	3.4772	3.5293	3.4913 (0.3, 4)
D_2^0 (Gy)	2.768	2.5914	2.9329	2.8794 (1, 50)

[a]Lower end of parameter 95% confidence interval
[b]Upper end of parameter 95% confidence interval
[c]Initialization value, lower (min), and upper (max) bound given to parameter during optimization

assume (1) an equal fraction of platelets is removed from each age dependent platelet subcompartment and (2) the removal of platelets is instantaneous. In one study, thrombopheresis was performed twice. To simulate this, we initialized the value of x_3 according to the first thrombopheresis and manually altered x_3 at the time of the second thrombopheresis without changing the values of the other state variables. This validation helps to confirm that the kinetic rates of cell maturation and feedback are correct in the model. These results are shown in Figure 4.5.

4.6.1 Relative compartment sizes

To further validate the thrombopoiesis model, the relative compartment sizes at equilibrium are calculated using model parameters and compared to experimental data. An equilibrium point of the model is a point in the steady state at which the vector field vanishes. Therefore, Eq. 25–30 imply that at an equilibrium point

$$
\begin{aligned}
0 &= \gamma x_1^{ud} - n\delta x_{2I,1}^{ud} \\
0 &= n\delta x_{2I,i-1}^{ud} - n\delta x_{2I,i}^{ud} \quad (i = 2, 3, ..., n/2) \\
0 &= n\delta x_{2I,n/2}^{ud} - n\delta_0 x_{2M,1}^{ud} \\
0 &= n\delta_0 x_{2M,i-1}^{ud} - n\delta_0 x_{2M,i}^{ud} \quad (i = 2, 3, ..., n/2) \\
0 &= \sigma n\delta_0 x_{2M,n/2}^{ud} - m\psi x_{3,1} \\
0 &= m\psi x_{3,i-1} - m\psi x_{3,i} \quad (i = 2, 3, ..., m)
\end{aligned}
$$

Moreover, at equilibrium $\delta = \delta_0$, so we must have

$$
\begin{aligned}
\frac{\bar{x}_1^{ud}}{\bar{x}_{2I,1}^{ud}} &= \frac{n\delta_0}{\gamma} \\
\frac{\bar{x}_{2I,i}^{ud}}{\bar{x}_{2I,j}^{ud}} &= 1 \quad (i = 1, 2, ..., n/2; j = 1, 2, ..., n/2)
\end{aligned}
$$

Table 4.4: Biological parameter values for thrombopoiesis

Parameter	Description	Value	Section (References)
α	Maximum rate of mitotic progenitor cell repopulation	2.0 d^{-1}	4.3.1
γ	Rate of mitotic progenitor cell maturation	0.26 d^{-1}	Optimized
δ_0	Rate of MK maturation	0.06 d^{-1}	Optimized
ψ	Rate of platelet decay	0.11 d^{-1}	4.3.2 (Mezzano et al. 1982; Finch et al. 1977)
n	Number of MK subcompartments	10	4.3.3
m	Number of platelet subcompartments	9	4.3.4 (Dowling et al. 2010; Scholz et al. 2010)
θ_2	Decay rate of mediator due to x_2 cells relative to decay rate due to x_1 cells	0.006	Optimized
θ_3	Decay rate of mediator due to x_3 cells relative by decay rate due to x_1 cells	0.00018	4.3.5 (Kuwaki et al. 1998; Broudy et al. 1997)
δ_{min}	Minimum rate of MK maturation	0.048	4.3.6
δ_{max}	Maximum rate of MK maturation	0.08	4.3.6
λ	Strength of x_3 feedback on immature MK maturation	3.5	Optimized
σ	Number of platelets per MK	3000	4.3.7 (Smirnova 2011; Deutsch and Tomer 2013)
D_1^0	Determines fraction of x_1 targets that are hit by radiation at dose D	0.79 Gy	4.3.8 (Kashiwakura et al. 2000)
n_1	Number of targets per x_1 cell	1	4.3.8 (Kashiwakura et al. 2000)
D_2^0	Determines fraction of x_2 targets that are hit by radiation at dose D	2.77 Gy	Optimized
n_2	Number of targets per x_2 cell	4	4.3.9
μ	Rate of moderately damaged cell death	1.0 d^{-1}	4.3.10

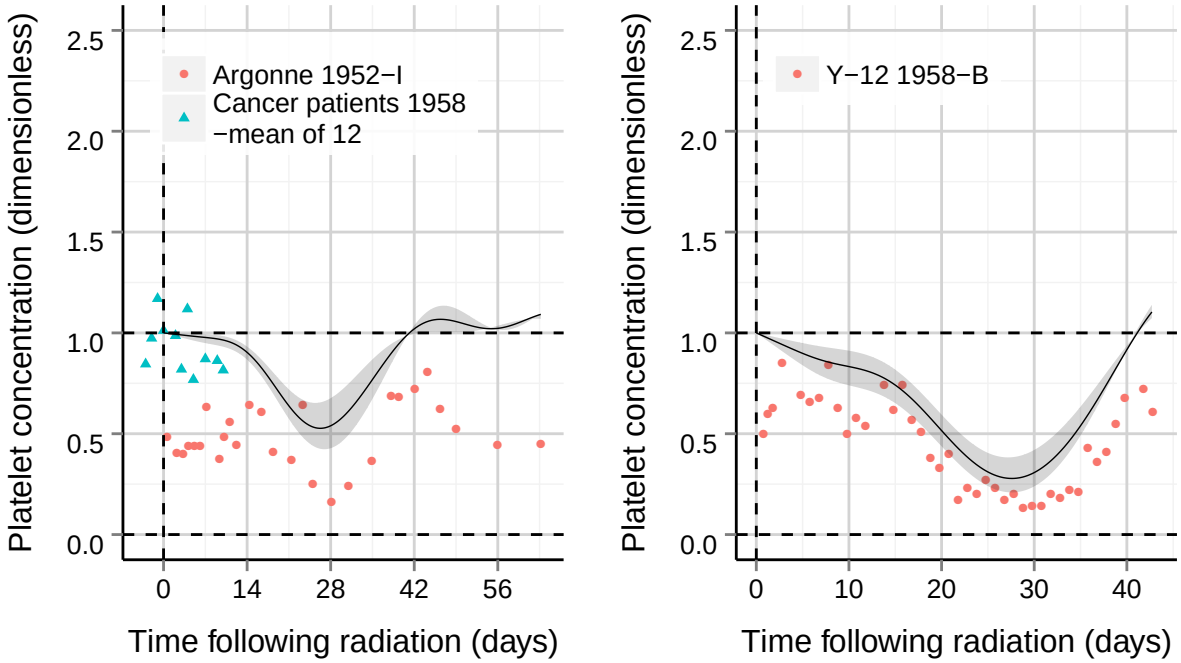

(a) Dose: 1.5 Gy (1-2 Gy; Argonnne)

(b) Dose: 2.97 Gy ± 25%

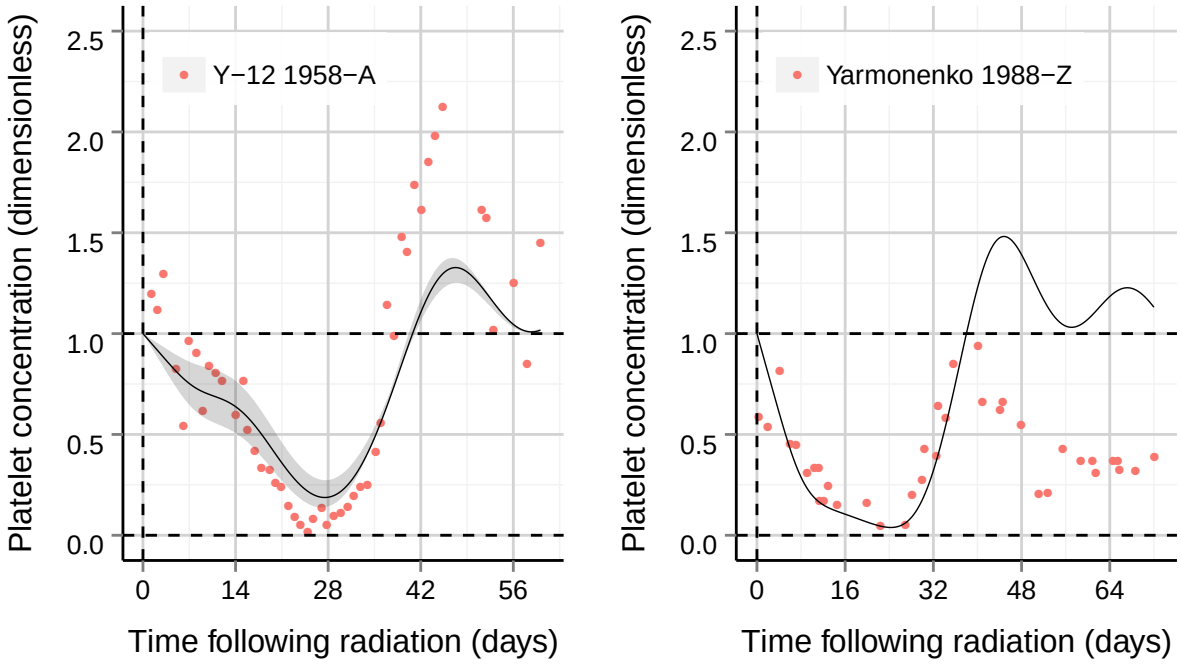

(c) Dose: 4.02 Gy ± 25%

(d) Dose: 9.8 Gy

Figure 4.3: Thrombopoiesis model compared to select optimization data. Model output at the specified dose is delineated by a black line and, if a dose range is provided, a shaded region.

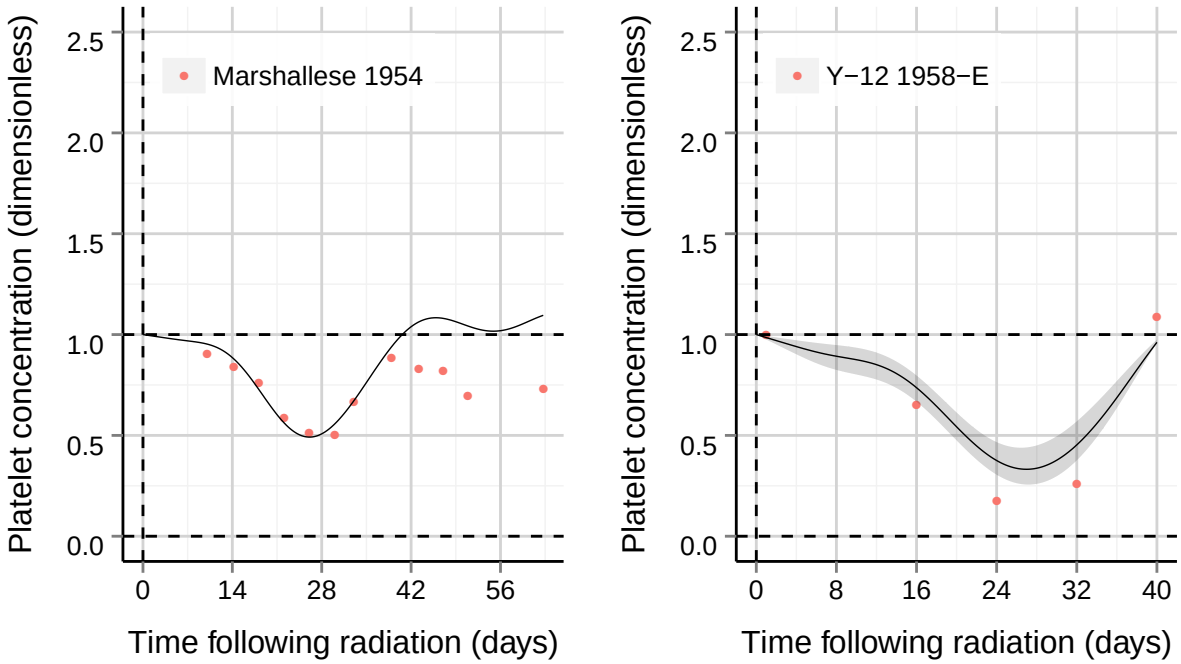

(a) Dose: 1.68 Gy

(b) Dose: 2.59 Gy ± 25%

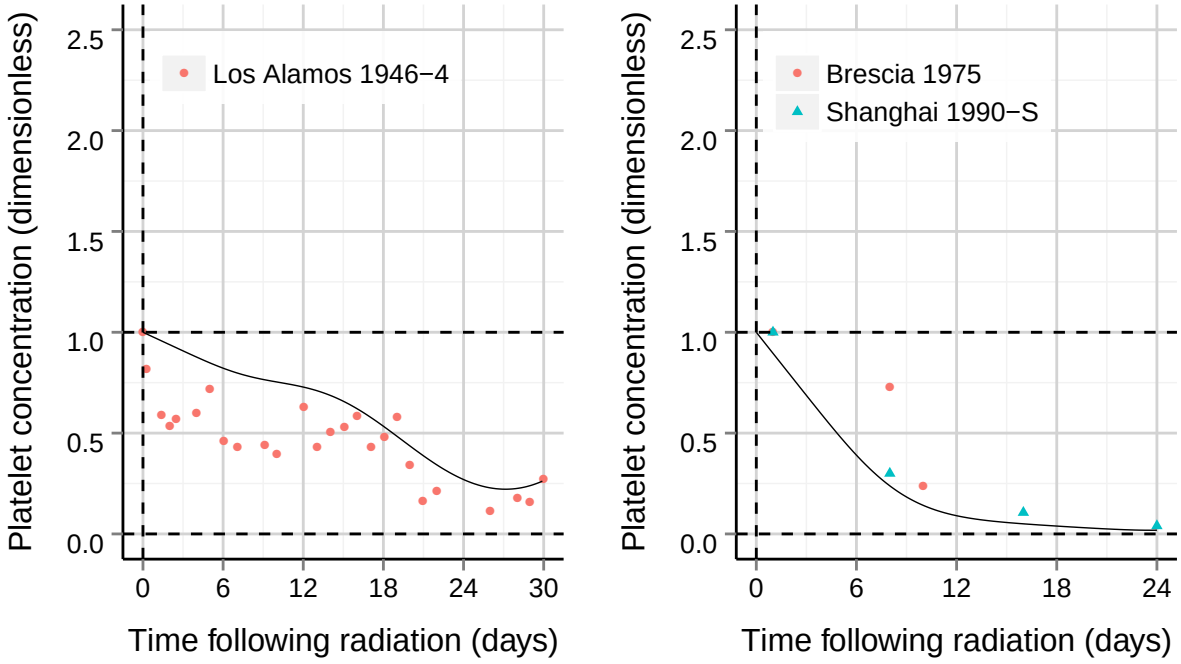

(c) Dose: 3.6 Gy

(d) Dose: 12.0 Gy

Figure 4.4: Thrombopoiesis model compared to select validation data. Model output at the specified dose is delineated by a black line and, if a dose range is provided, a shaded region.

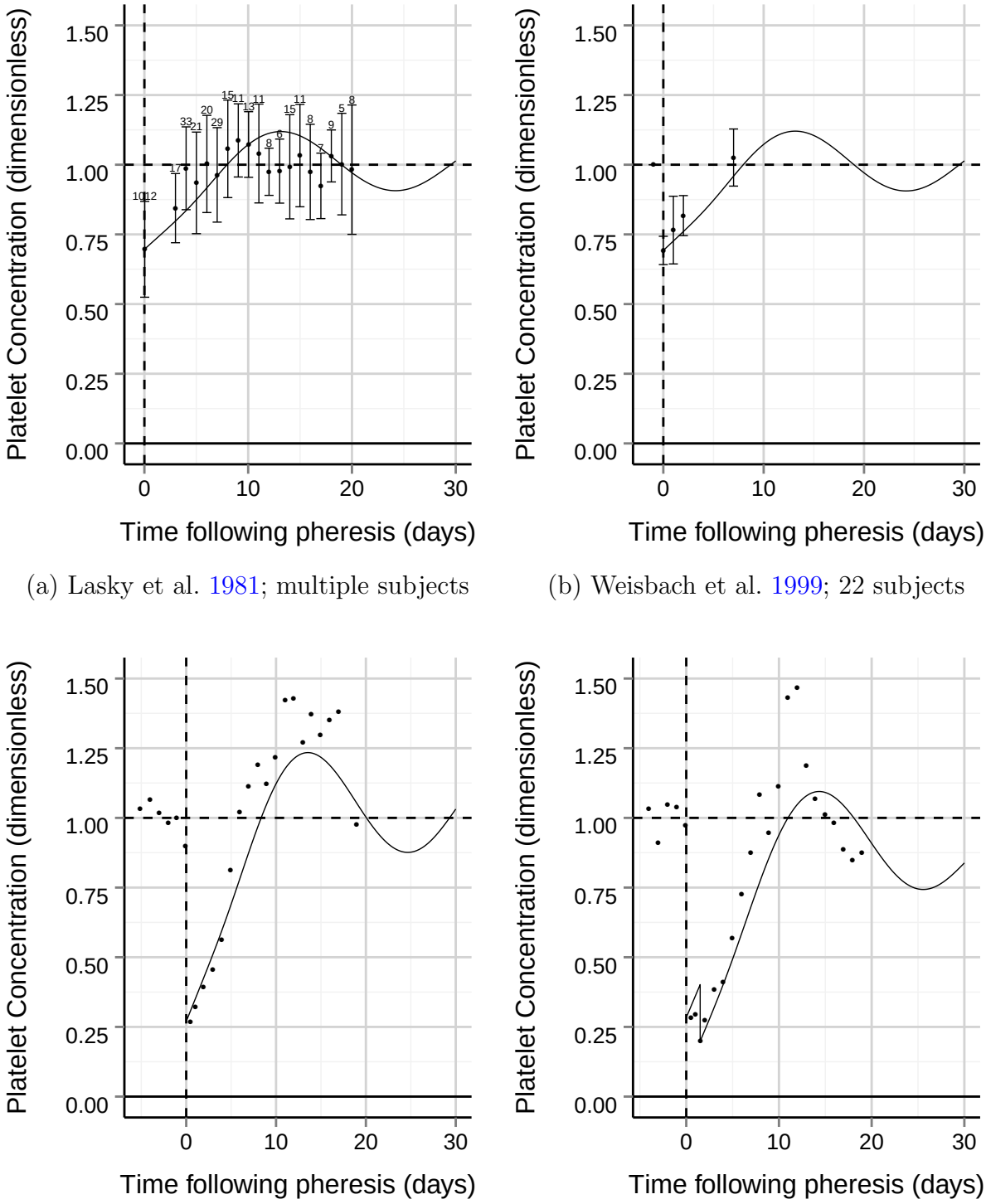

(a) Lasky et al. 1981; multiple subjects

(b) Weisbach et al. 1999; 22 subjects

(c) Sullivan et al. 1977; individual data

(d) Sullivan et al. 1977; individual data

Figure 4.5: Thrombopoiesis model overlaid on thrombopheresis data

$$
\begin{aligned}
\frac{\bar{x}^{ud}_{2M,i}}{\bar{x}^{ud}_{2I,j}} &= 1 \quad (i = 1, 2, ..., n/2; j = 1, 2, ..., n/2) \\
\frac{\bar{x}^{ud}_{2M,i}}{\bar{x}^{ud}_{2M,j}} &= 1 \quad (i = 1, 2, ..., n/2; j = 1, 2, ..., n/2) \\
\frac{\bar{x}^{ud}_{2M,n/2}}{\bar{x}_{3,1}} &= \frac{m\psi}{\sigma n \delta_0} \\
\frac{\bar{x}_{3,i}}{\bar{x}_{3,j}} &= 1 \quad (i = 1, 2, ..., m; j = 1, 2, ..., m)
\end{aligned}
$$

Since

$$
\begin{aligned}
\bar{x}^{ud}_2 &= \sum_{i=1}^{n/2} \bar{x}^{ud}_{2I,i} + \bar{x}^{ud}_{2M,i} \\
&= n\bar{x}^{ud}_{2I,i} \quad i = 1, 2, ..., n/2 \\
&= n\bar{x}^{ud}_{2M,i} \quad i = 1, 2, ..., n/2 \\
\bar{x}_3 &= \sum_{i=1}^{m} \bar{x}_{3,i} \\
&= m\bar{x}_{3,i} \quad i = 1, 2, ..., m,
\end{aligned}
$$

the relative compartment sizes at equilibrium are

$$
\begin{aligned}
\frac{\bar{x}^{ud}_1}{\bar{x}^{ud}_2} &= \frac{\delta_0}{\gamma} \\
&\rightarrow \frac{0.06}{0.26} = 0.23 \\
\frac{\bar{x}^{ud}_2}{\bar{x}_3} &= \frac{\psi}{\sigma \delta_0} \\
&\rightarrow \frac{0.11}{3000 \cdot 0.06} = 0.0006 \\
\frac{\bar{x}^{ud}_1}{\bar{x}_3} &= \frac{\psi}{\sigma \gamma} \\
&\rightarrow \frac{0.11}{3000 \cdot 0.26} = 0.0001
\end{aligned}
$$

In humans, the total number of bone marrow cells is approximately $2 \cdot 10^{10}$ per kg of body weight (Valentin 2002), and the fraction of those estimated to be MKs is 0.04% (Levine 1980). This gives a total MK count of $8 \cdot 10^6$ per kg body weight. The number of platelets circulating is approximately $250 \cdot 10^3$ per μL of blood (Valentin 2002). Humans have 71 mL of blood per kg of body weight (Starr and Taggart 1989), leading to a total platelet count of $1.775 \cdot 10^{10}$ cells per kg of body weight. This leads to an x_2 to x_3 ratio of 0.0005, which is comparable with the model prediction of 0.0006.

This page intentionally left blank.

5 Granulopoiesis Model

5.1 Conceptual Model

Granulopoiesis is the process by which mature granulocytes are generated from pluripotent HSCs. Granulocytes are a type of leukocyte and can be subdivided into neutrophils, eosinophils, and basophils. Neutrophils account for the majority of granulocytes and are involved in phagocytosis, the release of soluble anti-microbials, and generating neutrophil extracellular traps (NETs).

The granulopoiesis model has four compartments: mitotic precursors in the bone marrow (X_1), post-mitotic precursors in the bone marrow (X_2), granulocytes in circulation (X_3), and granulocytes in the tissues (X_4). Figure 5.1 illustrates the structure of the granulopoiesis model. In this diagram, the damaged compartments represent both the weakly damaged and the damaged cells in the system.

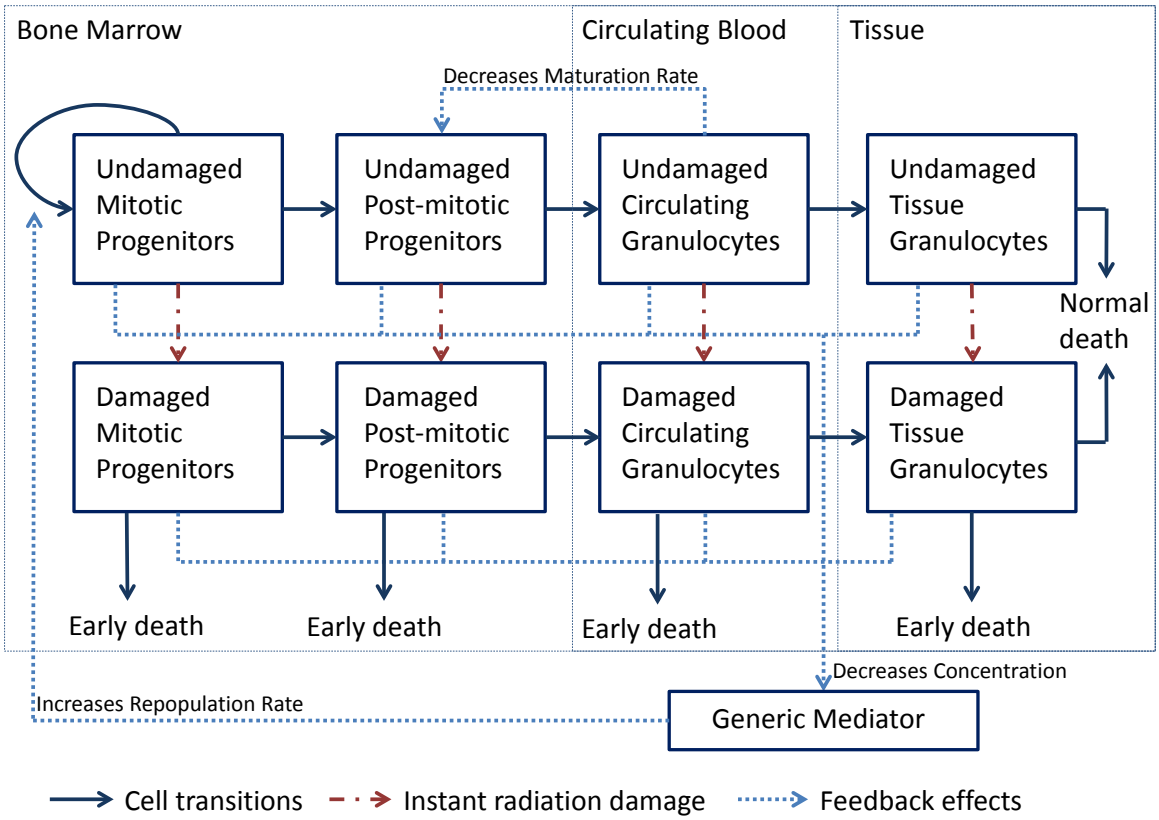

Figure 5.1: Granulopoiesis model diagram

5.1.1 Radiation damage

All cells in the granulopoietic lineage are radiosensitive. The mitotic cells in the bone marrow are the most radiosensitive and become either damaged or weakly damaged. The cells in the other three compartments are less radiosensitive than mitotic cells and enter a single damaged state following radiation exposure.

The weakly damaged cell compartment is used to model the late transient increase in granulocyte counts observed following radiation exposure (Bond et al. 1965). Weakly damaged cells reproduce like normal cells for a period of time defined by the following equation:

$$\Delta t_{ae} = \tau - vD \tag{43}$$

where D is the radiation dose, and τ and v are parameters. Once the elapsed time after radiation exposure is equal to Δt_{ae}, all weakly damaged cells and their progeny start decaying at rate η.

5.1.2 Feedback mechanisms

The model has two feedback mechanisms. The first involves the generic mediator which stimulates the repopulation rate of X_1. The mediator's concentration decreases as the population of granulopoietic cells increases. Because the action of the mediator is fast, its concentration can be written as a function of cell concentration, and thus the rate of repopulation (B) can also be written as a function of cell concentration (see Section 3.2 for derivation):

$$B = \frac{\alpha}{1 + \beta(x_1^{ud} + x_1^{d} + x_1^{wd} + \sum_{i=2}^{4} \theta_i (x_i^{ud} + x_i^{d} + x_i^{wd}))} \tag{44}$$

The second feedback mechanism affects the rate of granulocyte transition from the bone marrow into the blood. As the concentration of granulocytes in the blood increases, the rate of transition from the bone marrow (F) decreases resulting in a negative feedback loop. The equation for F is

$$F = \delta \frac{1 + M(x_3^{ud} + x_3^{d} + x_3^{wd})^2}{1 + L(x_3^{ud} + x_3^{d} + x_3^{wd})^2} \tag{45}$$

In the model, rather than defining M and L to describe the granulocyte rate of entry from the bone marrow to the blood (F), m and l are used. m is equivalent to $M(\bar{x}_3^{ud})^2$ and l is equivalent to $L(\bar{x}_3^{ud})^2$ where $\bar{x}_3$ represents the concentration of x_3 at equilibrium.

The sources for parameters defining the rates between compartments (γ, δ, m, l, κ), the rates of cell decay (ψ, μ, η), radiosensitivity parameters (D_1^0, D_1^{000}, n_1, D_2^0, n_2, D_3^0, n_3, D_4^0, n_4), and other parameters (α, θ_2, θ_3, θ_4, τ, v) are given in Section 5.3.

5.2 Mathematical Model

The mathematical model of granulopoiesis is described by a set of initial conditions and differential equations that describe the change in cell concentrations over time. The description of each cell type is given in Table 5.1.

At equilibrium cell concentrations in the X_1, X_2, X_3, and X_4 compartment are equal to $\bar{x}_1^{ud}$, $\bar{x}_2^{ud}$, $\bar{x}_3^{ud}$, and $\bar{x}_4^{ud}$, respectively. Following acute exposure, cells immediately transition into the damaged or weakly damaged compartments depending on their radiosensitivity. ϑ determines the ratio of the number of cells that transition into the damaged or weakly damaged compartment. The following equations describe how cell concentrations change

Table 5.1: Cell concentrations in each compartment of the granulopoiesis model

Variable name	Description
x_1^{ud}	Undamaged cells in the mitotic compartment X_1
x_2^{ud}	Undamaged cells in the post mitotic compartment X_2
x_3^{ud}	Undamaged granulocytes in the blood X_3
x_4^{ud}	Undamaged granulocytes in the tissues X_4
x_1^{d}	Damaged cells in the mitotic compartment X_1
x_2^{d}	Damaged cells in the post mitotic compartment X_2
x_3^{d}	Damaged granulocytes in the blood X_3
x_4^{d}	Damaged granulocytes in the tissue X_4
x_1^{wd}	Weakly damaged cells in the mitotic compartment X_1
x_2^{wd}	Weakly damaged cells in the post mitotic compartment X_2
x_3^{wd}	Weakly damaged granulocytes in the blood X_3
x_4^{wd}	Weakly damaged granulocytes in the tissue X_4
$\bar{x}_i^{ud}$	Concentration of cells in the X_i compartment at equilibrium (i=1,2,3,4)

following an acute exposure of dose D and determine initial conditions for the temporal model.

$$x_i^{ud} = \bar{x}_i^{ud}\left(1-(1-e^{-D/D_i^0})^{n_i}\right) \quad (i=1,2,3,4) \tag{46}$$

$$x_1^{wd} = \bar{x}_1^{ud}\frac{\vartheta}{1+\vartheta}\left(1-e^{-D/D_1^0}\right)^{n_1} \tag{47}$$

$$x_i^{wd} = 0 \quad (i=2,3,4) \tag{48}$$

$$x_1^{d} = \bar{x}_1^{ud}\frac{1}{1+\vartheta}\left(1-e^{-D/D_1^0}\right)^{n_1} \tag{49}$$

$$x_i^{d} = \bar{x}_i^{ud}\left(1-e^{-D/D_i^0}\right)^{n_i} \quad (i=2,3,4) \tag{50}$$

where

$$\vartheta = \frac{(1-e^{-D/D_1^0})^{n_1}-(1-e^{-D/D_1^{000}})^{n_1}}{(1-e^{-D/D_1^{000}})^{n_1}}$$

Once radiation exposure occurs, a series of differential equations are used to describe the compartmental transitions, repopulation and decay rates, and the feedback mechanisms shown in Figure 5.1. The following equations describe the model where Eq. 46–50 are used to calculate initial conditions. $\dot{x}_i$ represents dx_i/dt.

$$\dot{x}_1^{ud} = Bx_1^{ud} - \gamma x_1^{ud} \tag{51}$$

$$\dot{x}_2^{ud} = \gamma x_1^{ud} - F x_2^{ud} \tag{52}$$

$$\dot{x}_3^{ud} = F x_2^{ud} - \kappa x_3^{ud} \tag{53}$$

$$\dot{x}_4^{ud} = \kappa x_3^{ud} - \psi x_4^{ud} \tag{54}$$

$$\dot{x}_1^{wd} = \begin{cases} B x_1^{wd} - \gamma x_1^{wd} & t_o \leq t < t_o + \Delta t_{ae} \\ -\eta x_1^{wd} & t \geq t_o + \Delta t_{ae} \end{cases} \tag{55}$$

$$\dot{x}_2^{wd} = \begin{cases} \gamma x_1^{wd} - F x_2^{wd} & t_o \leq t < t_o + \Delta t_{ae} \\ -\eta x_2^{wd} & t \geq t_o + \Delta t_{ae} \end{cases} \tag{56}$$

$$\dot{x}_3^{wd} = \begin{cases} F x_2^{wd} - \kappa x_3^{wd} & t_o \leq t < t_o + \Delta t_{ae} \\ -\eta x_3^{wd} & t \geq t_o + \Delta t_{ae} \end{cases} \tag{57}$$

$$\dot{x}_4^{wd} = \begin{cases} \kappa x_3^{wd} - \psi x_4^{wd} & t_o \leq t < t_o + \Delta t_{ae} \\ -\eta x_4^{wd} & t \geq t_o + \Delta t_{ae} \end{cases} \tag{58}$$

$$\dot{x}_i^{d} = -\mu x_i^{d} \quad (i = 1, 2, 3, 4) \tag{59}$$

where

$$B = \frac{\alpha}{1 + \beta(x_1^{ud} + x_1^{d} + x_1^{wd} + \sum_{i=2}^{4} \theta_i (x_i^{ud} + x_i^{d} + x_i^{wd}))} \tag{60}$$

$$F = \delta \frac{1 + M(x_3^{ud} + x_3^{d} + x_3^{wd})^2}{1 + L(x_3^{ud} + x_3^{d} + x_3^{wd})^2} \tag{61}$$

$$M = \frac{m}{(\bar{x}_3^{ud})^2} \tag{62}$$

$$L = \frac{l}{(\bar{x}_3^{ud})^2} \tag{63}$$

5.3 Radiation Model Parameter Sources

Granulopoiesis parameters were determined using experimental data or through optimization. The optimized parameters include ψ, l, D_1^0, D_1^{000}, D_2^0 and η. The following gives a detailed explanation of the source of all other parameters in the human granulopoiesis model.

5.3.1 Maximum mitotic repopulation rate (α)

The maximum mitotic repopulation rate was set to 2.0 d^{-1} which results in a minimum division time of

$$T_{div} = \frac{ln(2)}{2d^{-1}} \cdot \frac{24h}{1d} = 8.3h \tag{64}$$

In adult humans, cells can divide up to about twice a day, and the DNA synthesis phase only takes approximately 8 h (Andreeff et al. 2000). Thus, a max repopulation rate of 2.0 d^{-1} is biologically reasonable.

5.3.2 Compartment transition rates (δ, m, l, κ, γ)

The mitotic and post-mitotic transition times of granulocytes have been experimentally determined (Price et al. 1996). The mitotic transition time is approximately 6.0 d, leading to $\gamma = 1/6 = 0.17$ d^{-1}. The post-mitotic transition time is 5.5 d leading to δ_{eq}=1/6.4=0.16 d^{-1}. Following G-CSF treatment, the minimum transit time is 2.9 d, leading to a maximum transition rate, or δ, of 0.34 d^{-1}.

Because

$$\delta_{eq} = \delta \frac{1+m}{1+l} \tag{65}$$

we can set m as a function of δ_{eq}, δ, and l.

$$m = \frac{\delta_{eq}}{\delta}(1+l) - 1 \tag{66}$$

δ_{eq} and δ have already been determined, l was included in the optimization procedure, and m was set using the above equation. The granulocyte half-life in the blood of humans is 10.4 h leading to a transit rate κ of 1.6 d^{-1} (Price et al. 1996).

5.3.3 Receptor concentration ratios (θ_2, θ_3, θ_4)

The ratio of receptors on x_2 and x_3 cells compared with x_1 cells was determined based on experimental data on the number of G-CSF receptors per granulocyte progenitor and peripheral granulocyte (Shinjo et al. 1995). Granulocyte progenitors are known to express both the CD33 and CD34 antigens. Using these markers for granulocyte progenitor selection, the relative number of G-CSF receptors on early progenitors in humans was measured to be 0.0446 ± 0.0068 and on later progenitors was 0.0988 ± 0.0250. The relative number of G-CSF receptors on peripheral granulocytes in humans was 8353 ± 623. This gives ratios of 998/446=2.24 and 8353/988=8.45 for θ_2 and θ_3, respectively. Because X_3 and X_4 both represent granulocytes, θ_4 was assumed to equal θ_3.

5.3.4 Granulocyte radiosensitivity (D_3^0, D_4^0)

Granulocyte radiosensitivity was assumed to be equal to the post-mitotic cell radiosensitivity ($D_3^0 = D_4^0 = D_2^0$). In Smirnova's original model, all three cell types also have the same radiosensitivity (Smirnova 2011).

5.3.5 Time of abortive rise Δt_{ae} (τ, v)

The time of abortive elevation Δt_{ae} is determined using the following equation:

$$\Delta t_{ae} = \tau - vD \tag{67}$$

where D is the radiation dose. τ and v were determined through examination of the time of

abortive rise in the granulopoiesis optimization data (see Section 5.4). In each case study, an approximate time of abortive rise was graphed against the acute radiation dose. Fitting Equation 67 to the data, resulted in values of $v = 1.25$ d Gy^{-1} and $\tau = 22.70$ d.

5.3.6 Targets per cell (n_1, n_2, n_3, n_4)

The number of targets per cell in the granulopoiesis model was assumed to be 1 for all cells in the lineage (n_i=1 for $i = 1, 2, 3, 4$) . Using this assumption, we are simplifying our radiation model to the single-target, single-hit model used by Smirnova (Smirnova 2011). Using this model of radiation damage, we are able to accurately match cell survivability following radiation exposure.

5.3.7 Effect of damaged states on mediator levels (μ)

The death rate of damaged cells was set to 1.0 d^{-1}. In Smirnova's original model, the moderately and heavily damaged compartments had death rates of 0.5 d^{-1} and 6.0 d^{-1} to simulate mitotic and interphase death, respectively (Smirnova 2011). Here, the damaged compartment contains both cells that die during mitosis and interphase. Thus, the value of 1.0 d^{-1} provides an approximate average lifespan of 1.0 d.

5.4 Optimization Data

For the radiation model optimization, the data was collected from multiple sources. Table 5.2 provides a summary of the radiation data used in optimizing the human granulopoiesis model. Information on the data reference, dose, and baseline values is given for all case studies. Data from 16 case studies were used in the optimization, 11 of which contained data points up to and beyond 30 days post-radiation exposure. The subjects received doses ranging from 0.12 to 9.8 Gy.

5.5 Results: Optimization and MCMC Analysis

The optimized parameter values and corresponding 95% confidence intervals are given in Table 5.3. Also provided are the initialization value, the lower bound, and the upper bound placed on each parameter prior to running the optimization. Table 5.4 gives a complete list of parameter values, descriptions, and bases. Figure 5.2 shows the optimized model compared to select data used for the optimization. Each dataset comes from the specified case study/patient. The remainder of the optimization data is compared to the model output either in the Discussion (Section 7; Figure 7.3b) or in Appendix B.1. For details on the MCMC results and identifiability analysis see Appendix C.

5.6 Validation

To validate the human granulopoiesis model, the model outputs were compared to data on granulocyte count following radiation in humans that were not included in the optimization (Hempelmann et al. 1952; Bond et al. 1965; Hirama et al. 2003; Stavem et al. 1985; Mettler

Table 5.2: Optimization data summary for granulopoiesis model

Incident/Subject	Reference	Dose (Gy)	Baseline ($10^3 \mu L^{-1}$)
Los Alamos 1945–2	Hempelmann et al. 1952	0.12	4.102[a]
UT CARL 1971	Andrews et al. 1961*	2.6	4.102[a]
Argonne 1952–I	Bond et al. 1965	1.5	4.102[a]
Y-12 1958–B	Andrews et al. 1961*	2.97	4.102[a]
Y-12 1958–C	Andrews et al. 1961*	3.73	4.102[a]
Y-12 1958–A	Bond et al. 1965	4.02	4.102[a]
Vinca 1958–B	Jammet et al. 1959	3.51	4.102[a]
Vinca 1958–H	Jammet et al. 1959	4.37	4.102[a]
Vinca 1958–M	Jammet et al. 1959	5.74	4.102[a]
Vinca 1958–G	Jammet et al. 1959	5.35	4.102[a]
Vinca 1958–D	Jammet et al. 1959	5.40	4.102[a]
Vinca 1958–V	Jammet et al. 1959	3.11	4.102[a]
Yarmonenko 1988–Z	Yarmonenko 1988	9.8	4.102[a]
Cancer patients 1958–mean of 18	Miller et al. 1958	1.0	6.22[b]
Cancer patients 1958–mean of 12	Miller et al. 1958	1.5	6.99[b]
Cancer patients 1958-mean of 30	Miller et al. 1958	2.0	8.13[b]

[a]Mean granulocyte concentration observed in humans (Valentin 2002)
[b]Mean of pre-radiation data points
*Data provided by Ron Goans
Additional details on the human case studies provided in Appendix A

et al. 2001; Mettler 2001). Select validation results are shown in Figure 5.3. The remainder of the validation results are given in Appendix B.2.

5.6.1 Relative compartment sizes

To further validate the granulopoiesis model, the relative compartment sizes at equilibrium are calculated using model parameters and compared to experimental data. An equilibrium point of the model is a point in the state space at which the vector field vanishes. Therefore, Eq. 52 - 54 imply that at an equilibrium point

$$0 = \gamma x_1^{ud} - \delta \frac{1+m}{1+l} x_2^{ud}$$
$$0 = \delta \frac{1+m}{1+l} x_2^{ud} - \kappa x_3^{ud}$$

Table 5.3: Granulopoiesis optimized parameters and confidence intervals

Parameter	Optimized Value	2.5%[a]	97.5%[b]	Initial Value (Lower,Upper)[c]
ψ (d^{-1})	1.0542	0.4409	1.6179	11.8422 (0.01, 20)
l	1.6906	1.1894	2.3066	1.1539 (1.126, 12)
D_1^{000} (Gy)	2.4591	1.9941	2.7815	2.3881 (1, 10)
D_2^0 (Gy)	45.76	43.3506	47.2832	10 (2, 50)
η (d^{-1})	0.08161	0.0524	0.1645	0.0865 (0.05, 5)
D_1^0 (Gy)	0.4605	0.3093	0.6766	0.4714 (0.3, 0.9)

[a]Lower end of parameter 95% confidence interval
[b]Upper end of parameter 95% confidence interval
[c]Initialization value, lower (min), and upper (max) bound given to parameter during optimization

$$0 = \kappa x_3^{ud} - \psi x_4^{ud}$$

Therefore, at equilibrium we must have

$$\begin{aligned}
\frac{\bar{x}_1^{ud}}{\bar{x}_2^{ud}} &= \frac{\delta^{\frac{1+m}{1+l}}}{\gamma} \\
&\rightarrow \frac{0.34^{\frac{1+0.27}{1+1.69}}}{0.17} = 0.94 \\
\frac{\bar{x}_2^{ud}}{\bar{x}_3^{ud}} &= \frac{\kappa}{\delta^{\frac{1+m}{1+l}}} \\
&\rightarrow \frac{1.60}{0.34^{\frac{1+0.27}{1+1.69}}} = 9.97 \\
\frac{\bar{x}_4^{ud}}{\bar{x}_3^{ud}} &= \frac{\kappa}{\psi} \\
&\rightarrow \frac{1.60}{1.05} = 1.52
\end{aligned}$$

In human granulopoiesis the total number of mitotic cell progenitors is $2.11 \cdot 10^9$ per kg of body weight, the total number of post-mitotic progenitors is $5.59 \cdot 10^9$ per kg of body weight, and the total number of granulocytes in the blood (both marginated and circulating) is $0.61 \cdot 10^9$ per kg of body weight (Dancey et al. 1976). This leads to the following ratios:

$$\frac{x_1}{x_2} = 0.377 \tag{68}$$

$$\frac{x_1}{x_3} = 3.459 \tag{69}$$

$$\frac{x_2}{x_3} = 9.164 \tag{70}$$

Based on this experimental data, the ratio given by the kinetic parameters of the granulopoiesis model defining x_2 to x_3 is approximately correct. The ratio of x_1 to x_2 predicted by the model is larger than the ratio predicted by the experimental data, suggesting the value of γ used by the model is too small. However, the value of γ used in our model has support from the literature (Price et al. 1996). The mitotic cell compartment in our model also contains early HSC progenitors, which may not be included in the granulocyte mitotic cell progenitor count given by Dancey et al. 1976. If this were the case, the calculated ratio of x_1 to x_2, based on relative cell compartment sizes, would be larger than 0.377 and closer to agreement with the model prediction of 0.94.

Table 5.4: Biological parameter values for granulopoiesis

Parameter	Description	Value	Section (References)
α	Maximum rate of mitotic progenitor cell repopulation	2.0 d^{-1}	5.3.1 (Andreeff et al. 2000)
γ	Rate of mitotic progenitor cell maturation	0.17 d^{-1}	5.3.2 (Price et al. 1996)
δ	Determines: Post-mitotic maturation rate	0.34 d^{-1}	5.3.2 (Price et al. 1996)
m	Determines: Post-mitotic maturation rate	0.27	5.3.2 (Price et al. 1996)
l	Determines: Post-mitotic maturation rate	1.69	Optimized
κ	Rate of transition from blood to tissue	1.60 d^{-1}	5.3.2 (Price et al. 1996)
ψ	Rate of granulocyte decay from tissue	1.05 d^{-1}	Optimized
η	Rate of weakly damaged cell death (when $t > \Delta t_{ae}$)	0.08 d^{-1}	Optimized
θ_2	Decay rate of mediator due to x_2 cells relative to decay rate due to x_1 cells	2.24	5.3.3 (Shinjo et al. 1995)
θ_3	Decay rate of mediator due to x_3 cells relative to decay rate due to x_1 cells	8.45	5.3.3 (Shinjo et al. 1995)
θ_4	Decay rate of mediator due to x_4 cells relative to decay rate due to x_1 cells	8.45	5.3.3 (Shinjo et al. 1995)
D_1^0	Determines fraction of damaged x_1 cells	0.46 Gy	Optimized
D_1^{000}	Determines ratio of weakly damaged to damaged x_1 cells.	2.46 Gy	Optimized
D_2^0	Determines fraction of damaged x_2 cells	45.76 Gy	Optimized
D_3^0	Determines fraction of damaged x_3 cells	45.76 Gy	5.3.4
D_4^0	Determines fraction of damaged x_4 cells	45.76 Gy	5.3.4
τ	Determines time of abortive rise: $\Delta t_{ae} = \tau - vD$	22.70 d	5.3.5
v	Determines time of abortive rise: $\Delta t_{ae} = \tau - vD$	1.25 d Gy^{-1}	5.3.5
n_i	Number of targets per cell x_i $(i = 1, 2, 3, 4)$	1	5.3.6
μ	Rate of damaged cell death	1.0 d^{-1}	5.3.7

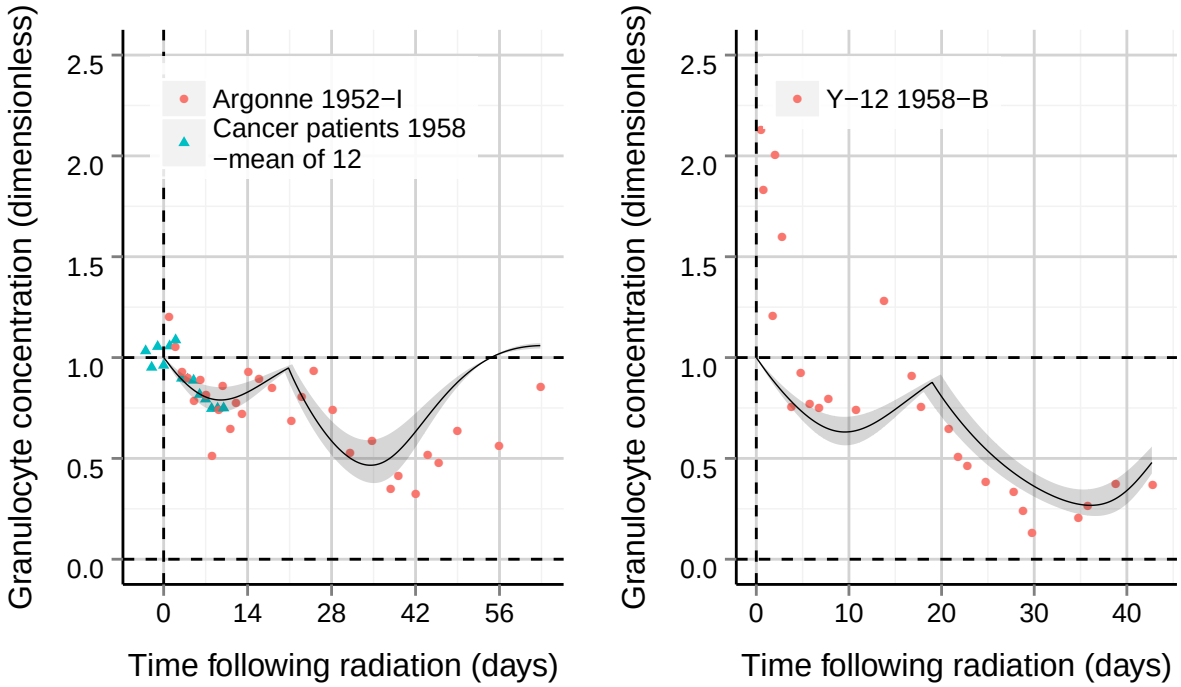

(a) Dose: 1.5 Gy (1-2 Gy; Argonne)

(b) Dose: 2.97 Gy ± 25%

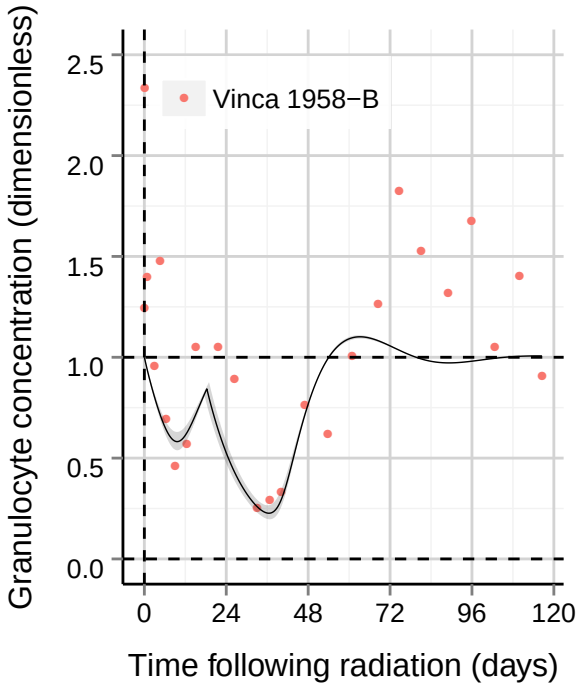

(c) Dose: 3.51 Gy ± 15%

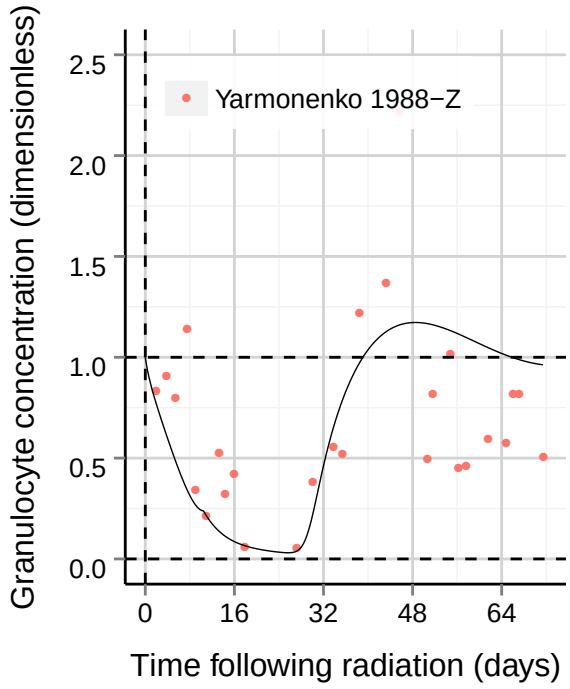

(d) Dose: 9.8 Gy

Figure 5.2: Granulopoiesis model compared to select optimization data. Model output at the specified dose is delineated by a black line and, if a dose range is provided, a shaded region.

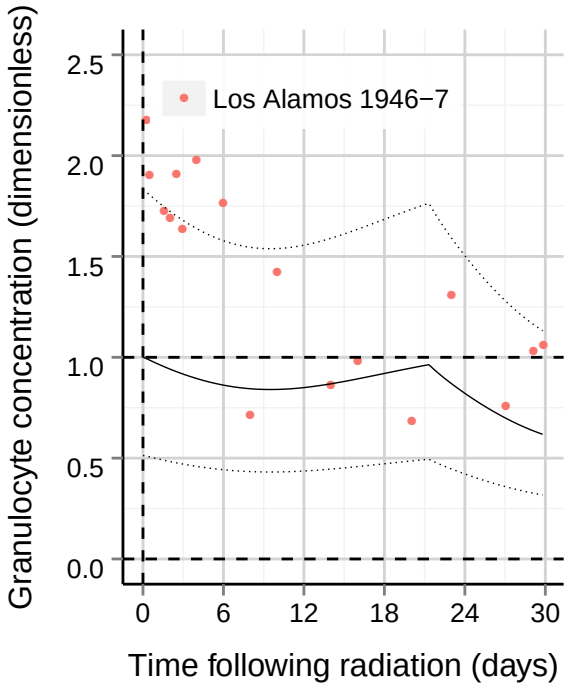

(a) Dose: 1.1 Gy

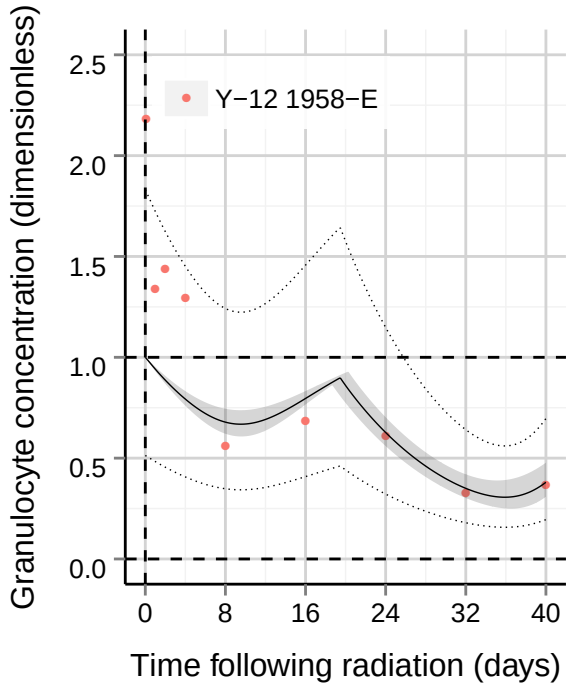

(b) Dose: 2.59 Gy ± 25%

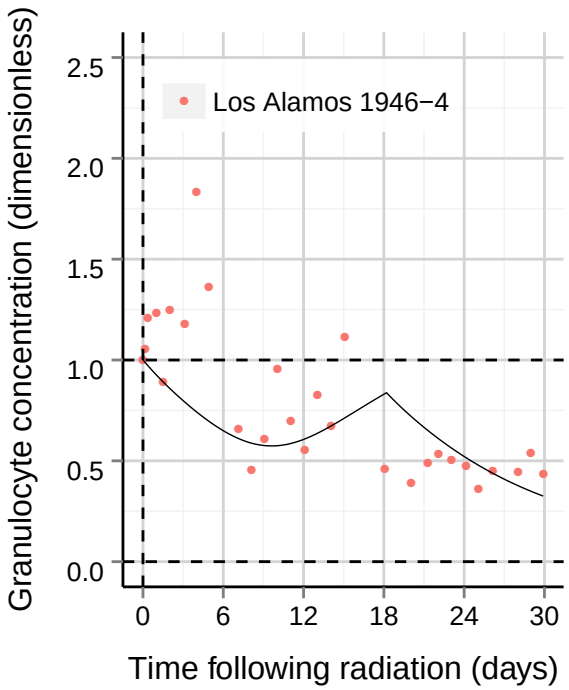

(c) Dose: 3.6 Gy

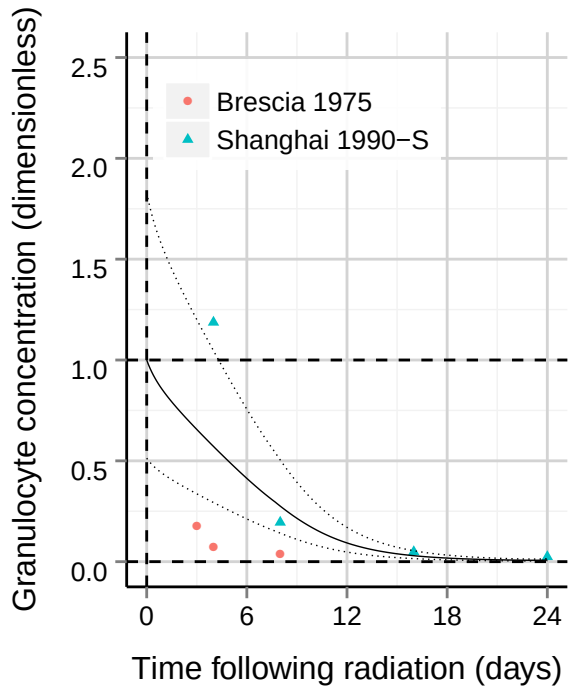

(d) Dose: 12 Gy

Figure 5.3: Granulopoiesis model compared to select validation data. Model output at the specified dose is delineated by a black line and, if a dose range is provided, a shaded region. If a generic baseline value was used, output initialized at the upper and lower end of the granulocyte range is shown by dotted lines.

6 Lymphopoiesis Model

6.1 Conceptual Model

Lymphopoiesis is the process by which lymphocytes are generated from the bone marrow. The three main types of lymphocytes are T cells, B cells, and natural killer (NK) cells. B and NK cells mature in the bone marrow, while T cell progenitors migrate to the thymus for maturation. Once mature, cells enter the circulation and peripheral lymphoid organs including the spleen and lymph nodes. The human lymphopoiesis model consists of three compartments: mitotic precursors in the bone marrow (X_1), post-mitotic precursors in the bone marrow or thymus (X_2), and lymphocytes in circulation (X_3). Figure 6.1 illustrates the structure of the model.

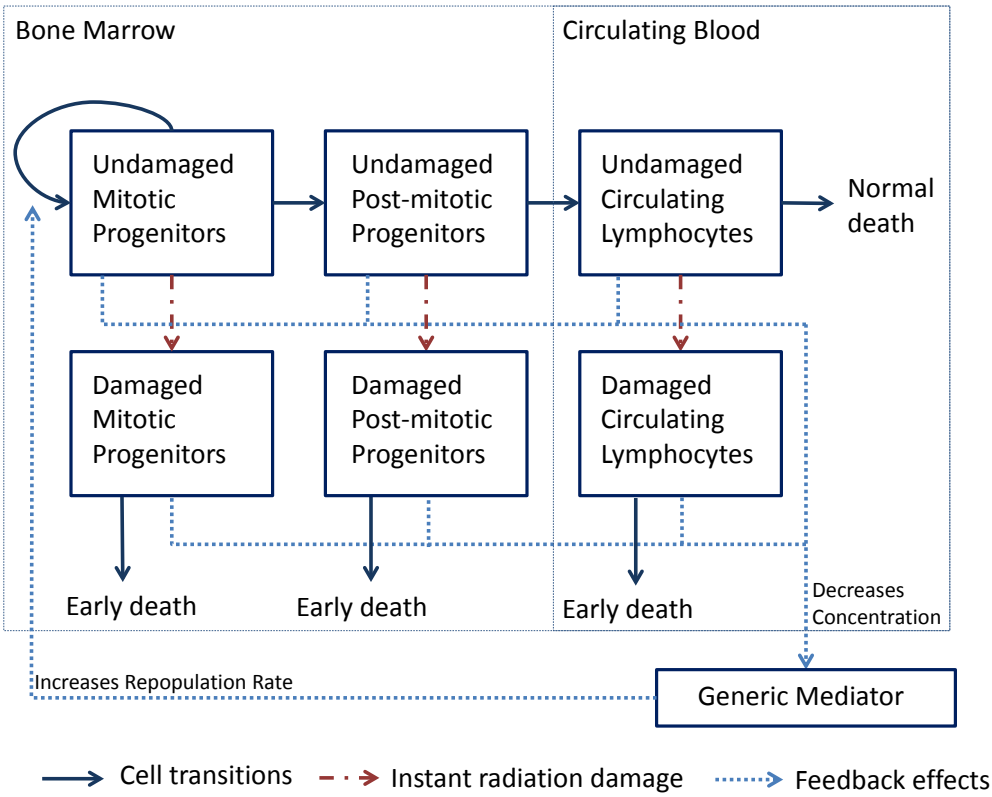

Figure 6.1: Lymphopoiesis model diagram

6.1.1 Radiation damage

All cells in the lymphopoiesis model are considered radiosensitive, and once damaged, decay at rate μ.

6.1.2 Feedback loops

The only feedback loop included in the lymphopoiesis model is the generic mediator that stimulates the repopulation rate of X_1. The mediator's concentration decreases as the pop-

ulation of lymphopoietic cells increases. Because the action of the mediator is fast, its concentration can be written as a function of cell concentration, and thus the rate of repopulation (B) can also be written as a function of cell concentration (see Section 3.2 for derivation):

$$B = \frac{\alpha}{1 + \beta(x_1^{ud} + x_1^d + \theta_2(x_2^{ud} + x_2^d) + \theta_3(x_3^{ud} + x_3^d))} \tag{71}$$

The sources for rates between compartments (γ, δ), the rates of cell decay (ψ, μ), radiosensitivity parameters (D_1^0, n_1, D_2^0, n_2, D_3^0, n_3), and other parameters (α, θ_2, θ_3) are given in Section 6.3.

6.2 Mathematical Model

The mathematical model of lymphopoiesis is described by a set of initial conditions and differential equations that describe the change in cell concentrations with time. The description of each cell type is given in Table 6.1.

Table 6.1: Cell concentrations in each compartment of the lymphopoiesis model

Variable name	Description
x_1^{ud}	Undamaged cells in the mitotic compartment X_1
x_2^{ud}	Undamaged cells in the post mitotic compartment X_2
x_3^{ud}	Undamaged lymphocytes in the blood X_3
x_1^d	Damaged cells in the mitotic compartment X_1
x_2^d	Damaged cells in the post mitotic compartment X_2
x_3^d	Damaged lymphocytes in the blood X_3
$\bar{x}_i^{ud}$	Concentration of cells in the X_i compartment at equilibrium (i=1,2,3)

At equilibrium cell concentrations in the X_1, X_2, and X_3 compartments are equal to $\bar{x}_1^{ud}$, $\bar{x}_2^{ud}$, and $\bar{x}_3^{ud}$, respectively. Following acute exposure, cells immediately transition into the damaged compartment depending on their radiosensitivity. The following equations describe how cell concentrations change following an acute exposure of dose D and determine initial conditions for the temporal model.

$$x_i^{ud} = \bar{x}_i^{ud}\left(1 - (1 - e^{-D/D_i^0})^{n_i}\right) \quad (i = 1, 2, 3) \tag{72}$$

$$x_i^d = \bar{x}_i^{ud}\left(1 - e^{-D/D_i^0}\right)^{n_i} \quad (i = 1, 2, 3) \tag{73}$$

Once radiation exposure occurs, a series of differential equations are used to describe the compartmental transitions, repopulation and decay rates, and the feedback mechanisms shown in Figure 6.1. The following equations describe the model where Eq. 72–73 are used to calculate initial conditions. $\dot{x}_i$ represents dx_i/dt.

$$\dot{x}_1^{ud} = Bx_1^{ud} - \gamma x_1^{ud} \tag{74}$$
$$\dot{x}_2^{ud} = \gamma x_1^{ud} - \delta x_2^{ud} \tag{75}$$
$$\dot{x}_3^{ud} = \delta x_2^{ud} - \psi x_3^{ud} \tag{76}$$
$$\dot{x}_i^{d} = -\mu x_i^{d} \quad (i = 1, 2, 3) \tag{77}$$

where

$$B = \frac{\alpha}{1 + \beta(x_1^{ud} + x_1^d + \theta_2(x_2^{ud} + x_2^d) + \theta_3(x_3^{ud} + x_3^d))} \tag{78}$$

6.3 Radiation Model Parameter Sources

Lymphopoiesis parameters were determined either using experimental data or through optimization. The optimized parameters include γ, θ_2, and D_1^0. The following gives a detailed explanation of the source of all other parameters in the human lymphopoiesis model.

6.3.1 Maximum mitotic repopulation rate (α)

The maximum mitotic repopulation rate was set to 2.0 d^{-1} which results in a minimum division time of

$$T_{div} = \frac{ln(2)}{2d^{-1}} \cdot \frac{24h}{1d} = 8.3h \tag{79}$$

In adult humans, cells can divide up to about twice a day, and the DNA synthesis phase only takes approximately 8 h (Andreeff et al. 2000). Thus, a max repopulation rate of 2.0 d^{-1} is biologically reasonable.

6.3.2 Rate of post-mitotic progenitor maturation (δ)

The rate of post-mitotic progenitor maturation was determined by estimating the number of post-mitotic progenitors in the bone marrow and thymus and deriving the lymphocyte turnover rate by this estimated post-mitotic cell concentration. In humans, the estimated percentage of lymphocytes in the bone marrow, thymus, and blood is 10.9%, 10.9%, and 2.2%, respectively (Trepel 1974). Assuming lymphocytes in the bone marrow and thymus comprise x_2, this leads to an x_3/x_2 ratio of 0.10. At equilibrium:

$$\delta = \psi \frac{\bar{x}_3}{\bar{x}_2} \tag{80}$$

Thus, δ is equal to 0.10ψ. In the next section, the value of ψ in humans is determined to be 0.01 d^{-1} meaning δ equals approximately 0.001 d^{-1} in humans.

6.3.3 Rate of lymphocyte clearance from blood (ψ)

In humans, the fractional replacement rates of $CD4^+$ and $CD8^+$ T cells are 0.008 ± 0.005 d^{-1} and 0.009 ± 0.013 d^{-1}, respectively (Hellerstein et al. 1999). At equilibrium in our model, the rate of replacement is equivalent to the rate of decay. B cells in young individuals (age=19-34) were found to have a mean proliferation rate of 0.0193 ± 0.0103 d^{-1} and a mean clearance rate of 0.0394 ± 0.0339 d^{-1} (Macallan et al. 2005). Because our model does not take into account lymphocyte proliferation, the value of ψ for B cells can be obtained by subtracting the clearance rate from the proliferation rate. This gives a decay rate applicable to our model of 0.0146 d^{-1}. This analysis leads to an approximate decay rate for all lymphocytes of 0.01 d^{-1}.

6.3.4 Effect of damaged states on mediator levels (μ)

The death rate of damaged cells was set to 1.0 d^{-1}. In Smirnova's original model, the moderately and heavily damaged compartments had death rates of 0.5 d^{-1} and 6.0 d^{-1} to simulate mitotic and interphase death, respectively (Smirnova 2011). Here, the damaged compartment contains both cells that die during mitosis and interphase. Thus, the value of 1.0 d^{-1} provides an approximate average lifespan of 1.0 d.

6.3.5 Radiosensitivity of post-mitotic precursors (D_2^0)

The radiosensitivity of post-mitotic precursors was assumed to be equal to that of mitotic precursors: $D_2^0 = D_1^0$. In Smirnova's murine model of lymphopoiesis the mitotic and post-mitotic precursors have the same radiosensitivity (Smirnova 2011), and we use that assumption here in the human model.

6.3.6 Radiosensitivity of lymphocytes (D_3^0, n_3)

The radiosensitivity of lymphocytes in humans was determined by fitting the survival curve to *in vitro* normalized lymphocyte survival data 4 days post irradiation (Kwan and Norman 1977). The optimized value of D_3^0 was 6.22 Gy, and the optimized value of n_3 was 0.40.

6.3.7 Targets per progenitor (n_1, n_2)

The average number of targets per cell in the lymphopoiesis model was assumed to be 1 for the mitotic ($n_1 = 1$) and post-mitotic progenitor cells ($n_2 = 1$). Using this assumption, we are simplifying our radiation model to the single-target, single-hit model used by Smirnova (Smirnova 2011). Using this model of radiation damage, we are able to accurately match cell survivability following radiation exposure.

6.3.8 Parameter dependencies (θ_3)

The amount of mediator decay caused by x_3 and x_2 cells is assumed to be identical ($\theta_2 = \theta_3$). To our knowledge there is no experimental data available to determine the relationship between θ_2 and θ_3. Perturbations to these parameters affect the model output in similar

Table 6.2: Optimization data summary for lymphopoiesis model

Incident/Subject	Reference	Dose (Gy)	Baseline ($10^3 \mu L^{-1}$)
Los Alamos 1945–2	Hempelmann et al. 1952	0.12	2.45[a]
UT CARL 1971	Andrews et al. 1961*	2.6	2.45[a]
Argonne 1952–I	Bond et al. 1965	1.5	2.45[a]
Y-12 1958–A	Bond et al. 1965	4.02	2.45[a]
Y-12 1958–B	Andrews et al. 1961*	2.97	2.45[a]
Y-12 1958–C	Andrews et al. 1961*	3.73	2.45[a]
Y-12 1958–E	Gusev et al. 2010*	2.59	2.45[a]
Vinca 1958–B	Jammet et al. 1959	2.97	2.45[a]
Vinca 1958–H	Jammet et al. 1959	4.37	2.45[a]
Vinca 1958–M	Jammet et al. 1959	5.74	2.45[a]
Vinca 1958–G	Jammet et al. 1959	5.35	2.45[a]
Vinca 1958–D	Jammet et al. 1959	5.40	2.45[a]
Vinca 1958–V	Jammet et al. 1959	6.11	2.45[a]
Cancer patients 1958 –mean of 30	Miller et al. 1958	1.0	1.395[b]
Cancer patients 1958 –mean of 12	Miller et al. 1958	1.5	1.385[b]
Cancer patients 1958 –mean of 18	Miller et al. 1958	2.0	1.35[b]
Yarmonenko 1988–Z	Yarmonenko 1988	9.8	2.45[a]
Lockport 1960–A	Bond et al. 1965	3.0	2.45[a]
Lockport 1960–B	Bond et al. 1965	3.0	2.45[a]

[a]Mean platelet concentration observed in humans (Valentin 2002)
[b]Mean of pre-radiation data points
*Data provided by Ron Goans
Additional details on the human case studies provided in Appendix A.

ways. Thus, when both are included in the optimization, the model is not identifiable. Here, the model was simplified by setting these parameters equal to each other.

6.4 Optimization Data

For the radiation model optimization, data was collected from multiple sources. Table 6.2 provides a summary of the radiation data used in optimizing the human lymphopoiesis model. Information on the data reference, dose, and baseline values is given for all case studies. Data from 19 case studies were used in the optimization, 12 of which contained

data points up to and beyond 30 days post-radiation exposure. The subjects received doses ranging from 0.12 to 9.8 Gy.

6.5 Results: Optimization and MCMC Analysis

Table 6.3 gives a complete list of parameter values, descriptions, and bases. The optimized parameter values and corresponding 95% confidence intervals are given in Table 6.4. Also provided are the initialization value, the lower bound, and the upper bound placed on each parameter prior to running the optimization. Figure 6.2 shows the optimized model compared to select data used for the optimization. Each dataset comes from the specified case study/patient. The remainder of the optimization data is compared to the model output either in the Discussion (Section 7; Figure 7.5b) or in Appendix B.1. For details on the MCMC results and identifiability analysis see Appendix C.

Table 6.3: Biological parameter values for lymphopoiesis

Parameter	Description	Value	Section (References)
α	Maximum rate of mitotic progenitor cell repopulation	2 d^{-1}	6.3.1 (Andreeff et al. 2000)
γ	Rate of mitotic progenitor cell maturation	0.06 d^{-1}	Optimized
δ	Rate of post-mitotic progenitor cell maturation	0.001 d^{-1}	6.3.2 (Trepel 1974)
ψ	Rate of lymphocyte clearance from the blood	0.01 d^{-1}	6.3.3 (Hellerstein et al. 1999; Macallan et al. 2005)
μ	Rate of damaged cell death	1 d^{-1}	6.3.4
D_1^0	Determines fraction of damaged x_1 cells	3.98 Gy	Optimized
D_2^0	Determines fraction of damaged x_2 cells	3.98 Gy	6.3.5 (Smirnova 2011)
D_3^0	Determines fraction of damaged x_3 cells	6.22 Gy	6.3.6 (Kwan and Norman 1977)
n_i	Number of targets per cell x_i $(i = 1, 2)$	1	6.3.7
n_3	Number of targets per x_3 cell	0.40	6.3.6 (Kwan and Norman 1977)
θ_2	Decay rate of mediator due to x_2 cells relative to decay rate due to x_1 cells	2.67	Optimized
θ_3	Decay rate of mediator due to x_3 cells relative to decay rate due to x_1 cells	2.67	6.3.8

Table 6.4: Lymphopoiesis optimized parameters and confidence intervals

Parameter	Optimized Value	2.5%[a]	97.5%[b]	Initial Value (Lower,Upper)[c]
γ (d^{-1})	0.0605	0.0534	0.1243	0.0447 (0.001, 1.99)
θ_2	2.6705	0.5312	3.167	19.9875 (0.001, 20)
D_1^0 (Gy)	3.9769	2.8992	4.4005	4.1128 (0.1, 20)

[a]Lower end of parameter 95% confidence interval
[b]Upper end of parameter 95% confidence interval
[c]Initialization value, lower (min), and upper (max) bound given to parameter during optimization

6.6 Validation

To validate the human lymphopoiesis model, the model outputs were compared to data on lymphocyte count following radiation in humans that were not included in the optimization (Hempelmann et al. 1952; Bond et al. 1965; Hirama et al. 2003; Stavem et al. 1985; Mettler et al. 2001; Mettler 2001). Select validation results are shown in Figure 6.3. An exception to this is the Mol 1965 case study which was a highly non-uniform exposure. The Mol exposure is included in the validation figure to provide a comparison with the Sarov 1963 case study, which is intended for validation, who received the same estimated dose of 5.5 Gy. The remainder of the validation results are given in Appendix B.2.

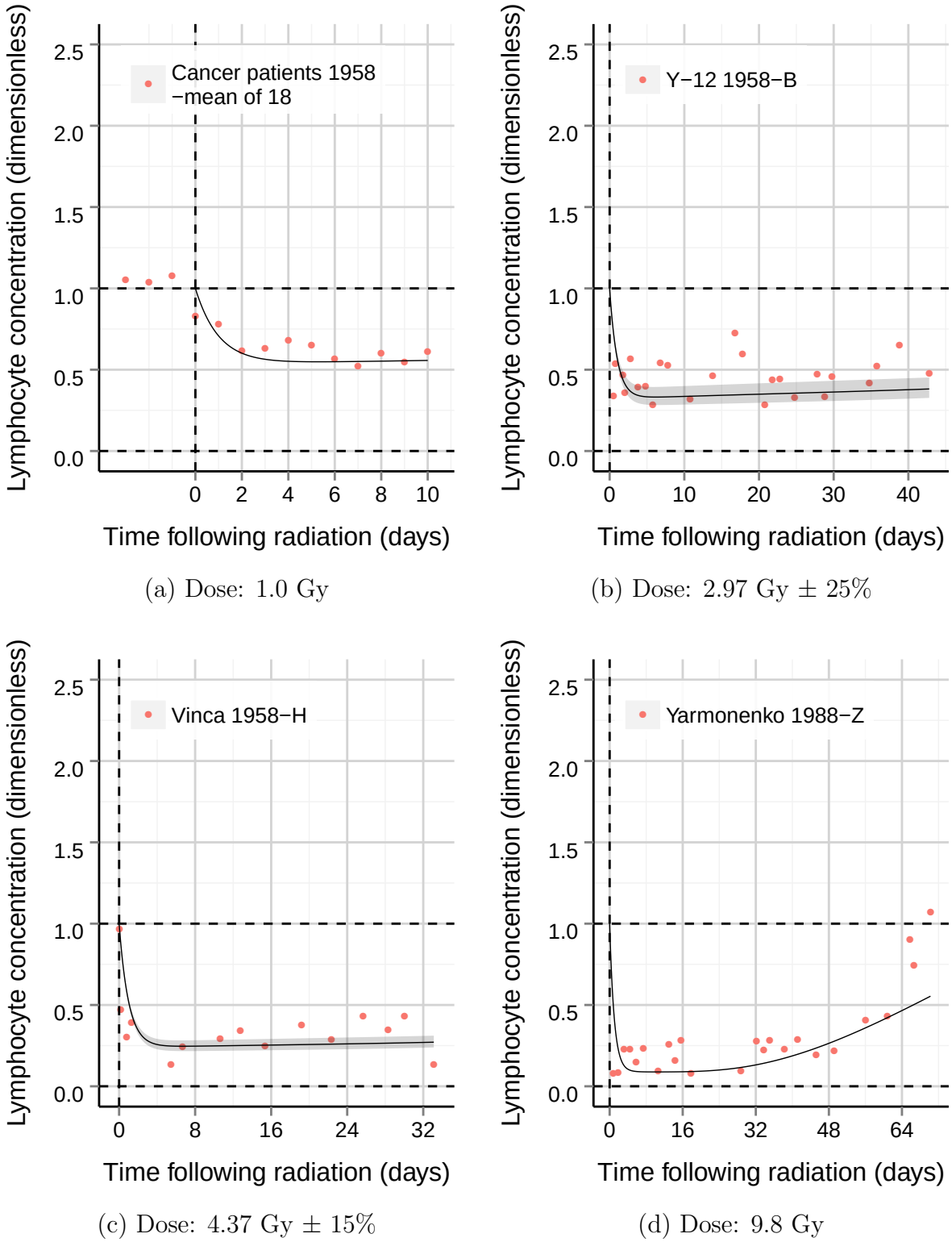

(a) Dose: 1.0 Gy

(b) Dose: 2.97 Gy ± 25%

(c) Dose: 4.37 Gy ± 15%

(d) Dose: 9.8 Gy

Figure 6.2: Lymphopoiesis model compared to select optimization data. Model output at the specified dose is delineated by a black line and, if a dose range is provided, a shaded region.

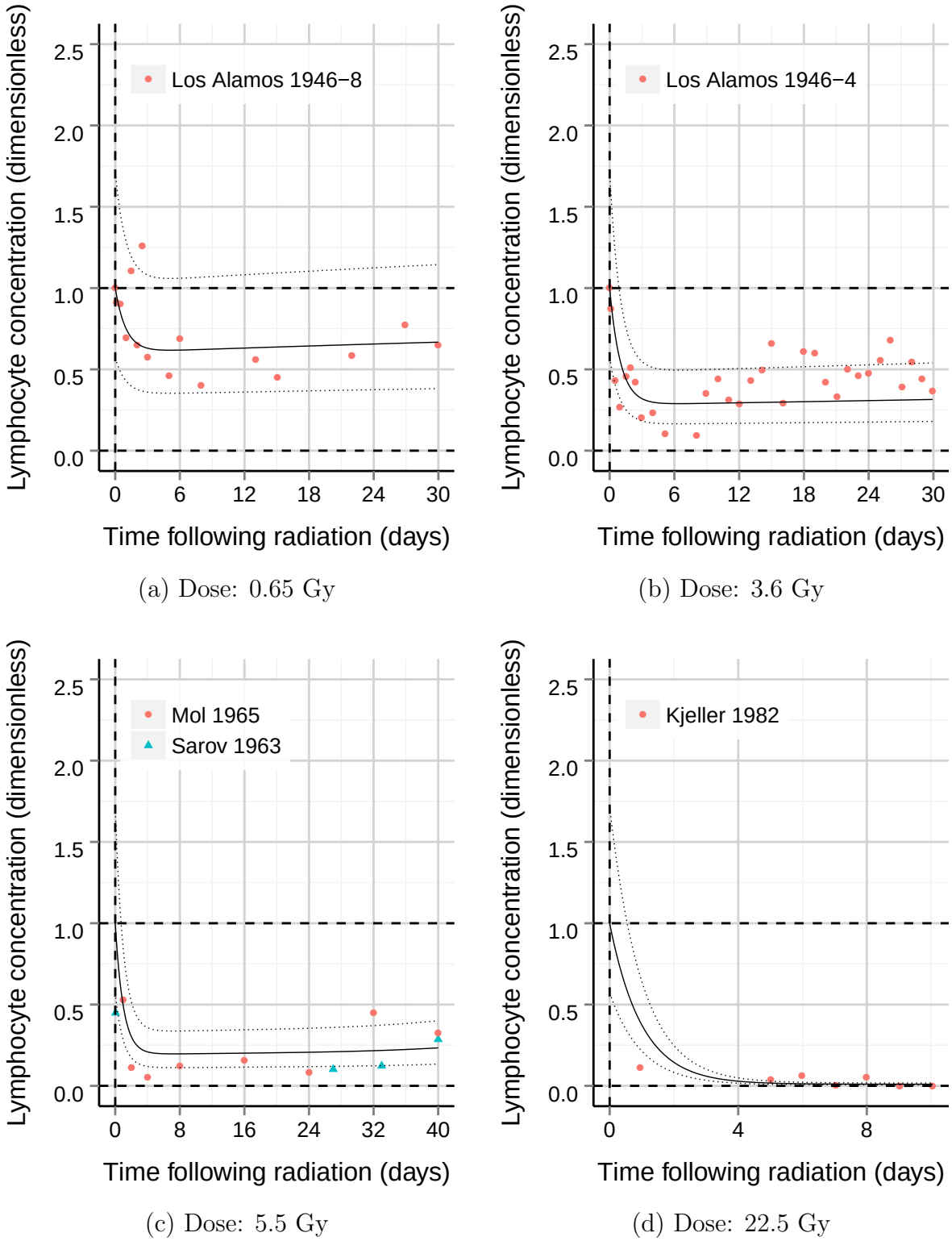

(a) Dose: 0.65 Gy

(b) Dose: 3.6 Gy

(c) Dose: 5.5 Gy

(d) Dose: 22.5 Gy

Figure 6.3: Lymphopoiesis model compared to select validation data. Model output at the specified dose is delineated by a black line. Output initialized at the upper and lower end of the lymphocyte range is shown by dotted lines.

This page intentionally left blank.

7 Discussion

Three hematopoietic mechanistic models which simulate blood cell kinetics following acute radiation exposure in humans are presented. These models have been optimized with and validated against available case study data. The aim of our modeling work was to develop models that represent the general hematopoietic response in humans after radiation exposure without treatment. Our models predict the average response in humans, provide realistic estimates of blood cell counts, and capture the important trends observed in blood cell dynamics following radiation exposure at a range of dose levels.

Several challenges arise when optimizing and validating the models. For both these procedures, we compare human data to model simulations. However, a number of factors impact the relevancy and reliability of these comparisons:

1. Baseline blood cell counts are not available in the majority of case studies. For each blood cell type, there is a large range for what this baseline value could be.

2. Uncertainty in acute radiation doses due to:

   (a) Variable reporting of free-in-air versus midline tissue doses

   (b) Uncertainty in physical dose reconstruction resulting in a large dose range

   (c) Uncertainty in the dose extrapolation for different radiation types (i.e. neutrons and x-rays)

   (d) Non-uniformity of dose delivered

   (e) Dose rate and duration; our models assume that the dose is received instantaneously

3. Treatments, such as transfusion and cytokine therapy, may impact the observed blood cell kinetics.

4. Inter-individual variabilities are observed in blood cell kinetics and cell radiosensitivities.

To perform comparisons to the dimensionless model output, data is divided by a baseline value specific to each individual. Healthy humans have a large range of possible blood cell concentrations; thus, an accurate baseline value is essential for comparisons. For optimization if the baseline value is incorrect, the calculated residual values may be artificially large or small. For granulocytes and lymphocytes when baseline cell counts specific to the individual were not available, the average concentration observed in humans was used as the baseline (Valentin 2002). For platelets, because there is a delayed response following radiation exposure, platelet counts obtained within three days of radiation exposure were used for determining baseline values. If values before three days were not available, the average concentration observed in humans was used (Valentin 2002).

To address concerns about the uncertainty in radiation dose estimates, case studies were reviewed in detail. An effort was made to identify studies that involved acute exposures that were primarily uniform with reliable dose estimates. Nevertheless, all exposures result in

some non-uniformity and uncertainty in the reported doses. Furthermore, due to limitations in available data, some comparisons are made in spite of known issues with the data. In these cases, the conditions must be taken into consideration when comparing with model outputs.

An effort was also made to identify treatment protocols for each case study. While most patients did receive some treatment, our main concern was to identify blood transfusions, stem cell transplants, and cytokine therapy since these procedures can have a significant impact on the observed blood cell kinetics. Again, due to limitations in available data, some comparisons are performed with data from treated subjects or from subjects where treatment information is unknown. The use of antibiotics for infections was not controlled for in the data. These factors may impact blood cell kinetics, and we plan to address this question in future work by analyzing experimental animal data in which other conditions are more tightly controlled.

Individual variability in cell kinetics and radiosensitivity also impacts comparisons of the model to individual data. Parameter values obtained from the literature are often presented as a mean value with an error measurement that provides information on the parameter variance. For example the granulocyte transit time through the mitotic compartment is 6.4 ± 0.3 d (Price et al. 1996). Also, when estimating parameter values through optimization, variance estimates on the optimized parameter values were obtained. However, in the current models, only the mean parameter value is used and information on the error associated with the parameter value is lost. Using a population based modeling approach which performs simulations accounting for these parameter variations may help understand and quantify the variance in output. In the future, we plan to conduct population analyses and Monte Carlo simulations to predict the range and likelihood of model outputs.

7.1 Thrombopoiesis

The thrombopoiesis model accurately captures important dose-dependent trends observed following acute radiation exposure. Figure 7.1a shows the thrombopoiesis model simulations at increasing radiation dose levels, and Figure 7.1b compares simulations to observational data. The purpose of these comparisons is to verify that trends observed in the data are reflected by the model.

At low acute radiation doses, there is a plateau phase prior to a decrease in platelet count. The duration of this phase represents the time needed for megakaryocyte maturation. As the radiation dose increases, megakaryocytes start becoming damaged and the plateau phase is eliminated. The platelet counts reach a nadir between 20 and 30 days following exposure and subsequently begin to recover. This recovery results in an overshoot where platelet levels temporarily rise above normal values. The significant trends observed in the data as the radiation dose increases are:

1. Platelet counts show a more drastic initial decline, and the plateau phase is eliminated.

2. The nadir is lower but occurs roughly around the same time.

The model of thrombopoiesis is able to capture these trends.

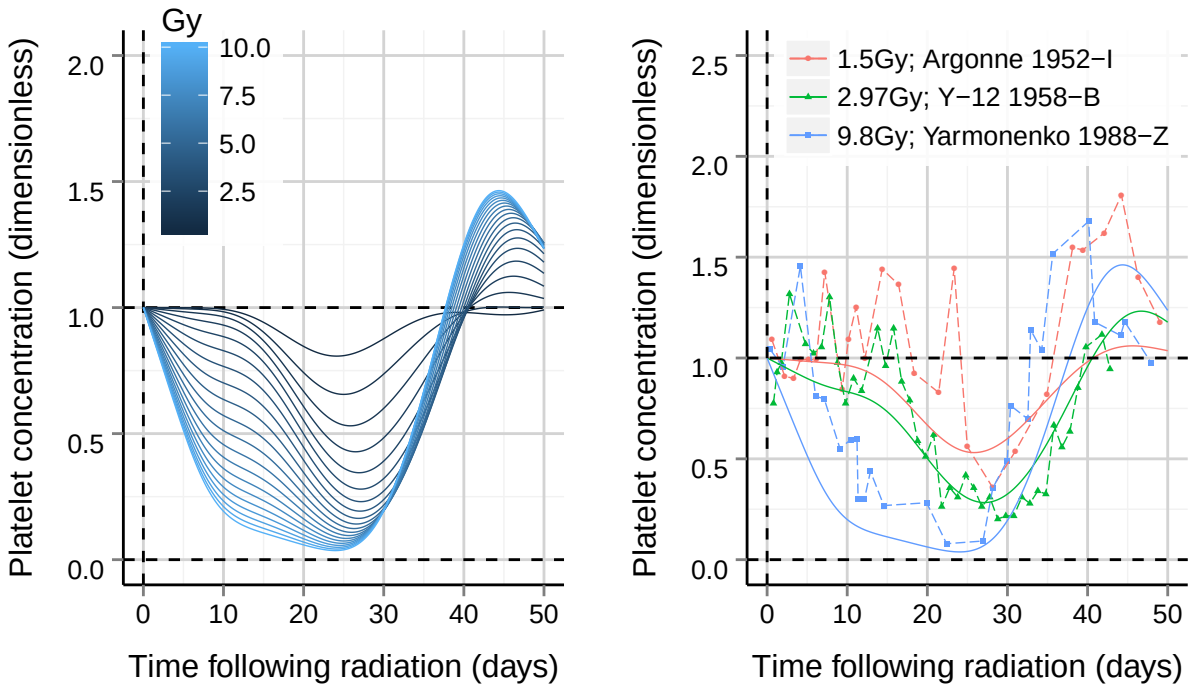

(a) (b)

Figure 7.1: Thrombopoiesis simulations

One challenge encountered in optimization of the thrombopoiesis model was reliably capturing the depth of the nadir. However, although there is a clear correlation between the nadir depth and the radiation dose; in some case study pairs, the depth of the nadir is not lower in the case study with the larger radiation dose. For example, as shown in Figure 7.2a, the minimum normalized platelet count for the 2.6 Gy case study from UT CARL (Goans 2012) was lower than that observed in the 3.51 Sv case study B from the Vinca incident (Jammet et al. 1959; Pešić 2012). This inconsistency could arise from individual variability in the response to radiation or result from uncertainty in the reported dose. Similarly, in the 5.35 Gy case study G from Vinca (Jammet et al. 1959; Pešić 2012), platelet counts decline less than in the Y-12 case A subject (Bond et al. 1965; Mettler et al. 2001; Kerr and Tankersley 2006) who received an estimated 4.02 Gy. A third comparison, shown in Figure 7.2b, shows the Vinca V subject who received an estimated 6.11 Gy dose and Subject Z from Yarmonenko 1988 who received an estimated 9.8 Gy dose. The Vinca V subject has a more drastic decline in platelet counts immediately following radiation exposure when compared with Subject Z; however, we would expect to see a faster decline in subject Z since that subject received a higher dose. Although all these comparisons are performed using the normalized data, the same issues arise when performing the comparisons using the absolute platelet counts. Such discrepancies in the case study data help explain why some of the simulation comparisons vary significantly.

Validation blood cell kinetic data following radiation exposure, presented in Figure 4.4 and Figure B.4, compare favorably with the simulation results. Considerable validity of the

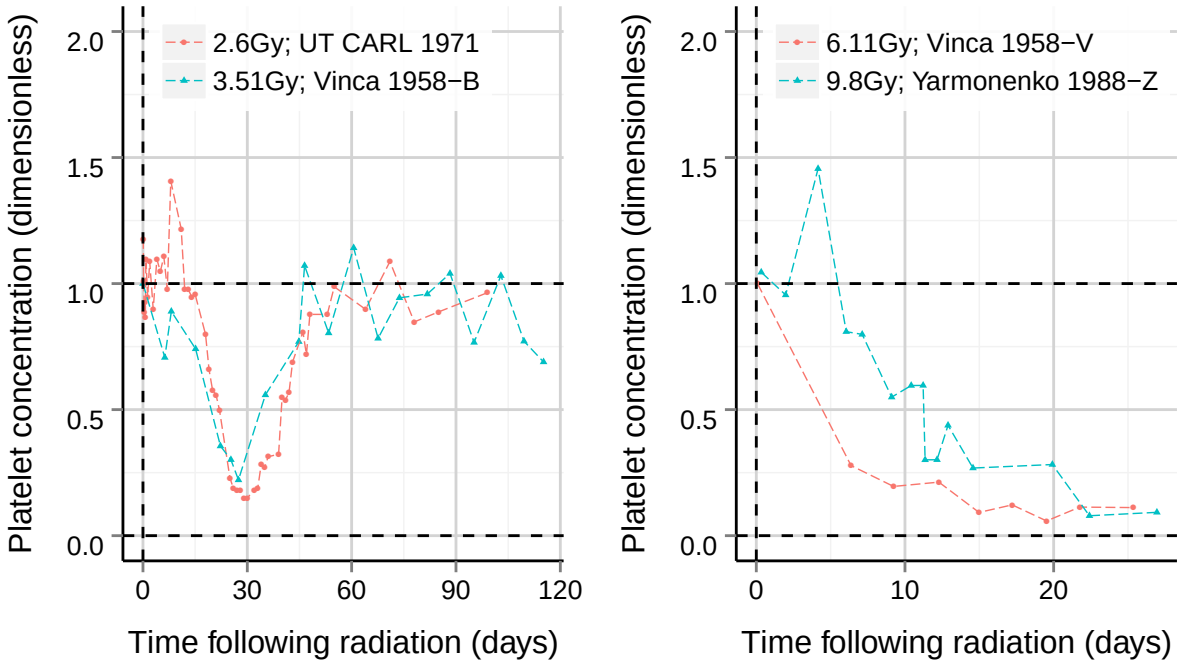

(a) (b)

Figure 7.2: Thrombopoiesis case study comparisons

thrombopoiesis model is also gained through the thrombopheresis data comparisons (Figure 4.5). In four separate studies, two of which had mean data from multiple subjects, the model was able to accurately predict the platelet count recovery following platelet removal. These comparisons reassure us that the kinetic parameters obtained from the literature and through optimization are accurate. Additionally, using model parameters to calculate the relative size of the MK compartment compared to the platelet compartment, as described in Section 4.6.1, led to relative compartment sizes that are in agreement with experimental data (Levine 1980; Valentin 2002; Starr and Taggart 1989).

While large variances are observed in some of the case study data, a general dose response has been established that reliably predicts the trends observed in platelet decline after radiation exposure. Further validation for the structure and parameter values of the model is added through both the thrombopheresis data comparisons and the compartment ratio analysis.

7.2 Granulopoiesis

The granulopoiesis model accurately predicts observed trends in circulating granulocyte count following acute radiation exposure. Figure 7.3a shows the granulopoiesis model simulations at increasing radiation dose levels, and Figure 7.3b compares similar simulations to observational data. The purpose of these comparisons is to verify that trends observed in the data are reflected by the model.

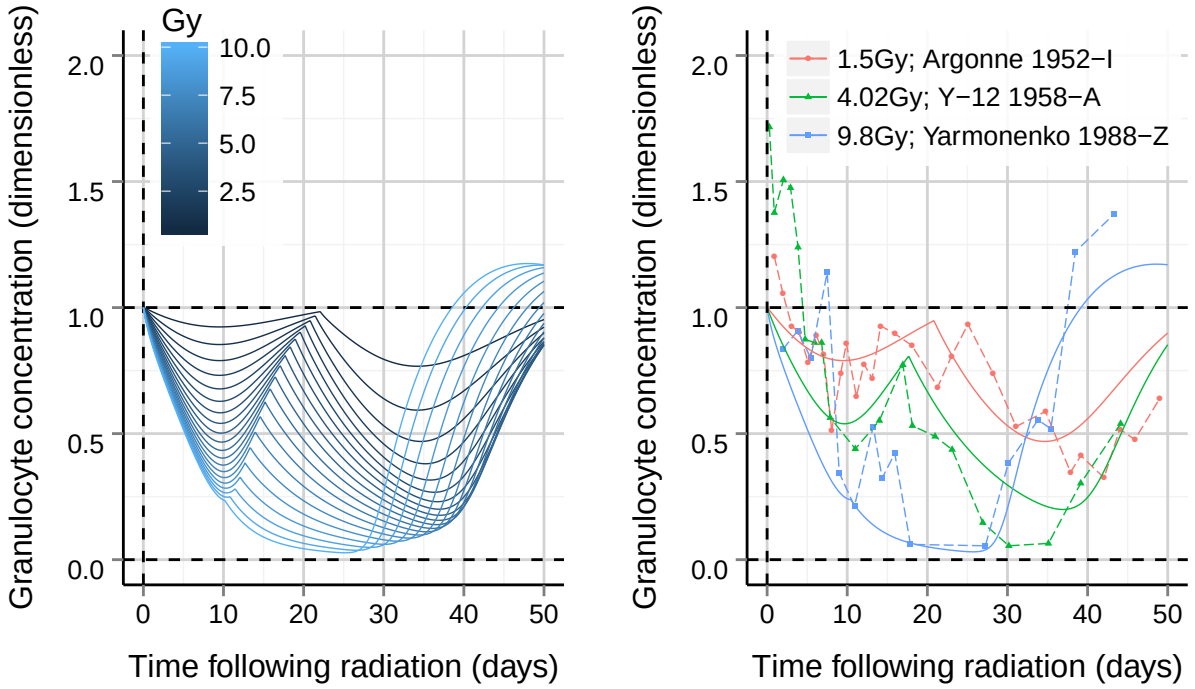

(a) (b)

Figure 7.3: Granulopoiesis simulations

Following radiation exposure there is an initial decrease in granulocyte count until the first nadir is reached. The system then appears to begin recovery; this phenomena is known to be an abortive rise in granulocyte count. At between 12 and 20 days, the granulocyte count decreases again until a second nadir is reached. The significant trends observed as the radiation dose increases are:

1. The time of abortive rise occurs earlier.
2. The nadirs before and after the time of abortive rise are lower.
3. The recovery of the system occurs earlier.

The model of granulopoiesis is able to predict these dose-dependent trends.

As seen in the thrombopoiesis work, in some case studies individual variability or environmental factors clearly impact general trends, making comparisons difficult. For example, the subject in the UT CARL case study (Goans 2012) experienced a lower radiation dose of 2.6 Gy compared with the 3.51 Gy dose received by subject B from the Vinca incident (Jammet et al. 1959; Pešić 2012). Figure 7.4a shows a comparison of the two datasets. As expected the first granulocyte nadir around day 10 is higher in UT CARL subject than in the Vinca B subject. However, for the second nadir, the UT CARL subject has a lower minimum granulocyte concentration compared to the Vinca B subject. If this were a trend observed between other datasets, we would consider revising the model structure. However, because

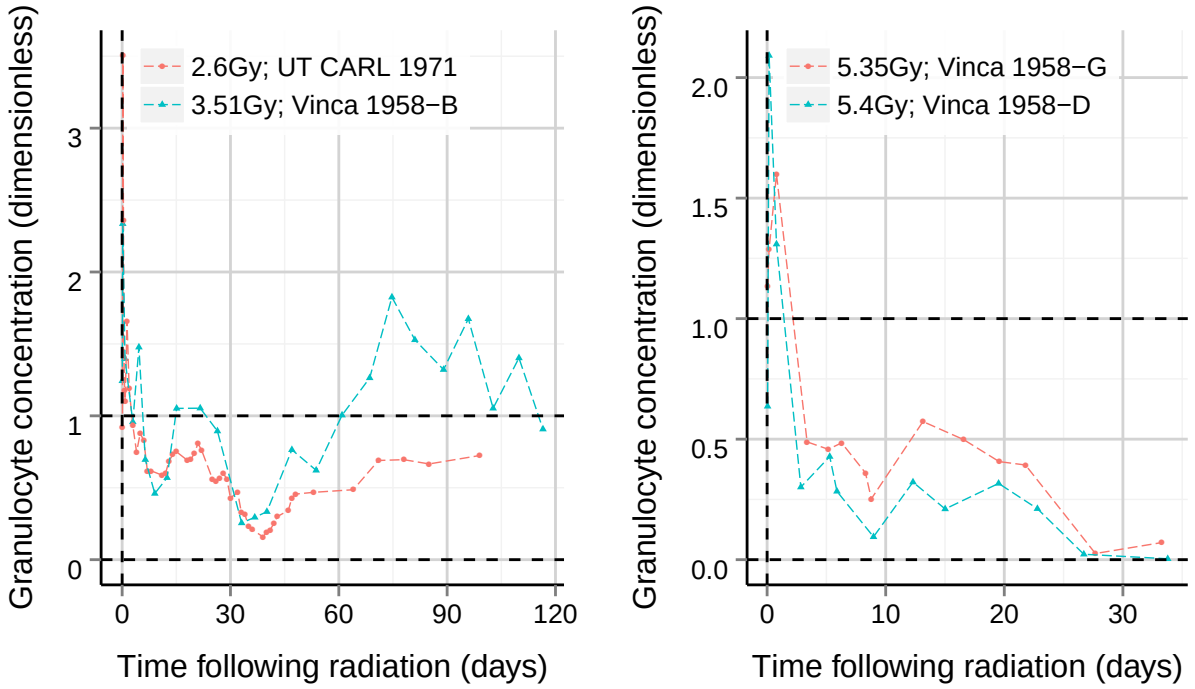

(a) (b)

Figure 7.4: Granulopoiesis case study comparisons

this switch in minimum nadir occurs rarely, we attribute it to the individual variability and treatment environment of the subjects rather than to an error in our model structure.

Figure 7.4b shows a second comparison between subjects G and D from the Vinca. Both subjects received a radiation dose of approximately 5.4 Gy. The granulocyte kinetics of subject G would suggest a lower dose compared with subject D. Since both these subjects have a radiation dose uncertainty of $\pm 15\%$, we attribute the differences in granulocyte kinetics to uncertainty in the dose. However, we can not say for sure that subject D received a higher dose because treatment and individual variations may still play a role.

In many subjects, an early abortive rise in granulocyte counts immediately following radiation is observed. The current model does not predict this early rise which is predicted to result from an immediate release of granulocytes from the marginated pool (granulocytes adhering to the walls of the endothelium) into circulation. The X_3 compartment of the granulopoiesis model includes both circulating and marginated granulocytes, and therefore the model does not depict the early increase in granulocyte count. Because the feedback mechanisms in the model depend on the total number of granulocytes, the release of granulocytes from the marginated pool does not affect these mechanisms. When making comparisons between the model and circulating granulocyte data, we assume that the ratio of marginated to circulating granulocytes remains constant. Although this assumption is not valid immediately following radiation exposure, once the ratio of marginated to circulating granulocytes returns to normal, the current model is still valid. Model adjustments to account for this early change in the marginated to circulating granulocyte ratio can be added if this infor-

mation is needed in the future.

Factors such as treatment, non-uniform exposures, and internal contamination limit the robustness of our validation comparisons for the granulocyte model. Since the granulocyte cell line responds quickly to radiation, assigning accurate baseline values for the case studies is difficult. Therefore, comparisons are presented with simulation outputs initialized at the population mean granulocyte concentration together with the upper and lower bounds of the granulocyte concentration observed in healthy humans.

Validation data presented in Figure 5.3 and Figure B.5 for the most part compare favorably with the simulation results, with a few exceptions. Los Alamos subject 6 appears to have very high granulocyte blood cell counts during the entire duration of the study, suggesting the baseline value used was low for that individual.

7.3 Lymphopoiesis

The lymphopoiesis model accurately captures observed trends in lymphocyte count following acute radiation exposure. Figure 7.5a shows the lymphopoiesis model simulations at increasing radiation dose levels, and Figure 7.5b compares four simulations to observational data. The purpose of these comparisons is to verify that trends observed in the data are reflected by the model.

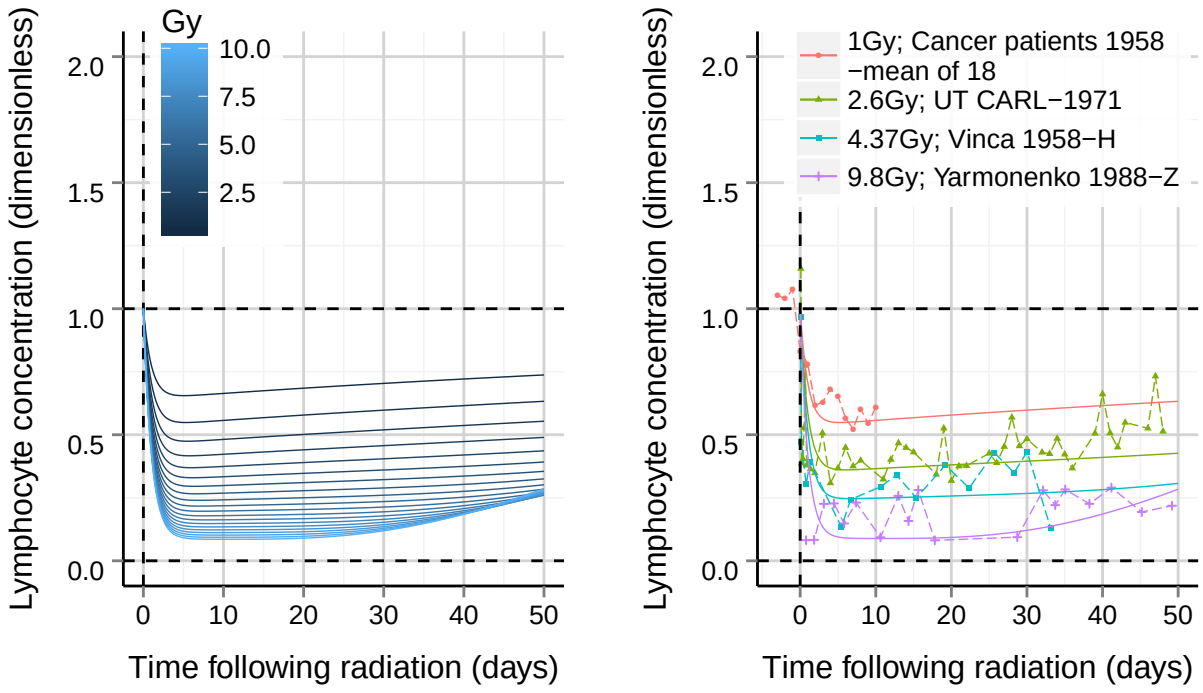

(a) (b)

Figure 7.5: Lymphopoiesis simulations

Radiation leads to a rapid decline in lymphocyte counts followed by a slow recovery. The main dose–dependent trend in the lymphopoiesis model is the rate of decline increases as

the radiation dose becomes greater. Our model of lymphopoiesis is able to accurately depict how the lymphocyte nadir changes as the dose increases and the subsequent recovery.

Once again, discrepancies between case studies and general dose-dependent trends exist; however, these issues are not as prominent as in the platelet and granulocyte cases. An example discrepancy is shown in Figure 7.6. Here, the Argonne I subject who received a 1.5 Gy radiation dose is compared to the Y-12 1958 E subject who received a 2.59 Gy radiation dose. In the 2.59 Gy case study, although the normalized values for the lymphocyte concentration reach a lower value sooner than in the Argonne 1.5 Gy case, at later time points the normalized lymphocyte concentration from the 2.29 Gy case study is either equal to or greater than the lymphocyte concentration from the Argonne 1.5 Gy case. The lymphopoiesis model output matches the Argonne 1.5 Gy study better than the Y-12 E study, suggesting the issue is due to dose uncertainty or individual variability in the Y-12 E study.

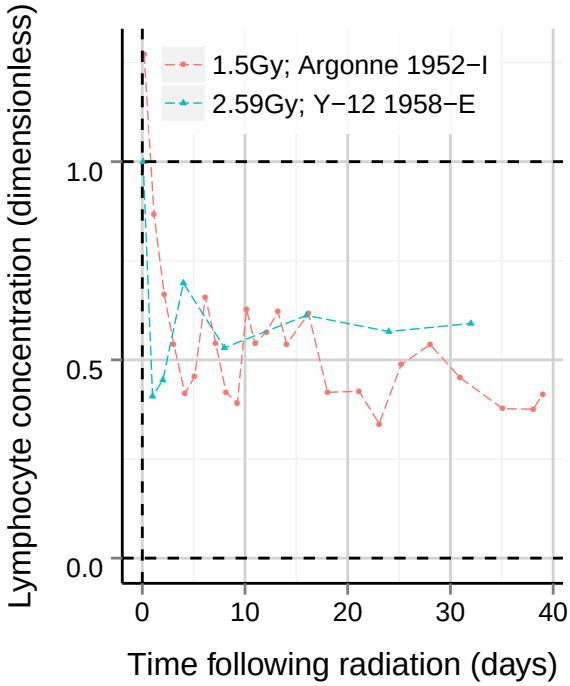

Figure 7.6: Lymphopoiesis case study comparisons

Validation data presented in Figure 6.3 and Figure B.6 compare favorably with the simulation results, with a few exceptions. At the higher doses, the lymphocyte count appears to drop faster than the model predicts (Case Study: Tokai-mura 1999–B, Shanghai–S, and Tokai-mura 1999–A). If this early response needs to be captured, future work would involve including the rate of damaged cell death in the optimization procedure.

7.4 Comparison with Expert Predictions

METREPOL (Medical Treatment Protocols for Radiation Accident Victims as a Basis for a Computerised Guidance System) provides an assessment of radiation injury severity based upon the hematopoietic response (Fliedner, Friesecke, et al. 2001). This severity ranking

system was developed by an international group of selected experts and is based on both experimental data and the analysis of data from radiation victims. There are four possible severity grades (H1: Mild damage; H2: Moderate damage; H3: Severe damage; H4: Fatal damage) which are not based on radiation dose but on the ensuing symptoms.

To verify that our hematopoietic models are in agreement with the predicted hematopoietic responses from METREPOL and to correlate these responses with a dose, we developed overlays of our model on the METREPOL predictions for the H2 and H3 severity levels (Figure 7.7). For an accurate comparison, our hematopoietic model outputs are shown for the normal range of blood cell counts as given in the METREPOL report (Fliedner, Friesecke, et al. 2001). Interestingly, for the same severity ranking the hematopoietic models were initialized at different acute radiation doses to compare to H2 and H3 METREPOL predictions. Since hematopoietic cell lines respond differently to radiation, the H1-H4 severity levels listed in METREPOL may correspond to different doses for the same severity level. For example, to match the predicted H2 response, the lymphopoiesis model was run with a radiation dose of 3 Gy while the granulopoiesis model was run at 7 Gy.

In general, the model predictions match the trends given by METREPOL. The platelet recovery predicted by our model is slightly faster and leads to an overshoot not predicted in the METREPOL hematopoietic response; however, this overshoot is observed in several of the individual case studies examined in this report. As examples see case studies Argonne 1952-I, Y-12 1958-A, and Yarmonenko 1988-Z shown in Figure 4.3. The granulopoiesis model has an abortive rise at a similar time as the METREPOL predictions, however at higher severity our granulopoiesis model predicts an earlier recovery due to the shortened time of abortive rise. METREPOL predicts a later granulocyte recovery at higher doses. Based on the dose-response data shown in Figure 7.3b, an early recovery of granulocytes at higher doses is not unfeasible.

In a second set of expert predictions, Annex G of the UNSCEAR 1988 report presents a schematic picture of the average time course of blood cell counts deduced from accidental human exposures (UNSCEAR 1988). Figure 7.8 shows a comparison of our hematopoietic models' outputs with this expert prediction. The UNSCEAR report presents the predicted blood cell responses at doses ranging from 0 to 20 Gy divided into four groups. Therefore, we plot our hematopoietic model outputs as a shaded region based on each dose range and overlay the predicted UNSCEAR response. Although the models are not in exact agreement with the UNSCEAR predictions, the general trends are supported and the dose response matches fairly well.

7.5 Treatment Effects

The purpose of our models is to show hematopoietic dynamics following untreated radiation exposure; however, in many case studies treatments were administered following acute radiation exposure. Comparing treated case studies to the model prediction provides hypotheses for how treatments affect the hematopoietic response. Here, we discuss one case study from Soreq 1990 (IAEA 1993; Mettler 2001) while other case study examples involving treatment are presented in Appendix B.2. The subject from Soreq received a whole-body exposure of 15 ± 5 Gy. He was treated with G-CSF one day following exposure, and platelet transfusions were given when the platelet count was less than $20 \cdot 10^3 \mu L^{-1}$. Platelet counts first

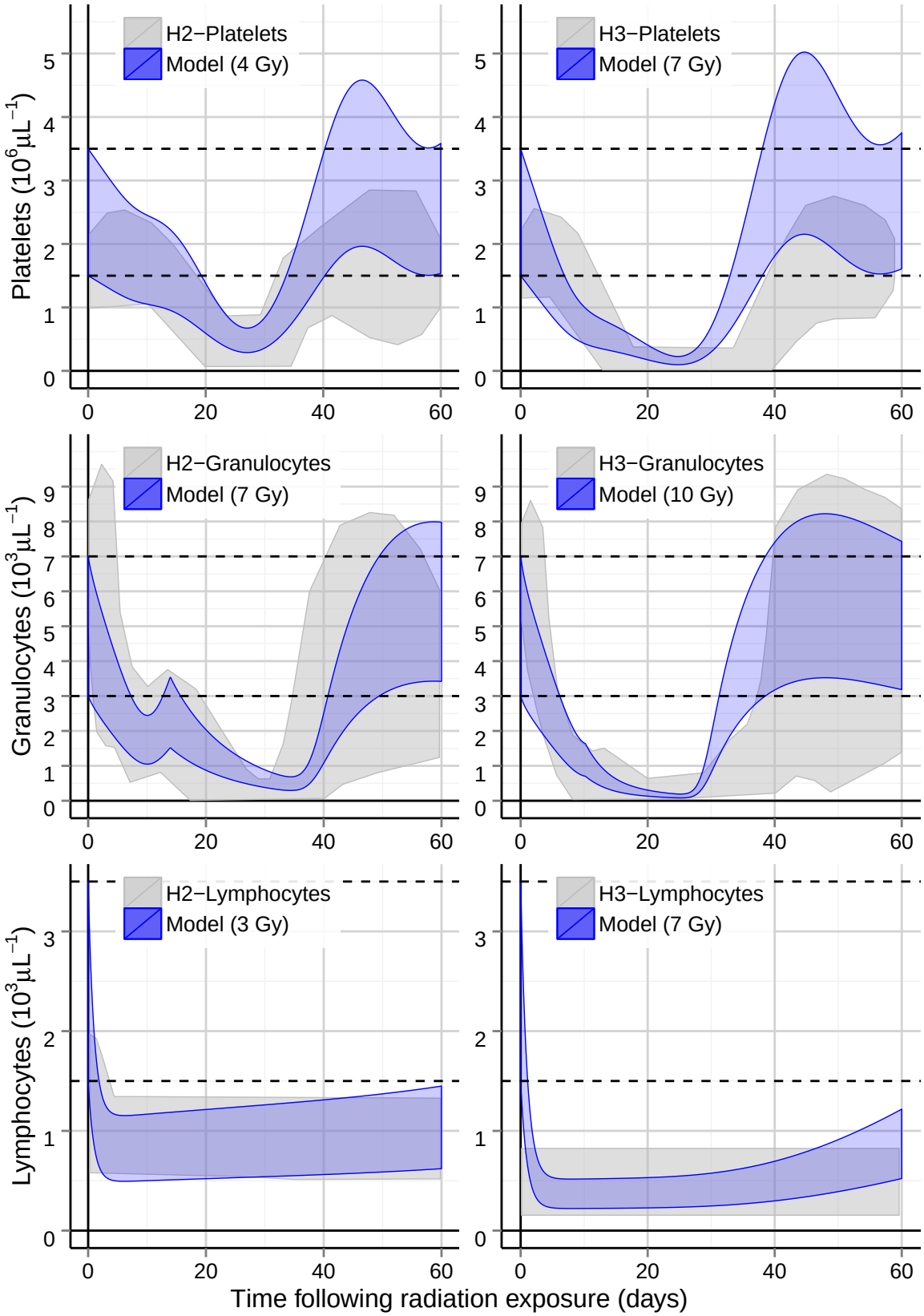

Figure 7.7: Comparison of hematopoietic model outputs to METREPOL

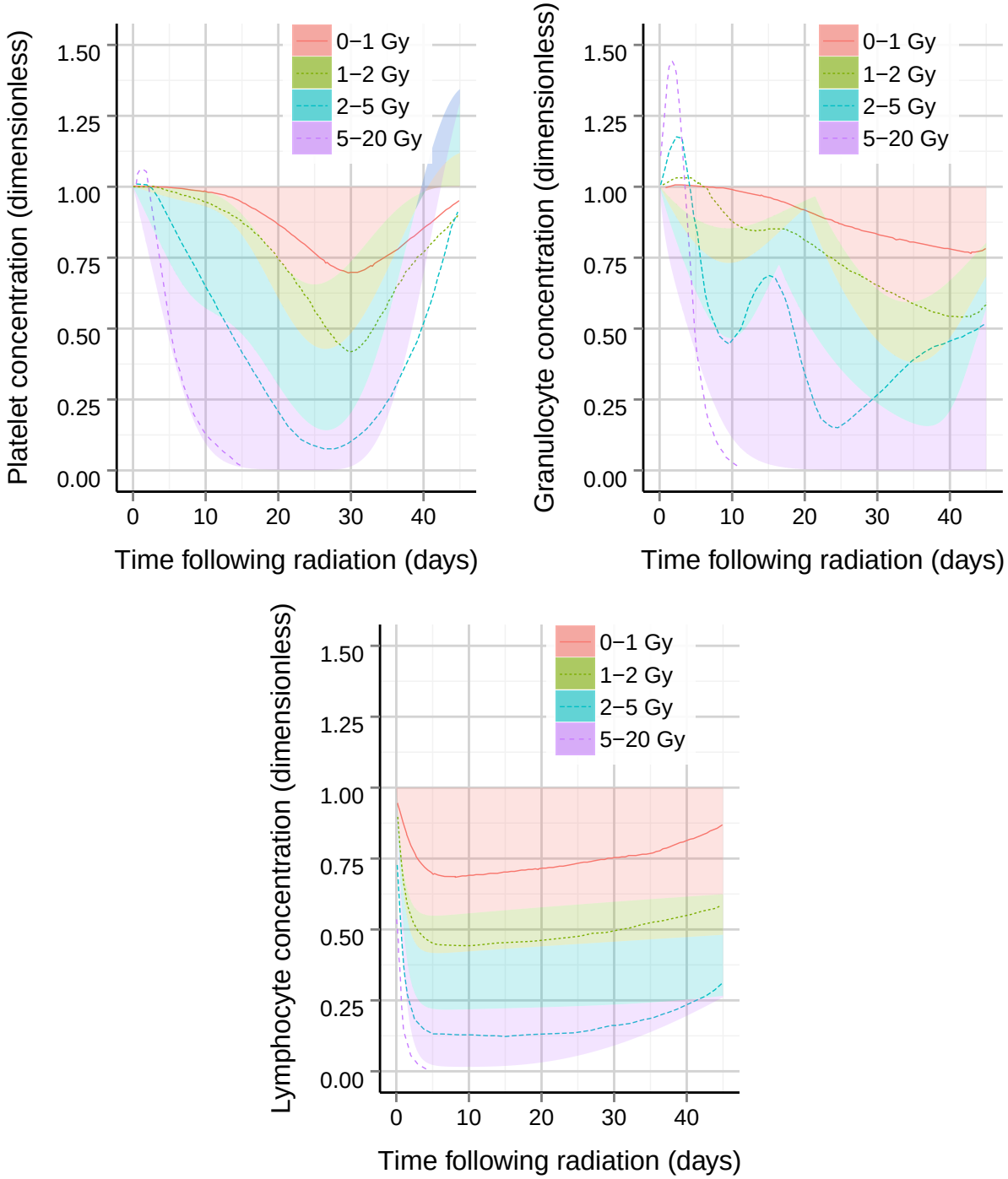

Figure 7.8: Comparison of hematopoietic model outputs (shaded regions for each dose range) with expert opinions on blood cell dynamics following radiation exposure (solid and dashed lines; UNSCEAR 1988)

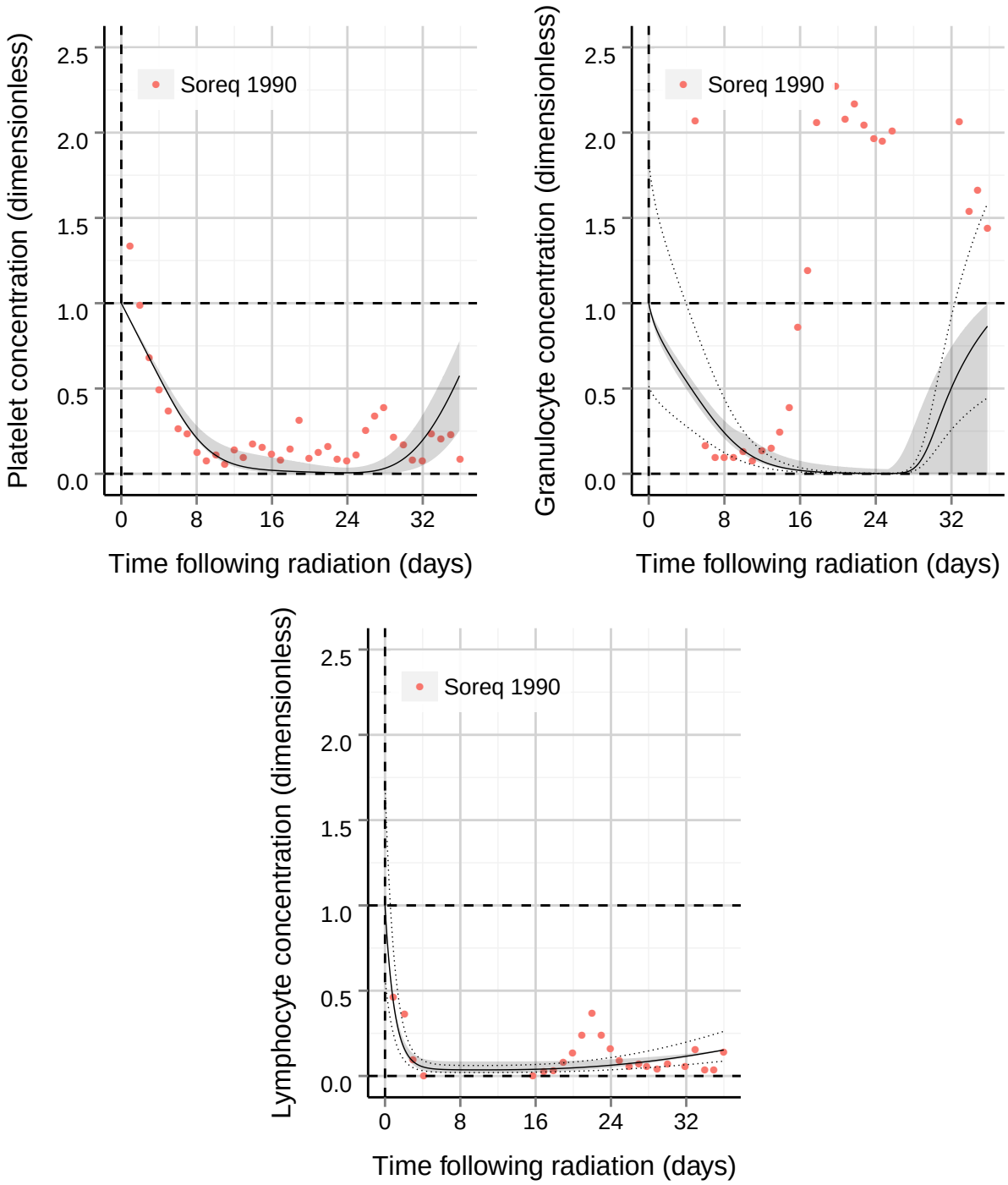

Figure 7.9: Hematopoietic dynamics following 15 Gy (10-20 Gy) and treatment. Model output at the specified dose (range) is delineated by a black line (shaded region). If a generic baseline value was used, output initialized at the upper and lower end of the healthy blood cell range is shown by dotted lines.

decreased below this point on the 9th day following radiation exposure. Figure 7.9 shows the kinetic blood cell count data from the Soreq subject. The granulocyte data suggests that G-CSF treatment causes a rapid recovery of the granulocytes, much faster than what the model predicts. The peripheral platelet and lymphocyte concentrations show temporary rises, which might be due to treatment as well. However, it would take more data collection and analysis to verify this.

7.6 Partial Body Effects

Several case studies were obtained where very non-uniform or partial body exposures occurred. These include Los Alamos 1945 subjects 1 and 3 (Hempelmann et al. 1952; Hempelmann 1961; Hoffman and Hempelmann 1957; Mettler et al. 2001) and subject K from Yarmonenko 1988. Here we present one case study, Los Alamos subject 1, who received an acute localized radiation exposure. Other case study examples involving non-uniform exposures are presented in Appendix B.2. For Los Alamos subject 1, the radiation dose was estimated as 12.75 Sv with a range from 5.5–20 Sv. Figure 7.10 shows a comparison between the data and model output for all three cell lines. In each case, the blood cell kinetics appear to be less severe than what the models predict. We would expect this since in partial body exposure some of the bone marrow is spared. HSCs in the spared bone marrow can continue to divide, contribute to recovery, and help alleviate the hematopoietic radiation effects.

7.7 Current and Future Effort

While the hematopoietic models for radiation alone provide useful insight into the clinical course of blood cell kinetics, mechanistic models also provide a way to evaluate the impact of additional insults on hematopoiesis. Therefore, model parameters for the impact of burn on hematopoiesis are also under development. The parameters will be integrated with radiation models to simulate the effects of combined radiation and burn injury in humans. These models will help to predict the synergistic effects of combined injury. The model outputs will also be used to facilitate predictions of time to and likelihood of mortality. This will be done by developing correlations between model outputs with mortality. Potential outputs worth examining include the time of the nadir and the duration in which blood cell counts are below specific threshold levels.

The hematopoietic models for radiation effects could also be used in the future to explore the overall systemic impact of partial body exposures and the potential decreased mortality risk afforded by partial shielding of progenitor (or stem) cells. In particular, these mechanistic models can help sort out the impact of global mediator response on blood cell kinetics and the associated ability of the hematopoietic system to recover after inhomogeneous radiation injury. The wealth of knowledge gleaned from more highly controlled animal experiments will be useful in establishing firm parameters for a partial body effects model, and partial body human exposures can provide data for optimization and validation of such models.

The effect of treatment on hematopoietic responses after radiation exposure is also an area where computational approaches may be useful. In separate work, we have integrated the effect of the cytokine IL-12 on hematopoietic kinetics on these models based on key changes observed in clinical data of patients that received IL-12 under normal circumstances (i.e.

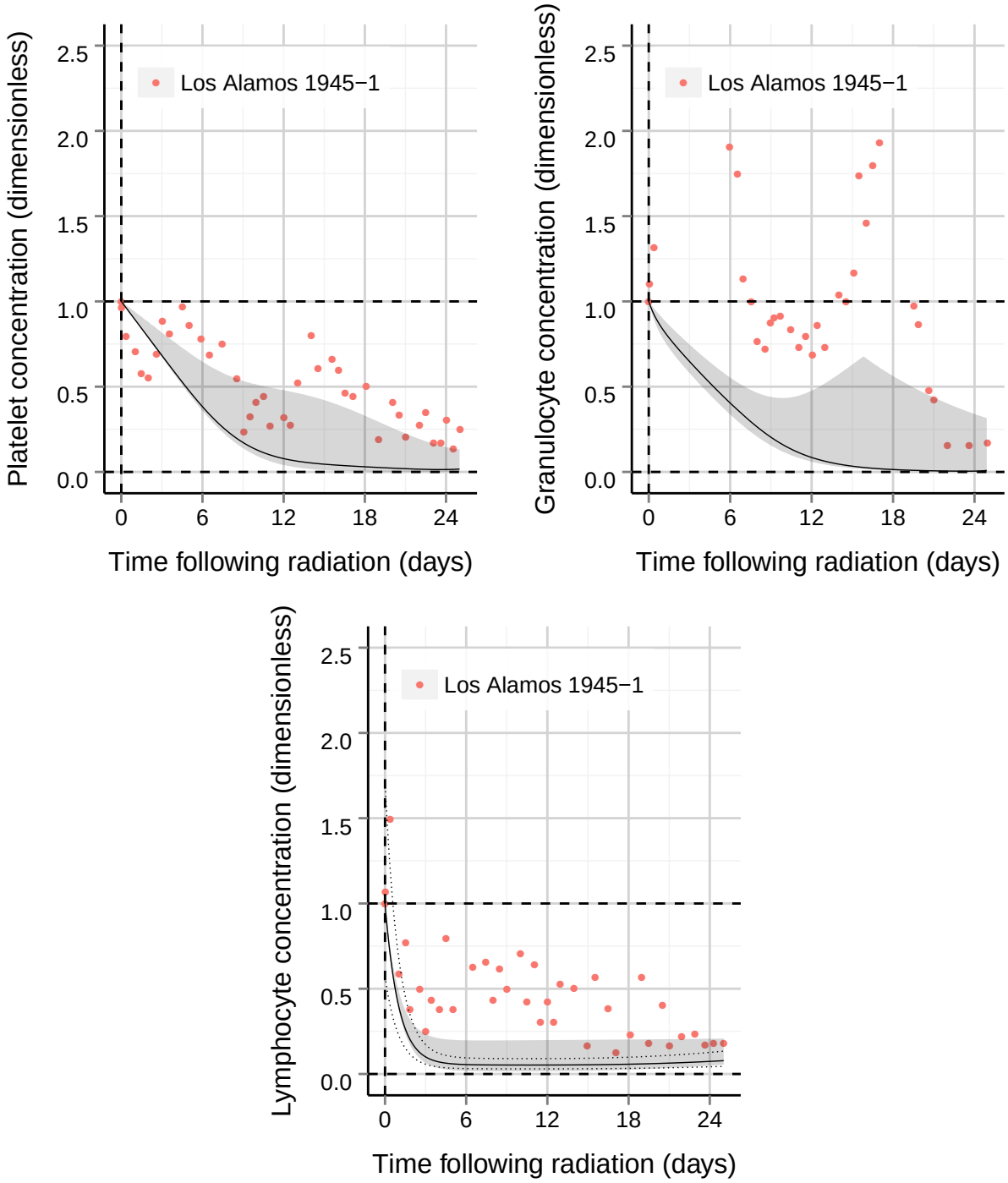

Figure 7.10: Hematopoietic dynamics following partial body exposure of 12.75 Sv (5.5-20 Sv). Model output at the specified dose (range) is delineated by a black line (shaded region). If a generic baseline value was used, output initialized at the upper and lower end of the healthy blood cell range is shown by dotted lines.

without radiation). Since G-CSF is currently the only Food and Drug Administration (FDA) approved therapeutic for the hematopoietic syndrome associated with radiation exposure, integration of its effect would be a logical next step in our modeling. A significant amount of data on G-CSF is available, including case studies of its use with highly irradiated persons, that would greatly facilitate parameterization of the treatment model. Treatment models can aid in scenario analyses involving large numbers of casualties and limited resources.

Finally, another important aspect to include in future modeling is population variability. In our current work, we have included the ability to adjust baseline blood cell counts so that the effects of radiation exposure in subpopulations with known variances in baseline cell counts can be examined. However, a more thorough population modeling approach could be taken to understand the population variances in other parameters that range from average blood volumes to cell turnover and regeneration rates. Integrating known parameters for vulnerable subpopulations such as young children and elderly would be particularly useful. This type of approach enables model users to understand the expected variability among a large, diverse population and obtain a more realistic picture of the health effects expected after a large scale nuclear or radiological incident.

This page intentionally left blank.

8 Conclusion

Hematopoietic models describing the effects of radiation on thrombopoiesis, granulopoiesis, and lymphopoiesis have been developed to better understand the clinical time course of blood cells after acute radiation exposure. The models have been optimized and validated against blood cell kinetic data from human radiation accidents and accurately illustrate the average observed trends in hematopoietic dynamics after acute radiation exposure. The models not only provide valuable information on the expected clinical course after radiation exposure, but, by integrating parameter changes for additional insults such as thermal injury, they also provide a mechanism for understanding the impact of combined injuries. By relating key clinical metrics obtained from the models, such as duration of neutropenia, the models may also assist in predicting the probability and time to mortality from combined injuries, facets for which little to no data currently exists. Future work will further increase the utility of these models by integrating treatment and population variability to support the application of these models in emergency preparedness scenario analyses and medical resource planning.

This page intentionally left blank.

9 References

Akushevich, I. V., Veremeyeva, G. A., Dimov, G. P., Ukraintseva, S. V., Arbeev, K. G., Akleyev, A. V., and Yashin, A. I., 2011. "Modeling hematopoietic system response caused by chronic exposure to ionizing radiation." *Radiation and Environmental Biophysics*, 50(2), 299–311.

Andreeff, M., Goodrich, D. W., and Pardee, A. B., 2000. "Cell proliferation, differentiation, and apoptosis," *Holland-Frei Cancer Medicine, 5th edition*. Ed. by R. C. Bast, D. W. Kufe, R. E. Pollock, R. R. Weichselbaum, J. F. Holland, and E. Frei. BC Decker, Ontario, Canada.

Andrews, G. A., Sitterson, B. W., Kretchmar, A. L., and Brucer, M., 1961. "Criticality accident at the Y-12 plant," *Diagnosis and Treatment of Acute Radiation Injury*, 27–48.

Auxier, J. A., 1961. "Dosimetric consideration in criticality accidents," *Diagnosis and Treatment of Acute Radiation Injury: Proceedings of a Scientific Meeting Jointly Sponsored by the IAEA and the WHO, Geneva, 17-21 Oct 1960*. Columbia University Press, New York, 27–48.

Baranov, A. E., 1981. "Assessment of doses and prediction of the dynamics of neutrophyl number in blood by making use of hematological data for gamma-irradiation of humans," *Meditsinskaia Radiologiia*, 26, 11–61.

Baranov, A. E., Selidovkin, G. D., Butturini, A., and Gale, R. P., 1994. "Hematopoietic recovery after 10-Gy acute total body radiation," *Blood*, 83(2), 596–599.

Bond, V. P., Fliedner, T. M., and Archambeau, J. O., 1965. *Mammalian radiation lethality: A disturbance in cellular kinetics*. Academic Press, New York, 78–83.

Broudy, V. C., Lin, N. L., Sabath, D. F., Papayannopoulou, T., and Kaushansky, K., 1997. "Human platelets display high-affinity receptors for thrombopoietin," *Blood*, 89(6), 1896–1904.

Brun, R., Reichert, P., and Kunsch, H. R., 2001. "Practical identifiability analysis of large environmental simulation models," *Water Resources Research*, 37(4), 1015–1030.

Cohn, S. H., and Milne, W. L., 1956. *The effects of combined administration of strontium-90 and external radiation*. USNRDL-TR-89, Naval Radiological Defense Lab., San Francisco.

Dancey, J. T., Deubelbeiss, K. A., Harker, L. A., and Finch, C. A., 1976. "Neutrophil kinetics in man," *Journal of Clinical Investigation*, 58(3), 705–715.

Dealy, J. B., and Tubiana, M., 1964. "Hematological responses to inhomogenous and homogenous whole-body irradiation," *Annals of the New York Academy of Sciences*, 114(1), 268–283.

Deutsch, V. R., and Tomer, A., 2013. "Advances in megakaryocytopoiesis and thrombopoiesis: From bench to bedside," *British Journal of Haematology*, 161(6), 778–793.

Dowling, M. R., Josefsson, E. C., Henley, K. J., Hodgkin, P. D., and Kile, B. T., 2010. "Platelet senescence is regulated by an internal timer, not damage inflicted by hits," *Blood*, 116(10), 1776–1778.

Ebbe, S., Stohlman, F., Donovan, J., and Overcash, J., 1968. "Megakaryocyte maturation rate in thrombocytopenic rats," *Blood*, 32(5), 787–795.

Finch, C. A., Harker, L. A., and Cook, J. D., 1977. "Kinetics of the formed elements of human blood," *Blood*, 50(4), 699–707.

Fliedner, T. M., Friesecke, I., and Beyrer, K., eds. 2001. *Medical management of radiation accidents: Manual on the acute radiation syndrome*. British Institute of Radiology.

Fliedner, T. M., Gräßle, D. H., Meineke, V., and Dörr, H., 2007. "Pathophysiological principles underlying the blood cell concentration responses used to assess the severity of effect after accidental whole-body radiation exposure: an essential basis for an evidence-based clinical triage." *Experimental Hematology*, 35(4), 8–16.

Goans, R. E., 2012. *Radiation exposure, illness, and injury*.

Gräßle, D. H., 2000. *Simulation of radiation effects using biomathematical models of the megakaryocytic cell renewal system*. Universität Ulm, Medizinische Fakultät.

Gusev, I., Guskova, A., and Mettler, F. A., eds. 2010. *Medical management of radiation accidents*. CRC Press.

Guskova, A. K., Barabanova, A. V., Baranov, A. Y., Gruszdev, G. P., Pyatkin, Y. K., Nadezhina, N. M., Metlyaeva, N. A., Selidovkin, G. D., Moiseev, A. A., Gusef, I. A., Dorofeeva, E. M., and Zykova, I. E., 1988. *UNSCEAR 1988 Report: Acute radiation effects in victims of the Chernobyl accident: Appendix to Annex: Early effects in man of high radiation doses*. United Nations Scientific Committee on the Effects of Atomic Radiation, New York.

Haario, H., Saksman, E., and Tamminen, J., 2001. "An adaptive Metropolis algorithm," *Bernoulli*, 7(2), 223–242.

Heath, M., 1997. *Scientific Computing: An Introductory Survey*. McGraw–Hill, Boston.

Hellerstein, M., Hanley, M. B., Cesar, D., Siler, S., Papageorgopoulos, C., Wieder, E., Schmidt, D., Hoh, R., Neese, R., Macallan, D., Deeks, S., and McCune, J. M., 1999. "Directly measured kinetics of circulating T lymphocytes in normal and HIV-1-infected humans," *Nature Medicine*, 5(1), 83–89.

Hempelmann, L. H., 1961. "The assessment of acute radiation injury," *Diagnosis and Treatment of Acute Radiation Injury: Proceedings of a Scientific Meeting Jointly Sponsored by the IAEA and the WHO, Geneva, 17-21 Oct 1960*. Columbia University Press, New York, 49–65.

Hempelmann, L. H., Lisco, H., and Hoffman, J. G., 1952. "The acute radiation syndrome: A study of nine cases and a review of the problem," *Annals of Internal Medicine*, 36(2), 279–510.

Hirama, T., Tanosaki, S., Kandatsu, S., Kuroiwa, N., Kamada, T., Tsuji, H., Yamada, S., Katoh, H., Yamamoto, N., Tsujii, H., Suzuki, G., and Akashi, M., 2003. "Initial medical management of patients severely irradiated in the Tokai-mura criticality accident," *British Journal of Radiology*, 76(904), 246–253.

Hoffman, J. G., and Hempelmann, L. H., 1957. "Estimation of whole-body radiation doses in accidental fission bursts," *American Journal of Roentgenology, Radium Therapy and Nuclear Medicine*, 77(1), 144–160.

Howland, J. W., Ingram, M., Mermagen, H., and Hansen, C. L., 1961. "The Lockport incident: Accidental partial body exposure of humans to large doses of X-irradiation," *Diagnosis and Treatment of Acute Radiation Injury: Proceedings of a Scientific Meeting Jointly Sponsored by the IAEA and the WHO, Geneva, 17-21 Oct 1960*. Columbia University Press, New York, 11–26.

Hu, S., and Cucinotta, F. A., 2011. "Characterization of the radiation-damaged precursor cells in bone marrow based on modeling of the peripheral blood granulocytes response." *Health Physics*, 101(1), 67–78.

Hu, S., Smirnova, O. A., and Cucinotta, F. A., 2012. "A biomathematical model of lymphopoiesis following severe radiation accidents–potential use for dose assessment," *Health Physics*, 102(4), 425–436.

Hurst, G. S., and Ritchie, R. H., 1959. *Radiation accidents: Dosimetric aspects of neutron and gamma-ray exposures*. No. ORNL-2748 (Pt. A), Oak Ridge National Lab., Tennessee.

Hurst, G. S., Ritchie, R. H., and Emerson, L. C., 1959. "Accidental radiation excursion at the Oak Ridge Y-12 plant-III: Determination of radiation doses," *Health Physics*, 2(2), 121–133.

Hurst, G. S., Ritchie, R. H., Sanders, F. W., Reinhardt, P. W., Auxier, J. A., Wagner, E. B., Callihan, A. D., and Morgan, K. Z., 1961. "Dosimetric investigation of the Yugoslav radiation accident," *Health Physics*, 5(2), 179–202.

IAEA, 1993. *The radiological accident in Soreq*. STI/PUB/925, International Atomic Energy Agency, Vienna, 1–72.

Jammet, H. P., 1961. "Treatment of victims at the zero-energy reactor accident in Vinca," *Diagnosis and Treatment of Acute Radiation Injury: Proceedings of a Scientific Meeting Jointly Sponsored by the IAEA and the WHO, Geneva, 17-21 Oct 1960*. Columbia University Press, New York, 83–103.

Jammet, H. P., Mathe, G., Pendić, B., Duplan, J. F., Maupin, B., Latarjet, R., Kalic, D., Schwarzenberg, L., Djukic, Z., and Vigne, J., 1959. "Study of six cases of accidental acute total irradiation," *Revue Française d'Études Cliniques et Biologiques*, 4(3), 210–225.

Joiner, M. C., 2009. "Quantifying cell kill and cell survival," *Basic Clinical Radiobiology Fourth Edition*. Ed. by M. C. Joiner and A. van der Kogel. CRC Press, 42–55.

Kashiwakura, I., Kuwabara, M., Inanami, O., Murakami, M., Hayase, Y., Takahashi, T. A., and Takagi, Y., 2000. "Radiation sensitivity of megakaryocyte colony-forming cells in human placental and umbilical cord blood," *Radiation Research*, 153(2), 144–152.

Kaushansky, K., 2005. "The molecular mechanisms that control thrombopoiesis," *Journal of Clinical Investigation*, 115(12), 3339–3347.

Kerr, G. D., and Tankersley, W. G., 2006. *External radiation dose estimates for individuals near the 1958 criticality accident at the Oak Ridge Y-12 plant*. ORAUT-OTIB-0057, Oak Ridge Associated Universities, Oak Ridge, TN.

Kuwaki, T., Hagiwara, T., Yuki, C., Kodama, I., Kato, T., and Miyazaki, H., 1998. "Quantitative analysis of thrombopoietin receptors on human megakaryocytes," *FEBS letters*, 427(1), 46–50.

Kwan, D. K., and Norman, A., 1977. "Radiosensitivity of human lymphocytes and thymocytes," *Radiation Research*, 69(1), 143–151.

Laine, M., 2008. *Adaptive MCMC methods with applications in environmental and geophysical models*. Finish Meteorological Institute.

Lasky, L. C., Lin, A., Kahn, R. A., and McCullough, J., 1981. "Donor platelet response and product quality assurance in plateletpheresis." *Transfusion*, 21(3), 247–260.

Levine, R. F., 1980. "Isolation and characterization of normal human megakaryocytes," *British Journal of Haematology*, 45(3), 487–97.

Macallan, D. C., Wallace, D. L., Zhang, Y., Ghattas, H., Asquith, B., de Lara, C., Worth, A., Panayiotakopoulos, G., Griffin, G. E., Tough, D. F., and Beverley, P. C. L., 2005. "B-cell kinetics in humans: Rapid turnover of peripheral blood memory cells," *Blood*, 105(9), 3633–3640.

Mathe, G., Amiel, J. L., and Schwarzenberg, L., 1964. "Treatment of acute total-body irradiation injury in man," *Annals of the New York Academy of Sciences*, 114(1), 368–392.

Matheson, L. N., Dore, M. A., Anno, G. H., and McClellan, G. E., 1998. *User's Manual: Radiation-Induced Performance Decrement (RIPD), Version 2.0*. DNA-TR-95-91, Pacific-Sierra Research Corp., Santa Monica, CA.

Mettler, F. A., 2001. "Accidents in industrial radiation facilities," *Medical Management of Radiation Accidents*. Ed. by I. A. Gusev, A. K. Guskova, and F. A. Mettler. 2nd ed. CRC Press, Boca Raton, 211–222.

Mettler, F. A., Voelz, B. L., Nénot, J. C., and Gusev, I. A., 2001. "Criticality accidents," *Medical Management of Radiation Accidents*. Ed. by I. A. Gusev, A. K. Guskova, and F. A. Mettler. 2nd ed. CRC Press, Boca Raton, 173–194.

Mezzano, D., Hwang, K., and Aster, R. H., 1982. "Characteristics of total platelet populations and of platelets isolated in platelet-rich plasma," *Transfusion*, 22(3), 197–202.

Miller, L. S., Fletcher, G. H., and Gerstner, H. B., 1958. "Radiobiologic observations on cancer patients treated with whole-body x-irradiation," *Radiation Research*, 8(2), 150–165.

Mole, R. H., 1984. "Sodium in man and the assessment of radiation dose after criticality accidents," *Physics in Medicine and Biology*, 29(11), 1307–1327.

Moré, J. J., 1978. "The Levenberg-Marquardt algorithm: Implementation and theory," *Numerical Analysis*. Springer Berlin Heidelberg, 105–116.

Murphy, E. A., and Francis, M. E., 1971. "The estimation of blood platelet survival. II. The multiple hit model," *Thrombosis et Diathesis Haemorrhagica*, 25(1), 53–80.

Pendić, B., 1961. "The zero-energy reactor accident at Vinca," *Diagnosis and Treatment of Acute Radiation Injury: Proceedings of a Scientific Meeting Jointly Sponsored by the IAEA and the WHO, Geneva, 17-21 Oct 1960*. Columbia University Press, New York, 67–81.

Pešić, M., 2012. "Estimation of doses received by operators in the 1958 RB reactor accident using the MCNP5 computer code simulation," *Nuclear Technology and Radiation Protection*, 27(3), 199–221.

Price, T. H., Chatta, G. S., and Dale, D. C., 1996. "Effect of recombinant granulocyte colony-stimulating factor on neutrophil kinetics in normal young and elderly humans," *Blood*, 88(1), 335–340.

R Core Team, 2013. *R: A language and environment for statistical computing*. R Foundation for Statistical Computing. Vienna, Austria.

Schmitt, A., Guichard, J., Massé, J. M., Debili, N., and Cramer, E. M., 2001. "Of mice and men: Comparison of the ultrastructure of megakaryocytes and platelets," *Experimental Hematology*, 29(11), 1295–1302.

Scholz, M., Gross, A., and Loeffler, M., 2010. "A biomathematical model of human thrombopoiesis under chemotherapy." *Journal of Theoretical Biology*, 264(2), 287–300.

Shinjo, K., Takeshita, A., Ohnishi, K., and Ohno, R., 1995. "Expression of granulocyte colony-stimulating factor receptor increases with differentiation in myeloid cells by a newly-devised quantitative flow-cytometric assay," *British Journal of Haematology*, 91(4), 783–794.

Smirnova, O. A., 2011. *Environmental radiation effects on mammals*. Springer.

Smirnova, O. A., 2012. "Comparative analysis of the dynamics of thrombocytopoietic, granulocytopoietic, and erythropoietic systems in irradiated humans: a modeling approach." *Health Physics*, 103(6), 787–801.

Soetaert, K., and Petzoldt, T., 2010. "Inverse modelling, sensitivity and Monte Carlo analysis in R using package FME," *Journal of Statistical Software*, 33(3), 1–28.

Soetaert, K., Petzoldt, T., and Setzer, R. W., 2010. "Solving differential equations in R: Package deSolve," *Journal of Statistical Software*, 33(9), 1–25.

Starr, C., and Taggart, R., 1989. *Biology: the Unity and Diversity of Life*. 5th ed. Wadsworth, California, 398.

Stavem, P., Brøgger, A., Devik, F., Flatby, J., van der Hagen, C. B., Henriksen, T., Hoel, P. S., Høst, H., Kett, K., and Petersen, B., 1985. "Lethal acute gamma radiation accident at Kjeller, Norway: Report of a case," *Acta Oncologica*, 24(1), 61–63.

Sullivan, L. W., Adams, W. H., and Liu, Y. K., 1977. "Induction of thrombocytopenia by thrombopheresis in man: Patterns of recovery in normal subjects during ethanol ingestion and abstinence," *Blood*, 49(2), 197–207.

Trepel, F., 1974. "Number and distribution of lymphocytes in man. A critical analysis," *Klinische Wochenschrift*, 52(11), 511–515.

Tubiana, M., Lalanne, C. M., and Surmont, J., 1961. "Total body irradiation for organ transplantation," *Proceedings of the Royal Society of Medicine*, 54(12), 1143–1150.

UNSCEAR, 1988. *Sources, effects, and risks of ionizing radiation. 1988 report to the General Assembly*. United Nations Scientific Committee on the Effects of Atomic Radiation, New York.

Vainstein, V., Ginosar, Y., Shoham, M., Ranmar, D. O., Ianovski, A., and Agur, Z., 2005. "The complex effect of granulocyte colony-stimulating factor on human granulopoiesis analyzed by a new physiologically-based mathematical model," *Journal of Theoretical Biology*, 234(3), 311–27.

Valentin, J., 2002. "Basic anatomical and physiological data for use in radiological protection: Reference values. ICRP Publication 89," *Annals of ICRP*, 32(3-4), 1–277.

Weisbach, V., Friedlein, H., and Glaser, A., 1999. "The influence of automated plateletpheresis on systemic levels of hematopoietic growth factors," *Transfusion*, 39(8), 889–94.

Wentz, J., Oldson, D., and Stricklin, D., 2014. *Hematopoietic models for humans and rhesus monkeys with the effects of radiation and IL-12 treatment*. Applied Research Associates, Inc., Arlington, VA.

Yarmonenko, S. P., 1988. "Radiation sickness in man," *Radiobiology of Humans and Animals*. Trans. by G. Leib. Mir Publishers, Moscow, 153–70.

This page intentionally left blank.

Appendix A Human Case Study Data

Here the process used to evaluate case study data for use in optimization and validation of the mechanistic hematopoietic models is described. Case study data was collected from published literature on reactor and industrial accidents, the Chernobyl accident, and early radiation therapy studies. A larger number of case studies were identified than are reported here, however, many of them lacked detail on hematological parameters over time, had significant treatment, or were overtly localized exposures. This review focuses on the initial down-selection of case studies that could potentially provide valuable data for our work. Nevertheless, many of the case studies have details that must be carefully considered before their associated data are used in our modeling work.

A.1 General Considerations and Criteria

Case studies were reviewed with consideration of factors that could impact hematopoietic response in humans, which include: partial body or non-uniform exposures, uncertainty in dose estimates, differential neutron (or x-ray) energies and contributions to dose and the biological response to them, existing individual variability (due to different baseline cell counts, co-morbidities, and/or individual responses), and the application of treatment and/or therapeutics. Data was obtained on as many of these details as possible. Some case studies, such as the Marshallese and Chernobyl patients, were exposed to radioactive fallout that included beta emitting radionuclides resulting in some cases to cutaneous injury and some level of internalized contamination. Case studies recommended for use in optimizations were prioritized according to relative reliability of dose estimates, uniformity of doses, availability of time course data on the cell counts, and cases without significant hematological treatment.

Where possible, doses in Sv were used to account for the relative biological effectiveness (RBE) of the neutrons that were involved in the criticality accidents. In two specific cases, absorbed doses in Gy were recorded without regard to neutron RBE due to uncertainties associated with the dose estimates resulting in unrealistic doses given the observed effects in these case studies. These studies are discussed below. The large uncertainty placed on the doses estimates for these case studies account for any effect of neutron RBE. Special care was needed to ensure that doses used for the modeling were consistently input as free-in-air (FIA) or midline tissue (MLT) doses. The reporting of dose estimates for the studies was highly variable. The doses reported here reflect the values used as inputs as FIA gamma equivalent doses for modeling hematopoietic responses across the different types of radiation and exposure scenarios.

Although a few case studies that involved treatment with significant transfusions, cytokines, and/or stem cell transplantation were included in the optimization, data points collected after these treatments were removed from the optimization data. Some case study data for treated patients remained in the validation data out of necessity, however, model comparisons (reported elsewhere) discuss the limitations of the data and relevance of the comparisons.

Our current modeling work has the aim of predicting hematopoietic response resulting from relatively uniform whole body exposures. Since significant acute localized injury results in a different overall clinical picture than uniform whole body exposures, case studies

involving highly non-uniform/partial body exposures were avoided for use in optimization. Such cases would be expected to significantly deviate from our modeling results as well. Although an attempt was made to avoid significant partial body exposure case studies that could not afford reasonable comparisons, nearly all of the studies involved some degree of inhomogeneity in the exposure.

A.2 Case Study Descriptions

A.2.1 Criticality accidents

Los Alamos, 1945 and 1946

The criticality accident at Los Alamos National Laboratory in 1945 resulted in two exposures; one fatality and one minor exposure (Hempelmann et al. 1952; Hempelmann 1961; Hoffman and Hempelmann 1957; Bond et al. 1965; Mettler et al. 2001). The fatality, referred to as Case 1, had sustained severe localized exposure to the hand, resulting in significant complications leading to death. Case 2 had a relatively minor exposure to the back. Although hematological data was available for both cases, only Case 2, the low dose exposure, was used in the optimization. The acute partial body nature of the exposure in Case 1 prevents its utility in the model and was instead used to visual the effects of non-uniform exposures (5.5-20 Sv).

Another criticality occurred in 1946 in which eight persons were exposed (Cases 3-10). Hematological data was available on seven of these persons. Cases 3 and 4 were significant but highly non-uniform, prohibiting use in model optimization. Case 4 deemed fit for validation, while Case 3 was used to visualize the potential effects of partial body exposure. Other cases were moderate to insignificant exposures, were fairly uniform, and were not treated. Cases 6-10 had hematological data and were included in validation.

It is important to note that the methods used for determining platelets for these studies differ significantly from methods applied in later studies. Therefore, the platelet data in these studies must be normalized and only relative platelet changes can be reliably evaluated in these studies. However, several of the patients from these accidents had baseline cell count data on file since they were nuclear workers that were being monitored. The baseline data aids interpretation of the hematological response after the exposures.

Doses in Sv as reported in Mettler et al. 2001 were used for these case studies since the conversion to Sv accounts for neutron RBE. The original doses reported in Hempelmann et al. 1952 vary considerably from the doses reported later since neutron doses were not accounted for in the original work. Also note that Bond et al. 1965 reports other doses than those in Mettler et al. 2001 (for example, Bond reports 13.5 Gy for Case 3, vs 13–21 Sv as reported in Mettler et al. 2001). However, due to the completeness of data and doses provided in Sv found in Mettler et al. 2001, these are the data used for these case studies. In cases where a dose range is reported, the median value was used for modeling purposes.

Argonne, 1952

Four workers were exposed to mixed field exposure at Argonne National Laboratory in 1952. The doses ranged from 1.59 to 0.11 Gy (Bond et al. 1965; Mettler et al. 2001). Hematological data was obtained on Cases I and II (1.59 and 1.26 Gy, respectively). Details on uniformity,

proportion of neutron contribution to dose, and treatment were not available. Since the workers were on a platform some distance from the source, relative uniformity is assumed. Only Case I showed any clinical symptoms, however, blood count changes were observed. A median dose of 1.5 Gy (1–2 Gy range) was assigned for both of cases, and Case I was used in the optimization. There is some concern over the appropriate baseline counts for Case II, so this case was not included in the optimization.

Y-12, 1958

The criticality accident that occurred at the Y-12 facility in Oak Ridge, TN in 1958 resulted in eight exposed persons with significant doses to five of the individuals (Mettler et al. 2001). The doses were mixed neutron and gamma. Useful hematological data was obtained on four of these individuals: patients A, B, C, and E (Mettler et al. 2001; Andrews et al. 1961; Bond et al. 1965). All of these patients were in the room at the time of the criticality at different distances from the source. The exposures were total body but were not completely uniform.

Although total doses in Sv were reported in Mettler et al. 2001, upon review we found several dosimetric studies that reported different doses for the case study (Hurst and Ritchie 1959; Hurst, Ritchie, and Emerson 1959; Mole 1984; Kerr and Tankersley 2006). In particular, the study by Mole 1984, indicated that the sodium ratios used to calculate the neutron contributions in the early dose estimates for this accident and the Vinca accident were off. Therefore, the revised doses in Gy as reported in the Kerr and Tankersley 2006 dose reconstruction in 2006 were used as the MLT dose input for the model optimization. For these studies, the RBEs were not accounted for because the estimates were unrealistic given observed health effects when an RBE was used for the neutron contribution. However, the uncertainty provided for the dose estimates is considerable (25% for both neutron and gamma contributions).

Although bone marrow transplantation was considered, patients were expected to recover and in the end only received antibiotics as necessary. Due to the relative reliability of the dose estimated, relative uniformity of exposure, and lack of treatment, these studies were all used in the optimization of the models. The one exception to this was thrombopoiesis and granulopoiesis data from patient E which was reserved for validation.

Vinca, 1958

The Vinca reactor criticality that occurred in 1958 resulted in six exposed individuals and one fatality (Mettler et al. 2001). Doses were relatively uniform, however, there are significant discrepancies in the doses reported (Jammet et al. 1959; Hurst, Ritchie, Sanders, et al. 1961; Pendić 1961; Auxier 1961; Mole 1984; Pešić 2012). Originally, the midpoint of the total dose range reported in Jammet et al. 1959 was used for modeling purposes, however, the dose ranges were not realistic given observed health effects. After review of the collective dosimetry studies for this accident, the doses calculated after correcting the sodium ratios (referenced in the Y-12 accidents, see Mole 1984) and as reported in Pešić 2012 were used.

The patients received only nominal blood transfusions to compensate for blood draws. Bone marrow transplantations were attempted in five of the six cases; therefore, only data up to the point of transplantation was used. The majority of the data from this case study was obtained from the original graphs found in Jammet et al. 1959. However, the early

time points were particularly difficult to reconstruct. Data for three early time points were reported in Pendić 1961 and included in our data for optimization.

Los Alamos, 1958

A third criticality at Los Alamos National Laboratory resulted in an operator being exposed to an extremely high dose mixed field of neutrons and gamma radiation (Mettler et al. 2001; Bond et al. 1965). Few data hematological data points were available since the patient died at 35 hours. Two other workers were exposed to 1.35 and 0.54 Gy, but detailed hematology was not available on these cases.

Sarov-1963

Two persons (KH and M) were involved in this criticality accident, having received approximately 5.5 and 3.7 Gy of neutron and gamma exposure, respectively. The patients received blood transfusions and survived the incident. Data on patient KH was obtained from Mettler et al. 2001 and included for validation.

Mol-1965

An operator standing above the tank received a non-uniform dose of mixed field radiation. The dose in the pelvic region was 10 Gy but was 2-5 Gy in the chest; a mean bone marrow dose was estimated to be 5 Gy. One heavily irradiated leg (50 Gy) was amputated, but the patient survived. Details on hematological was lacking. Due to the amputation and highly localized injury, this study was not considered for optimization or validation. However, data was obtained from Mettler et al. 2001 and used for model comparisons.

Tokai-mura, 1999

The Japanese criticality resulted in two highly exposed individuals that eventually died and a third that was moderately exposed (Hirama et al. 2003; Mettler et al. 2001). All patients received aggressive care. Data from subjects A and B were included in the validation, while data from subject C was compared to the model output to examine potential effects of treatment.

A.2.2 Radiation therapy

In the early days of radiation therapy, a number of patients were treated with single doses of whole body irradiation followed by minimal hematological therapy. The advantage to data from radiation therapy case studies is that baseline blood cell counts are obtained and the radiation dose is known with much more certainty than in radiation accidents. The obvious shortcoming in using radiation therapy data is that patients have co-morbidities that may impact the observed hematological effects. From the literature evaluated, potentially useful data from two studies were identified: one study on patients with cancer not involving the hematopoietic system and one study on patients with renal dysfunction receiving radiation before kidney transplantation.

Non-hematological cancer

Hematological data was collected in cancer patients receiving therapeutic exposures to 250 kvp x-rays in three different dose ranges: 2, 1.5, and 1 Gy (population sizes were 30, 12, and 18, respectively). Although tumors in these patients originated in organs systems other than the hematopoietic system (kidney, lung, colon, etc.), the disease state may still affect the hematopoietic response. Nevertheless, the data provided good baselines for each cohort, relatively precise doses, and mean and standard deviation for the cohorts. Unfortunately, the data only extends out to about 10 days post-exposure.

Renal disorders

Hematological data in a cohort of patients receiving radiation therapy before kidney transplantation was studied (Dealy and Tubiana 1964; Mathe et al. 1964; Tubiana et al. 1961). Most of these patients received fractionated doses of 250 kvp x-rays or exposure to a Co-60 gamma source. The fractionated exposures could not be used in the modeling effort, however, two patients in the cohort received single 4 Gy gamma exposures. The hematological data was reported as an average for these two patients. When hemorrhages were observed, platelet transfusions were performed (Tubiana et al. 1961), however, it was noted that the transfusions did relieve the bleeding but did not restore circulating platelet levels.

A.2.3 Industrial irradiator accidents

UT CARL Co-60, 1971

An individual was relatively uniformly exposed to Co-60 source at the Variable Dose Rate Irradiation Facility (VDRIF; UT CARL, TN in 1971, Goans 2012). The estimated dose was 2.6 Gy; details on treatment were not available and are assumed to be negligible given the moderate dose.

Nesvizh, Belarus Co-60, 1991

At a Nesvizh, Belarus commercial irradiation facility in 1991, an individual was exposed to a Co-60 sterilization source (Baranov et al. 1994; Mettler et al. 2001). The person received a relatively uniform whole body gamma exposure estimated between 10–15 Gy. The midpoint of 12.5 Gy was used for modeling. Granulocyte and platelet data was available for the case study, however, IL-3 and granulocyte macrophage colony-stimulation factor (GM-CSF) as well as blood products were administered from day 3, limiting the amount of data available for use.

Brescia 1975

One individual was exposed at a Co-60 irradiation facility in Italy with limited details available (Mettler 2001). Details on medical treatment were not available. The patient died after 12 days. This was used for validation.

Kjeller 1982

An individual was lethally irradiated by an exposed Co-60 source at a sterilization facility in Norway (Stavem et al. 1985). The exposure was non-uniform and there was considerable uncertainty in the dose estimate. Antibiotic treatments were delivered, and neutrophil,

platelet, and/or whole blood transfusions were administered as needed from 7–8 days.

Soreq 1990

An individual received a whole body exposure to a Co-60 source at an irradiation facility in Israel (IAEA 1993; Mettler et al. 2001). The estimated dose was between 10 and 20 Gy. Supportive care and aggressive therapy were administered. G-CSF was given on day 3, IL-3 on day 5, platelet transfusions as needed, and eventual bone marrow transplantation. The patient died day 36 with a wide range of complications.

Shanghai 1990

A total of seven workers were irradiated by a Co-60 source at an industrial irradiation facility in China (Mettler et al. 2001). The exposures were very non-uniform, and the two most heavily irradiated patients, S and W, received average whole body doses of 12 and 11 Gy, respectively. The mid-section of the patients received the highest doses. Both patients received whole blood and platelet transfusions starting day 2. Bone marrow transplantation was performed on day 11 and 4 for S and W, respectively. S died on day 25, and W died of respiratory failure on day 90.

A.2.4 Miscellaneous

Marshallese 1954

The mean hematological responses observed in 64 Marshallese on the Rongelap atoll exposed to fallout radiation from the atomic bomb testing in the Pacific Ocean was reviewed in Bond et al. 1965. The average whole-body gamma dose for this group was 1.68 Gy. In this cohort, the exposures resulted from the radioactive fallout and was considered somewhat uniform. Internal contamination and skin doses were not taken into account for the doses reported here. Some of the Marshallese did receive burns to the skin, and the doses were received over a period of time. These factors limit the relevance of comparisons to our acute exposure hematological models.

Lockport 1960

This incident involved nine persons being exposed to a pulse of x-rays from a powerful radar generator due to the protective shielding having been removed (Howland et al. 1961; Bond et al. 1965). The doses received to the persons were very non-uniform, ranging from 15 Gy to the head to 3 Gy to the trunk. Although one individual was severely injured, all nine persons recovered. Data on two of the patients with average whole body doses of 3 Gy have been included in the validation for comparison; however, Bond et al. 1965 notes the unusually slow recovery as compared to uniform whole body doses. The RBE of the x-rays, the non-uniformity, and the uncertainty in the doses may contribute to the unusual observations in this study.

Chernobyl 1986

The average hematological response of eleven patients Chernobyl nuclear power plant accident was summarized and reviewed by Fliedner, Gräßle, et al. 2007. This cohort was

referenced as having level 3 hematopoietic syndrome with an estimated whole body dose of 4.85 Gy gamma dose. It was noted that these patients experienced hematopoietic recovery without cytokine therapy. This cohort includes beta irradiation, skin contamination, and internal contamination. Exposures were obtained over an extended period of time that spanned up to several weeks.

UNSCEAR 1988: Case Studies from Chernobyl

The overall experience from the Chernobyl accident was reviewed in the Guskova et al. 1988 report. In this review, the hematological responses of four moderately exposed patients are provided. It was noted that treatment for these patients was conservative, with no antibiotics or transfusions unless symptoms warranted. However, no specific mention of administration of either of these was provided. One patient in particular was noted to have significant skin burns (case 39). These patients received no specialized therapy. As indicated previously, the Chernobyl cohort includes beta irradiation, skin contamination, internal contamination, and protracted exposures.

Russian Examples

Exposures occurring in the former Soviet Union described originally by Guskova and Baranov in Russian, were cited for illustrative examples for a radiobiological review of radiation sickness in man (Yarmonenko 1988; Baranov 1981). Therefore, details of these exposures are vague but note that they are both non-uniform, neutron and gamma exposures. Details on treatment are lacking.

A.3 Summary and Conclusions

A sufficient amount of data for optimization and validation of the hematopoietic model under development was obtained from peer review literature on radiation accident case studies and therapy patients. However, much care was needed in consistently assigning radiation doses and controlling for therapeutic factors in observed hematopoietic responses. Although much of the data was removed due to treatment and/or significant partial body effects, these additional data or case studies can be used in the future to better understand the impact of partial body exposures and bone marrow sparring as well as the impact of treatment on hematopoietic recovery.

Table A.1: (1 of 2) Case studies used in optimization

Case Study–Patient	References	Estimated Dose; Range (Type)	Exposure Details	Treatment Details
Los Alamos 1945–2[abc]	Hempelmann et al. 1952 Hempelmann 1961 Hoffman and Hempelmann 1957 Mettler et al. 2001	0.12 Gy (n, γ)	Insignificant exposure to back	None
Argonne 1952–I[abc]	Bond et al. 1965 Mettler et al. 2001	1.59;1-2 Gy (n, γ)	Assumed uniform	Some clinical effects, assume no significant treatment
Y-12 1958–A[abc]	Bond et al. 1965 Mettler et al. 2001 Andrews et al. 1961 Kerr and Tankersley 2006	4.02 Gy±25% (n, γ)	Criticality, relatively uniform exposure	Antibiotics
Y-12 1958–B[abc]	"	2.97 Gy±25% (n, γ)	"	"
Y-12 1958–C[abc]	"	3.73 Gy±25% (n, γ)	"	None
Y-12 1958-E[c]	"	2.59 Gy±25% (n, γ)	"	"
Vinca 1958–V[abc]	Jammet et al. 1959 Jammet 1961 Pendić 1961 Pešić 2012	6.11 Gy±15% (n, γ)	Criticality, relatively uniform exposure	Bone marrow transfusion wk 5 small blood transfusion platelets during hemorrhage supportive care
Vinca 1958–D[abc]	"	5.4 Gy±15% (n, γ)	"	"
Vinca 1958-H[abc]	"	4.37 Gy±15% (n, γ)	"	"
Vinca 1958–M[abc]	"	5.74 Gy±15% (n, γ)	"	Bone marrow transfusion wk 5 small blood transfusion supportive care
Vinca 1958–G[abc]	"	5.35 Gy±15% (n, γ)	"	"
Vinca 1958-B[abc]	"	3.51 Gy±15% (n, γ)	"	Small blood transfusion supportive care
Cancer patients 1958–mean of 30[abc]	Miller et al. 1958	2 Gy (250 kvp x-ray)	Uniform, whole-body	None
Cancer patients 1958–mean of 18[abc]	"	1 Gy (250 kvp x-rays)	"	"
Cancer patients 1958–mean of 12[abc]	"	1.5;1.25-1.75 Gy (250 kvp x-rays)	"	"

[a] Case study used in thrombopoiesis optimization
[b] Case study used in granulopoiesis optimization
[c] Case study used in lymphopoiesis optimization

Table A.1: (2 of 2) Case studies used in optimization

Case Study–Patient	References	Estimated Dose; Range (Type)	Exposure Details	Treatment Details
UT CARL 1971[abc]	Goans 2012	2.6 Gy (γ)	Relatively uniform	No treatment assumed
Nesvizh 1991[a]	Baranov et al. 1994	12.5;10-15 Gy (γ)	Relatively uniform	Cytokines and blood transfusions
Lockport 1960–A[c]	Bond et al. 1965 Howland et al. 1961	3 Gy –x-rays	Very non-uniform	Conservative treatment noted Antibiotics and transfusions only if necessary
Lockport 1960–B[c]	"	"	"	"
Yarmonenko 1988-Z[abc]	"	9.8 Sv –n, γ	Non-uniform	No details

[a] Case study used in thrombopoiesis optimization
[b] Case study used in granulopoiesis optimization
[c] Case study used in lymphopoiesis optimization

Table A.2: (1 of 3) Case Studies for potential use in validation and future work

Case Study–Patient	References	Estimated Dose; Range (Type)	Exposure Details	Treatment Details	Notes on applicability
Most reliable case studies					
Los Alamos 1946-4[abc]	Hempelmann et al. 1952 Hempelmann 1961 Hoffman and Hempelmann 1957 Mettler et al. 2001	3.6 Sv (n, γ)	Non-uniform criticality, some localized exposure	Antibiotics, fluids, blood transfusions	Limitations: some treatment
Los Alamos 1946-6[abc]	"	1.6 Sv (n, γ)	Relative uniform criticality	No effects observed, no treatment	
Los Alamos 1946-7[abc]	"	1.1 Sv (n, γ)	"	"	
Los Alamos 1946-8[abc]	"	0.65 Sv (n, γ)	"	"	
Los Alamos 1946-9[abc]	"	0.47 Sv (n, γ)	"	"	
Los Alamos 1946-10[abc]	"	0.37 Sv (n, γ)	"	"	
Argonne 1952-II[c]	Bond et al. 1965 Mettler et al. 2001	1.26;1-2 Gy (n, γ)	Assumed uniform	No clinical effects, no treatment assumed	
Y-12 1958-E[ab]	Bond et al. 1965 Mettler et al. 2001 Andrews et al. 1961 Kerr and Tankersley 2006	2.59 Gy±25% (n, γ)	Criticality, relatively uniform exposure	Antibiotics	
Lockport 1960–A[ab]	Bond et al. 1965 Howland et al. 1961	3 Gy (x-rays)	Very non-uniform	Conservative treatment noted, antibiotics and transfusions only if necessary	Limitations: non-uniform
Lockport 1960–B[ab]	"	"	"	"	"
Kidney transplants 1964 –mean of 2[d]	Mathe et al. 1964 Tubiana et al. 1961 Dealy and Tubiana 1964	4 Gy (γ)	Uniform, whole-body	Platelet transfusions noted amelioration of hemorrhage but not platelet levels	Limitations: repeated transfusion
Kjeller 1982[abc]	Stavem et al. 1985 Mettler 2001	22.5 Gy (γ)	Dosimetry uncertain, non-uniform	Antibiotics, transfusions on days 8, 9, 12; died day 13	Limitations: non-uniform and treatment

[a] Case study used in thrombopoiesis validation
[b] Case study used in granulopoiesis validation
[c] Case study used in lymphopoiesis validation
[d] Case study used to visualize treatment effects

Table A.2: (2 of 3) Case studies for potential use in validation and future work

Case Study–Patient	References	Estimated Dose; Range (Type)	Exposure Details	Treatment Details	Notes on applicability
Case studies with mild limitations					
Marshallese 1954–mean of 64[abc]	Bond et al. 1965	1.68 Gy (γ, β)	Uniform fallout, included skin contamination	No details, none assumed	Limitations: cutaneous doses, internal contamination and protracted doses
Sarov 1963[abc]	Mettler et al. 2001	5.5 Gy (n, γ)	Non-uniform criticality	Antibiotics and blood transfusions every 3-5 days	Limitations: non-uniform and treatment
Brescia 1975[ab]	Mettler 2001	12 Gy (γ)	No details	No details, died day 12	Limitations: details on exposure and treatment lacking
Chernobyl 1986-mean of 11	Fliedner, Gräßle, et al. 2007	4.85;2.6-7.1 Gy (γ, β)	Variable exposure, may include beta contamination	No cytokine therapy, hematopoietic recovery	Limitations: large dose range, cutaneous doses, internal contamination and protracted doses
Chernobyl 1986–Case 21	Guskova et al. 1988	3.9;3.6-4.2 Gy (γ, β)	Variable exposure, beta and internal contamination	Supportive care only	Limitations: skin burns, internal contamination and protracted doses
Chernobyl 1986–Case 39	"	2.85;2.4-3.3 Gy (γ, β)	"	"	Limitations: cutaneous doses, internal contamination and protracted doses
Chernobyl 1986–Case 48	"	1.25;1.1-1.4 Gy (γ, β)	"	"	"
Chernobyl 1986–Case 97	"	0.6;0.3-0.9 Gy (γ, β)	"	"	"
Shanghai 1990-S[abc]	Mettler 2001	12 Gy (γ)	Very non-uniform	Antibiotics, whole blood and platelet transfusions, bone marrow transplant	Limitations: details on non-uniformity not available and significant treatment
Shanghai 1990-W[d]	"	11 Gy (γ)	"	"	Limitations: some non-uniformity and significant treatment

[a] Case study used in thrombopoiesis validation
[b] Case study used in granulopoiesis validation
[c] Case study used in lymphopoiesis validation
[d] Case study used to visualize treatment effects

Table A.2: (3 of 3) Case studies for potential use in validation and future work

Case Study–Patient	References	Estimated Dose; Range (Type)	Exposure Details	Treatment Details	Notes on applicability
Tokai-mura 1999-A[abc]	Hirama et al. 2003 Mettler et al. 2001	>20 GyEq (n, γ)	Non-uniform criticality	Antibiotics, G-CSF day 1, eventual stem cell transplant, died after 82 days	Limitations: non-uniform and some treatment
Tokai-mura 1999-B[abc]	"	7.4;6-10 GyEq (n, γ)	Non-uniform criticality	Antibiotics, G-CSF day 1, eventual stem cell transplant, died after 210 days	"
Tokai-mura 1999-C[d]	"	2.3;1-4.5 GyEq (n, γ)	Relatively uniform criticality	Antibiotics, G-CSF day 2, recovered	Limitations: treatment
Case studies with dramatic limitations					
Los Alamos 1945-1[e]	Hempelmann et al. 1952 Hempelmann 1961 Hoffman and Hempelmann 1957 Mettler et al. 2001	12.75;5.5-20 Sv (n, γ)	Non-uniform criticality, acute localized exposure	Antibiotics, died day 25	Not useful: Acute localized exposure; useful in showing partial body effects
Los Alamos 1946-3[e]	"	17;13-20 Sv (-n, γ)	Non-uniform criticality, acute localized exposure	Antibiotics, fluids, blood transfusions, died day 9	Not useful: Limited data and acute localized exposure
Mol 1965[abc]	Mettler et al. 2001	5.5 Gy (n, γ)	Non-uniform criticality	Antibiotics and amputation	Not useful: Acute localized exposure resulting in amputation
Baranov 1981	Baranov 1981	2.3;2-2.6 Gy (γ)	No details	No details, assume no treatment	Not useful: no details available on exposure, data inconsistent with known hematological response
Yarmonenko 1988-K[e]	Yarmonenko 1988	5.8;2.8-10 Sv (n, γ)	Non-uniform: 10 and 2.8 Sv to each side	No stem cell transplant, details limited, spontaneous recovery	Not useful: Highly non-uniform; useful in showing partial body effects
Soreq 1990[d]	IAEA 1993 Mettler 2001	15;10-20 Gy (γ)	Whole-body	Antibiotics, G-CSF day 1, IL-3 day 5, platelet transfusions, bone marrow transplant, died day 36	Not useful: Highly treated; useful in showing effect of treatment

[a] Case study used in thrombopoiesis validation
[b] Case study used in granulopoiesis validation
[c] Case study used in lymphopoiesis validation
[d] Case study used to visualize treatment effects
[e] Case study used to visualize partial body effects

Appendix B Supplemental Model Comparisons

B.1 Optimization Data Comparisons

This section provides all the comparisons between the optimization data and the corresponding model simulation not included in the the main body of the report. Figure B.1, Figure B.2, and Figure B.3 show these comparisons for thrombopoiesis, granulopoiesis, and lymphopoiesis, respectively. Each dataset presented in these plots comes from the specified case study/patient. Details on each optimization case study are provided in Appendix A.

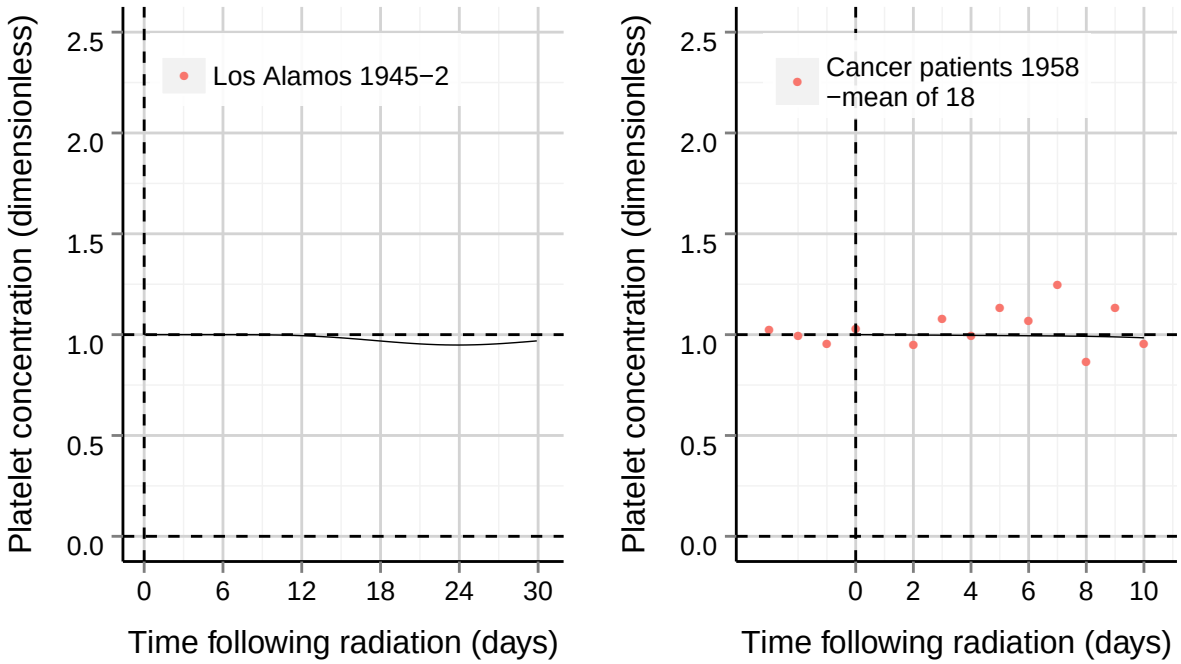

(a) Dose: 0.12 Gy

(b) Dose: 1.0 Gy

Figure B.1: (1 of 4) Thrombopoiesis model compared to optimization data. Model output at the specified dose is delineated by a black line and, if a dose range is provided, a shaded region.

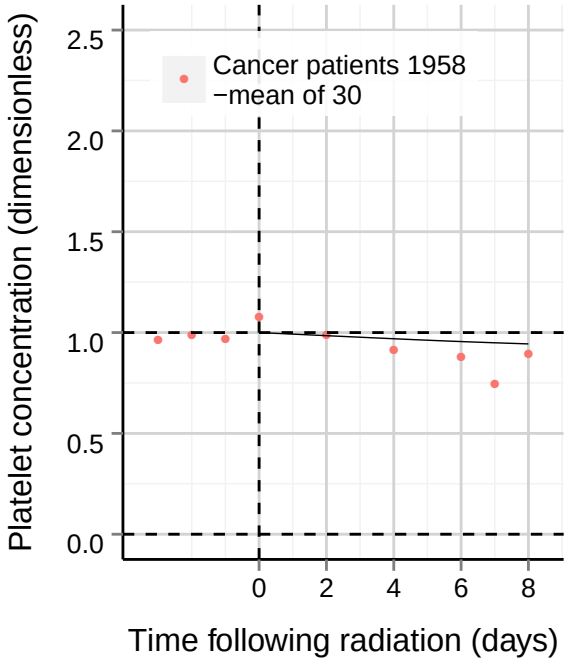

(c) Dose: 2.0 Gy

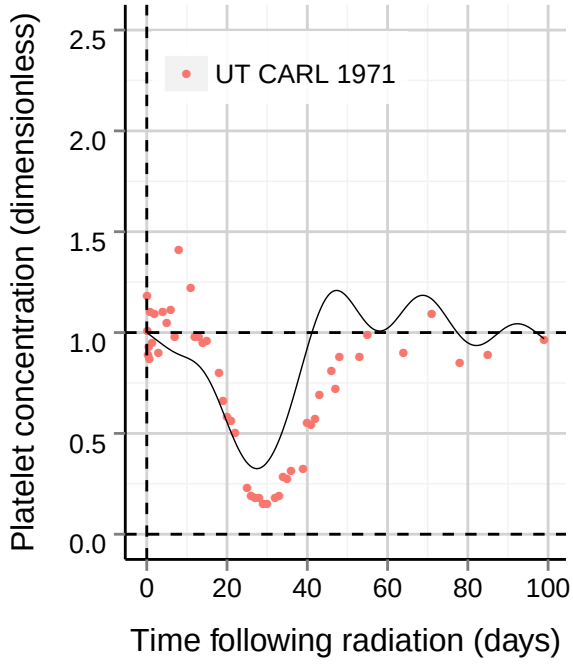

(d) Dose: 2.6 Gy

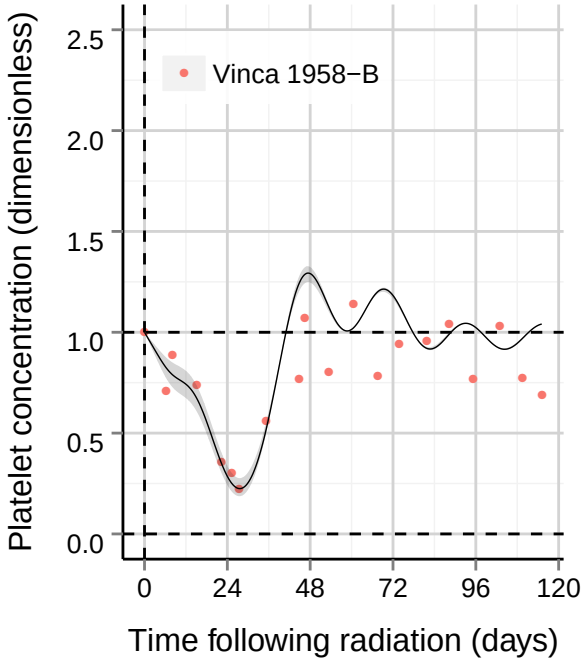

(e) Dose: 3.51 Gy ± 15%

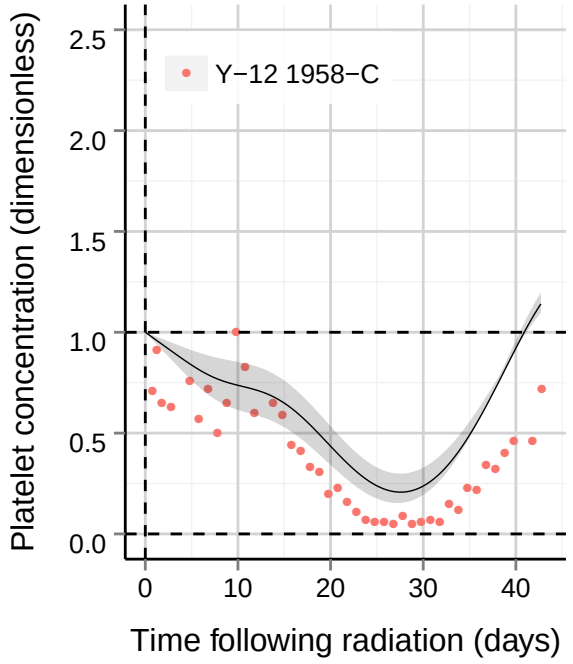

(f) Dose: 3.73 Gy ± 25%

Figure B.1: (2 of 4) Thrombopoiesis model compared to optimization data. Model output at the specified dose is delineated by a black line and, if a dose range is provided, a shaded region.

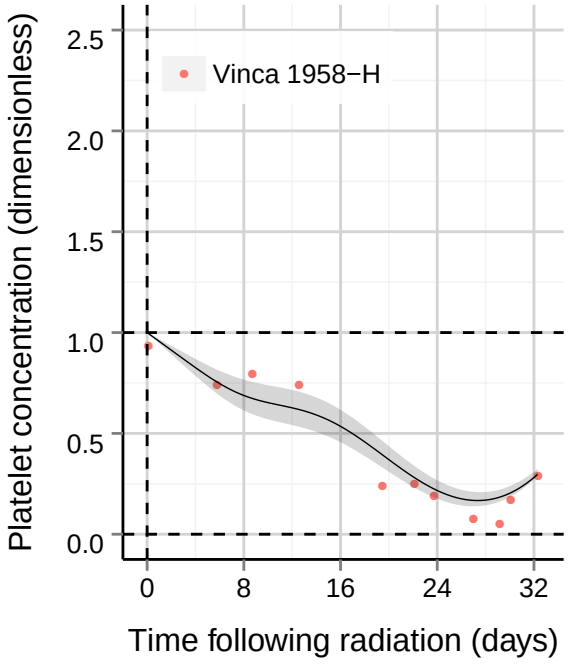

(g) Dose: 4.37 Gy ± 15%

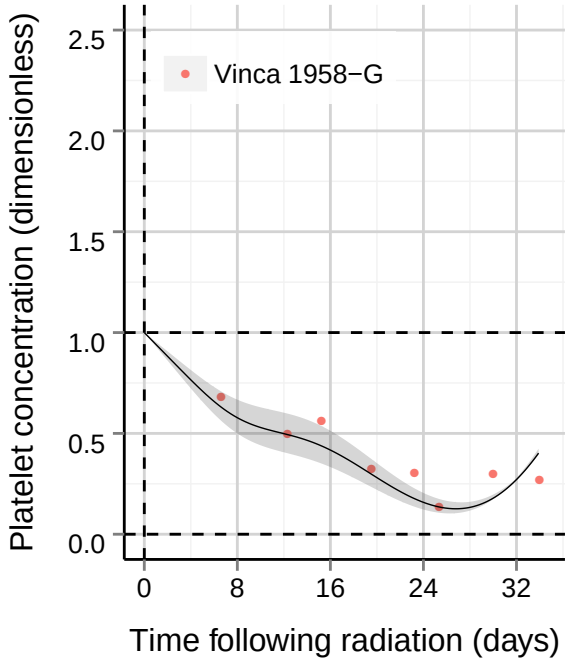

(h) Dose: 5.35 Gy ± 15%

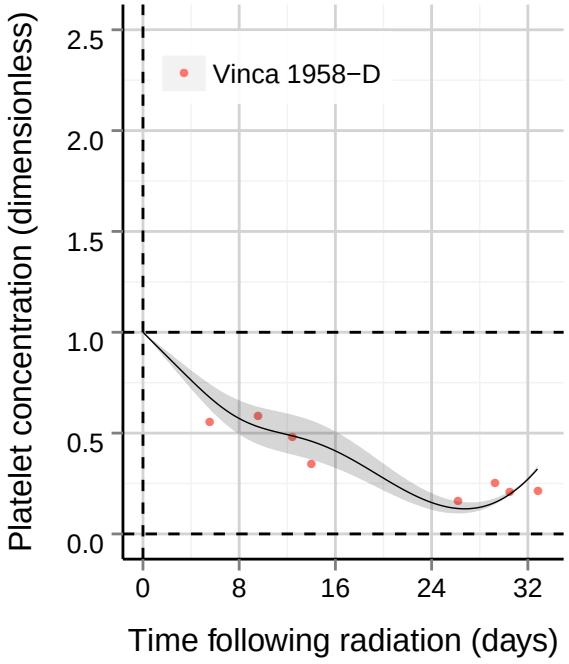

(i) Dose: 5.4 Gy ± 15%

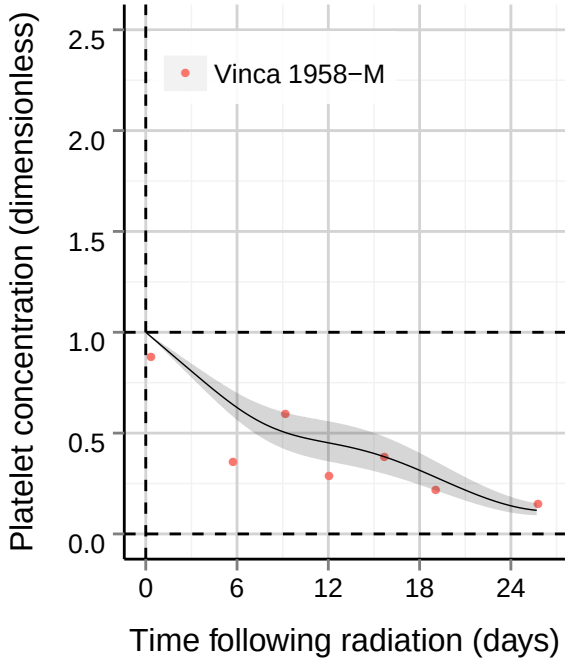

(j) Dose: 5.74 Gy ± 15%

Figure B.1: (3 of 4) Thrombopoiesis model compared to optimization data. Model output at the specified dose is delineated by a black line and, if a dose range is provided, a shaded region.

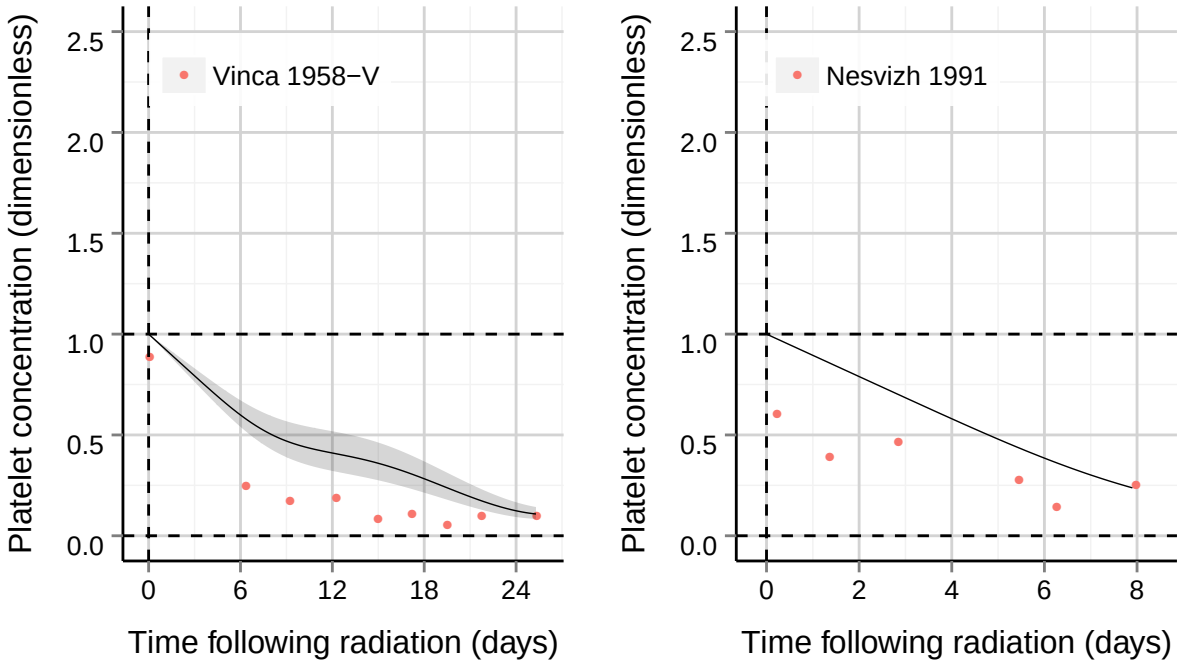

(k) Dose: 6.11 Gy ± 15%

(l) Dose: 12.5 Gy

Figure B.1: (4 of 4) Thrombopoiesis model compared to optimization data. Model output at the specified dose is delineated by a black line and, if a dose range is provided, a shaded region.

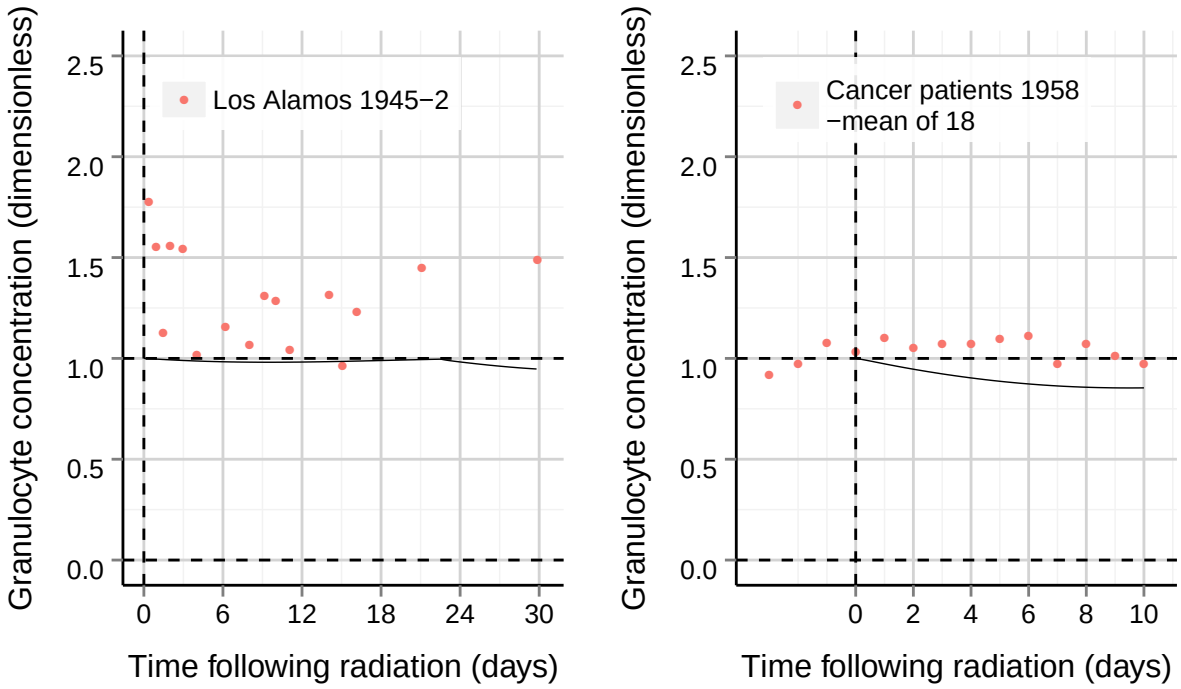

(a) Dose: 0.12 Gy

(b) Dose: 1.0 Gy

Figure B.2: (1 of 3) Granulopoiesis model compared to optimization data. Model output at the specified dose is delineated by a black line and, if a dose range is provided, a shaded region.

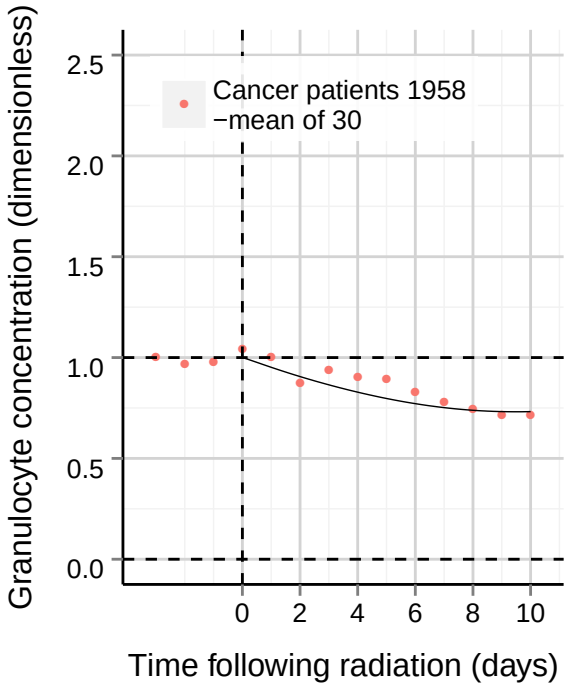

(c) Dose: 2.0 Gy

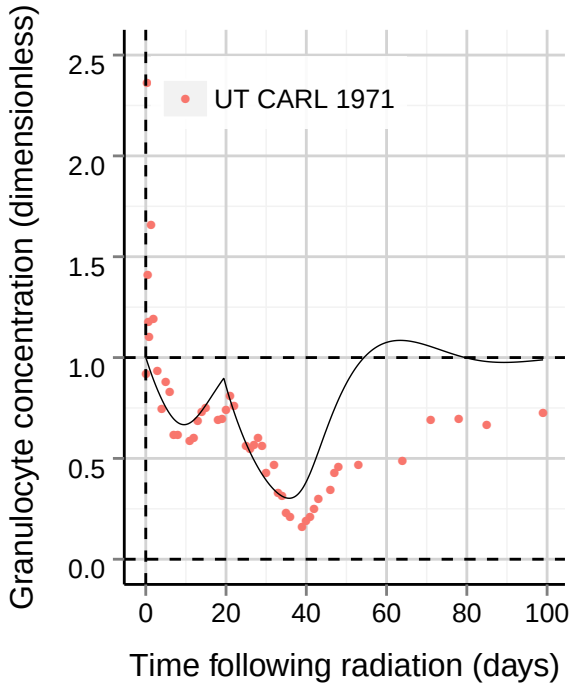

(d) Dose: 2.6 Gy

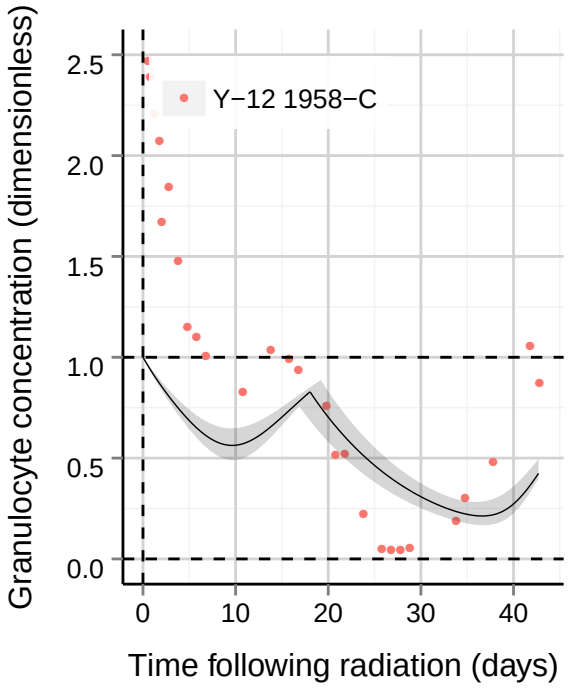

(e) Dose: 3.73 Gy ± 25%

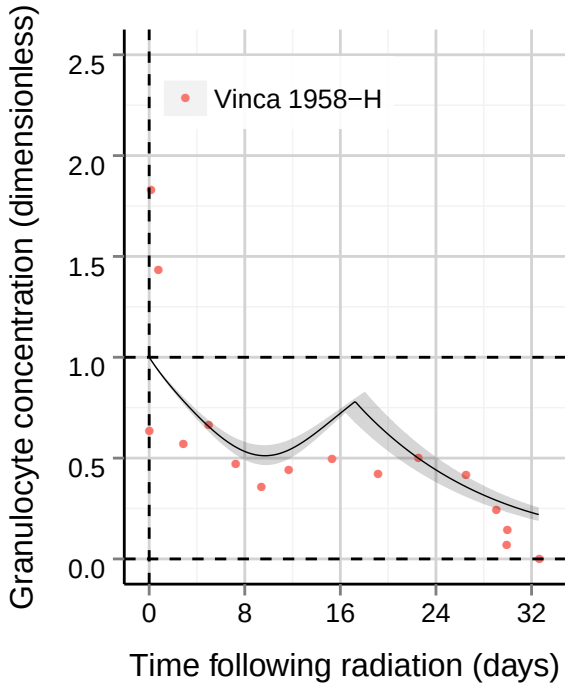

(f) Dose: 4.37 Gy ± 15%

Figure B.2: (2 of 3) Granulopoiesis model compared to optimization data. Model output at the specified dose is delineated by a black line and, if a dose range is provided, a shaded region.

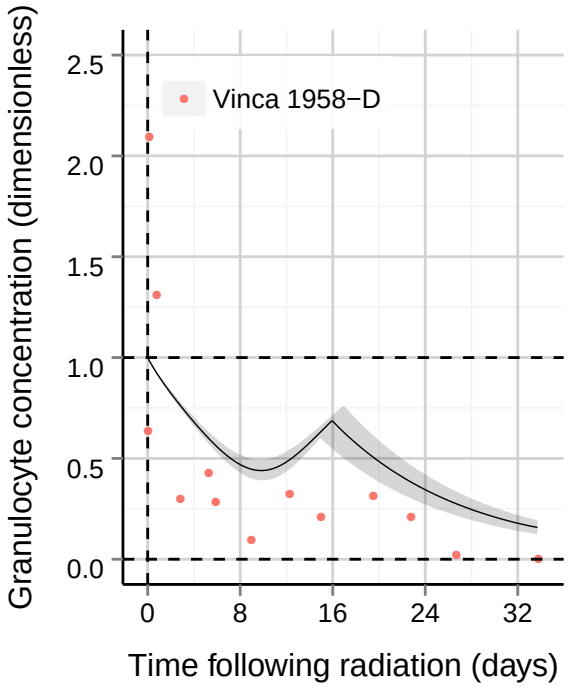

(g) Dose: 5.4 Gy ± 15%

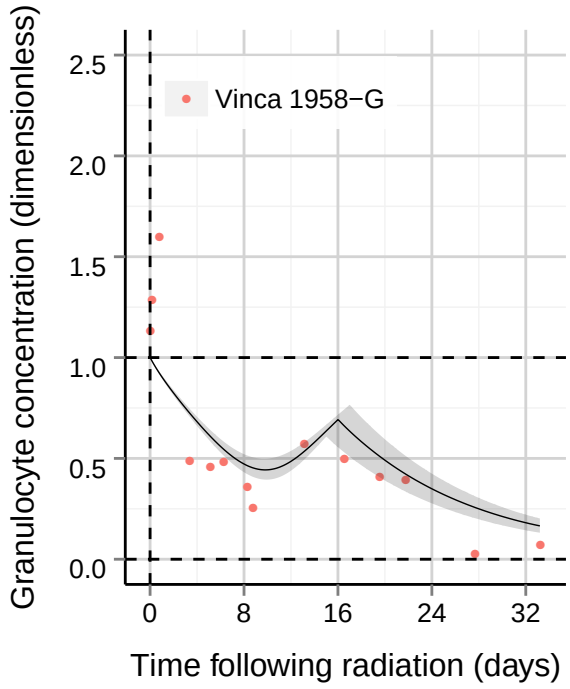

(h) Dose: 5.35 Gy ± 15%

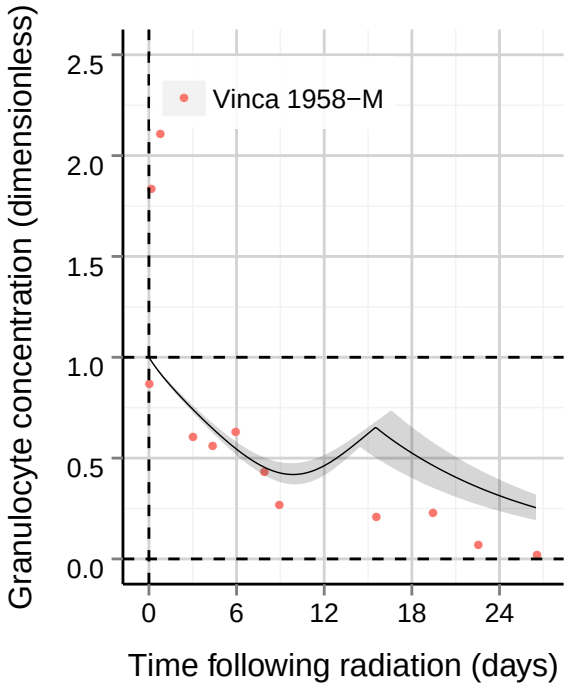

(i) Dose: 5.74 Gy ± 15%

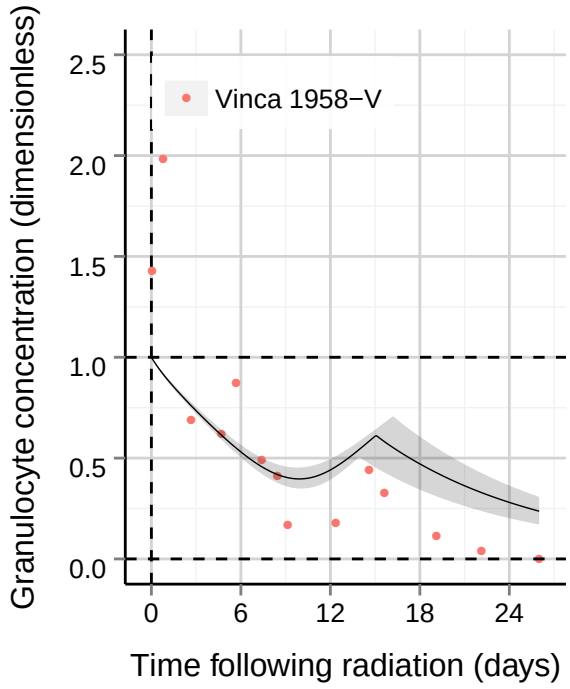

(j) Dose: 6.11 Gy ± 15%

Figure B.2: (3 of 3) Granulopoiesis model compared to optimization data. Model output at the specified dose is delineated by a black line and, if a dose range is provided, a shaded region.

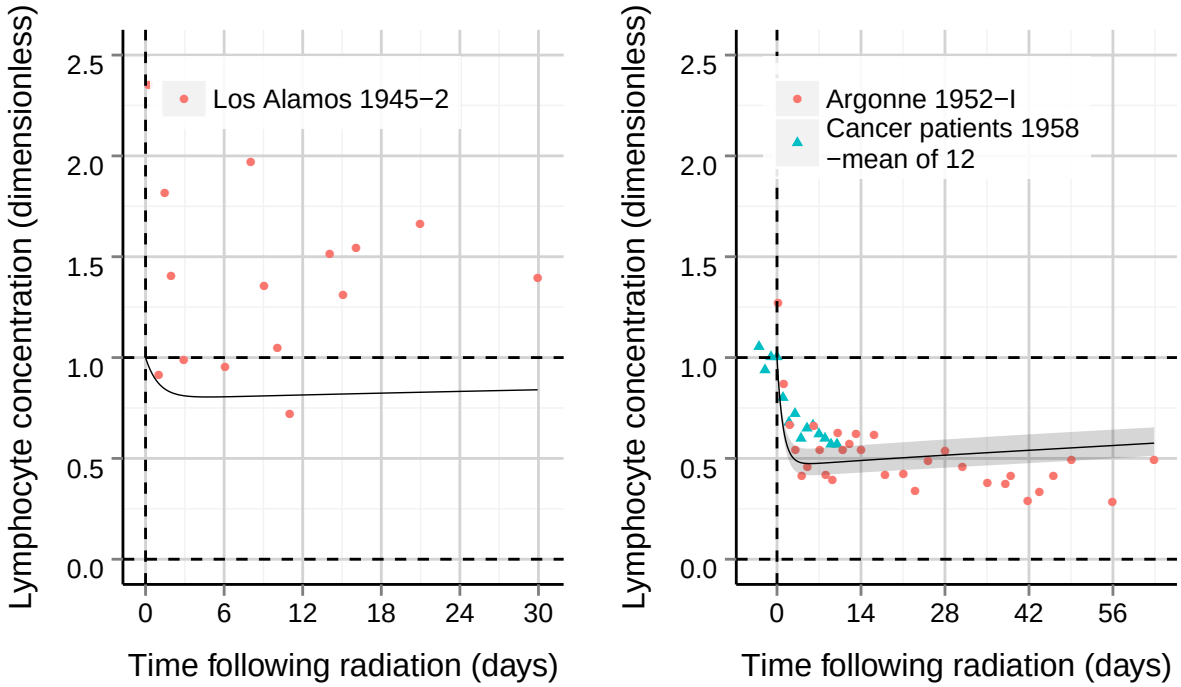

(a) Dose: 0.12 Gy

(b) Dose: 1.5 Gy (1-2 Gy; Argonne)

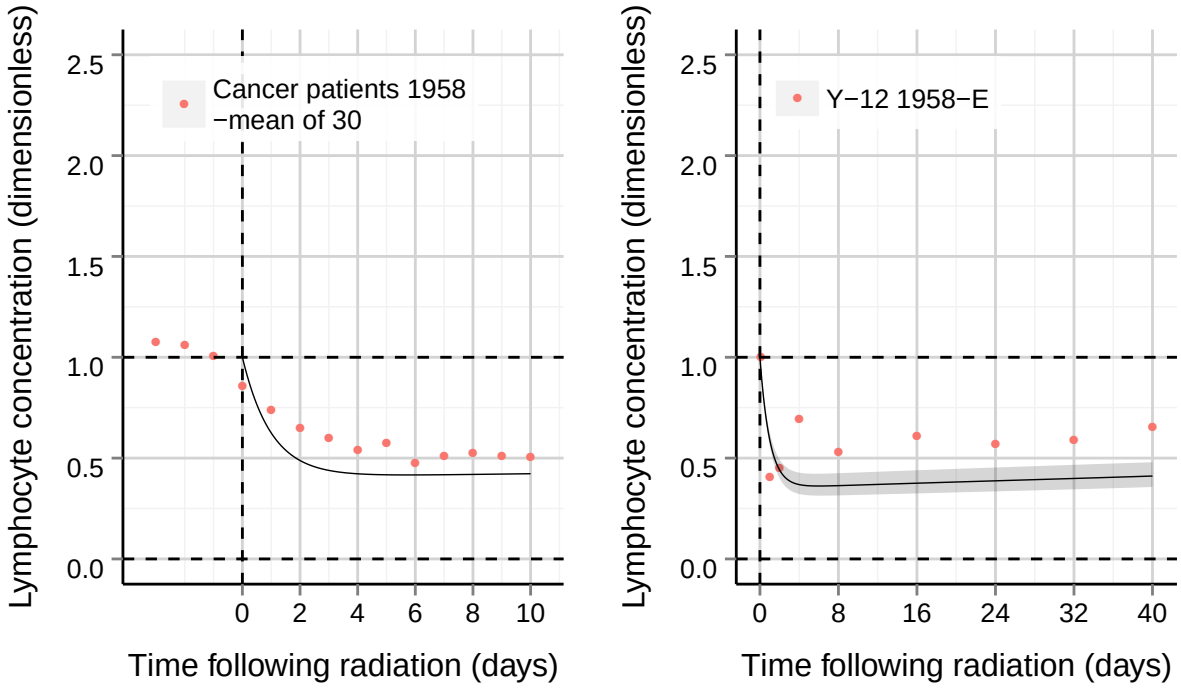

(c) Dose: 2.0 Gy

(d) Dose: 2.59 Gy ± 25%

Figure B.3: (1 of 3) Lymphopoiesis model compared to optimization data. Model output at the specified dose is delineated by a black line and, if a dose range is provided, a shaded region.

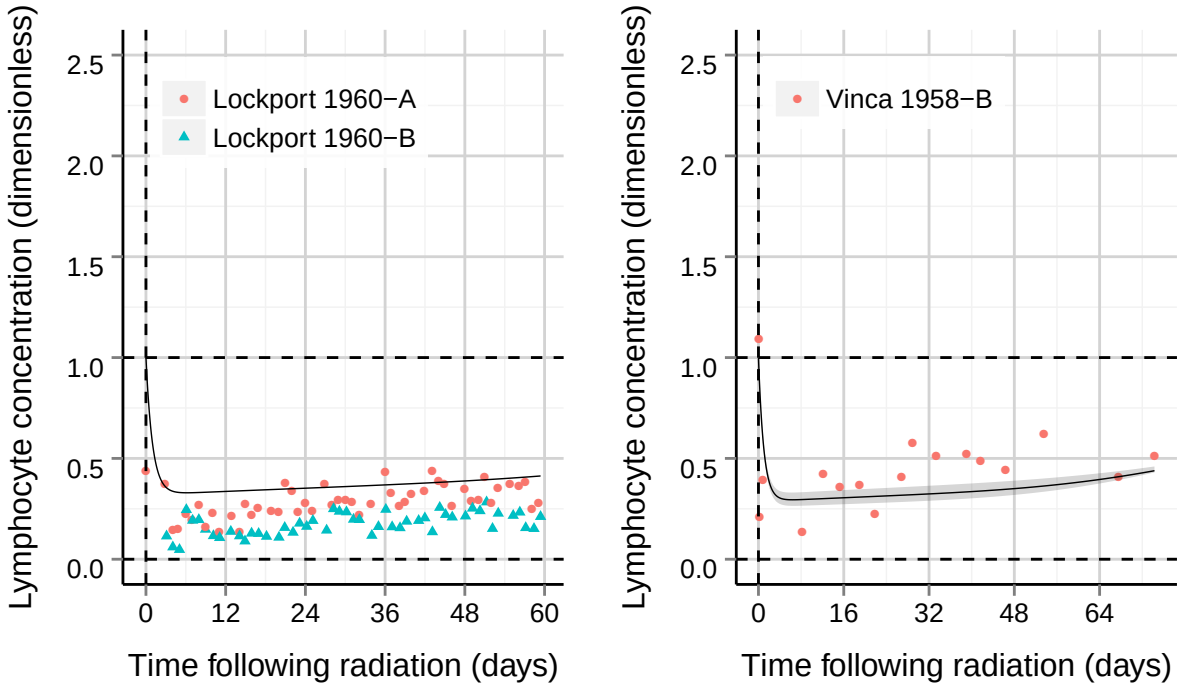

(e) Dose: 3.0 Gy

(f) Dose: 3.51 Gy ± 15%

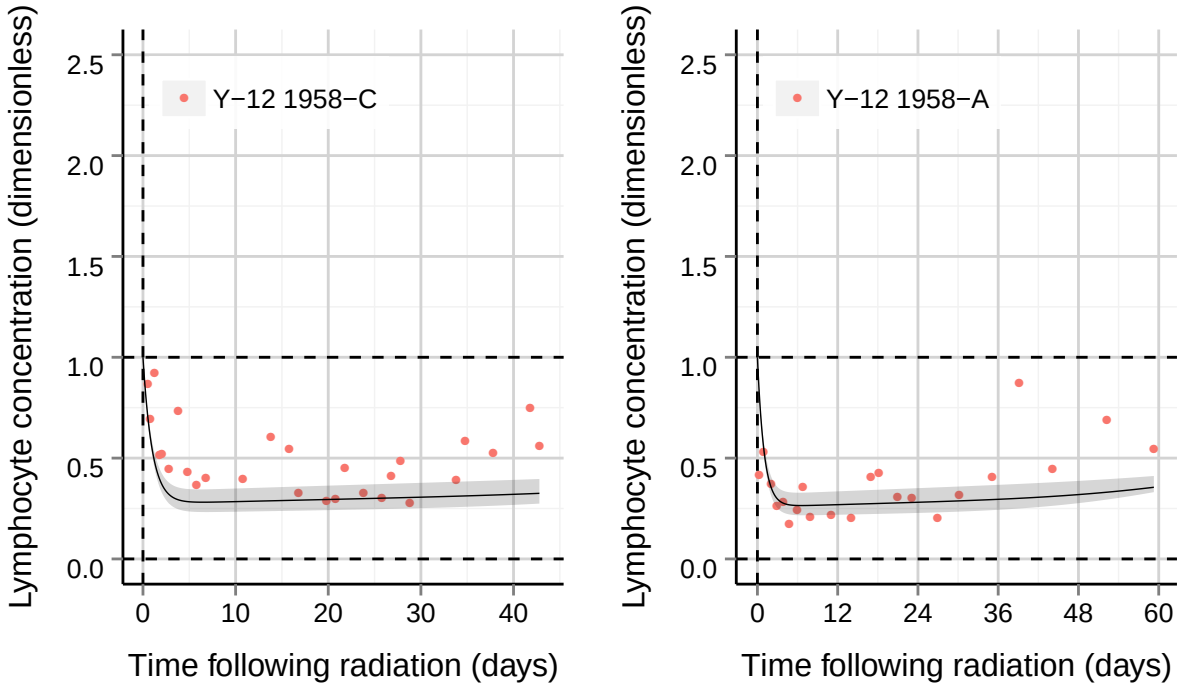

(g) Dose: 3.73 Gy ± 25%

(h) Dose: 4.02 Gy ± 25%

Figure B.3: (2 of 3) Lymphopoiesis model compared to optimization data. Model output at the specified dose is delineated by a black line and, if a dose range is provided, a shaded region.

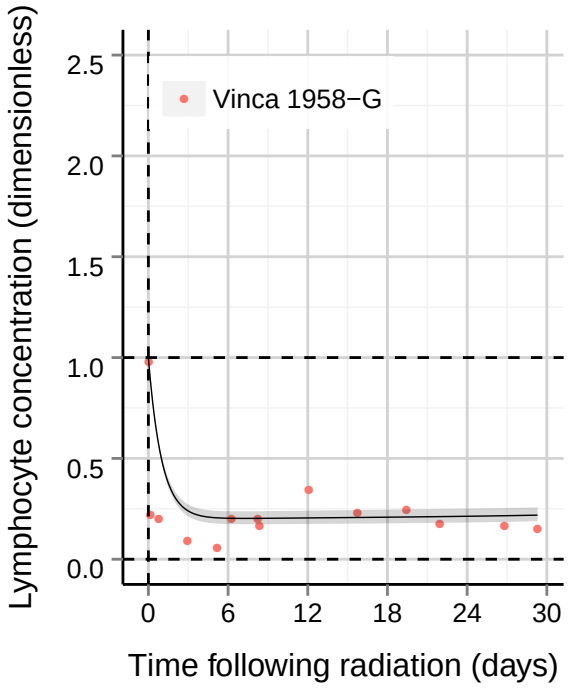

(i) Dose: 5.35 Gy ± 15%

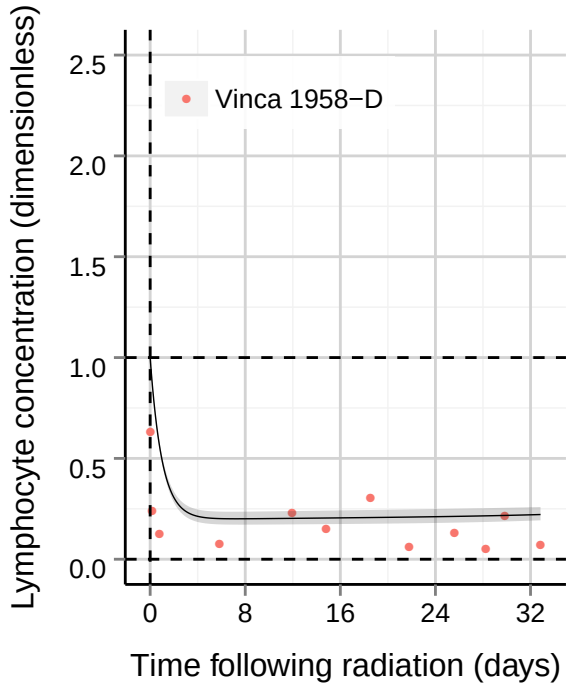

(j) Dose: 5.4 Gy ± 15%

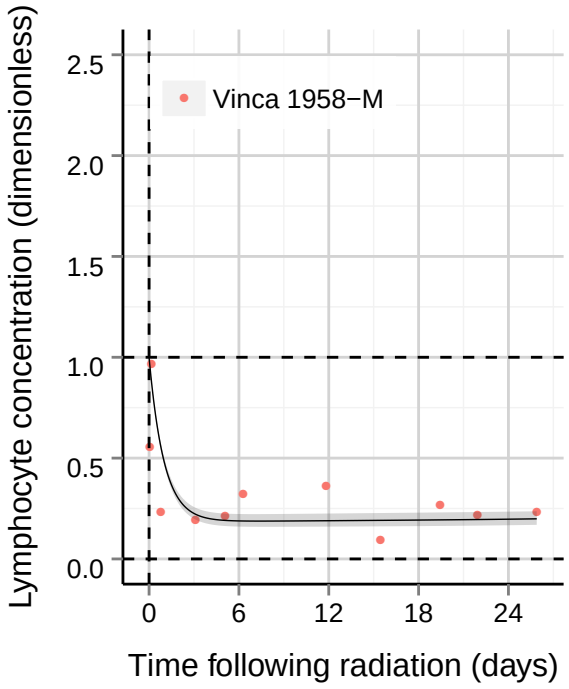

(k) Dose: 5.74 Gy ± 15%

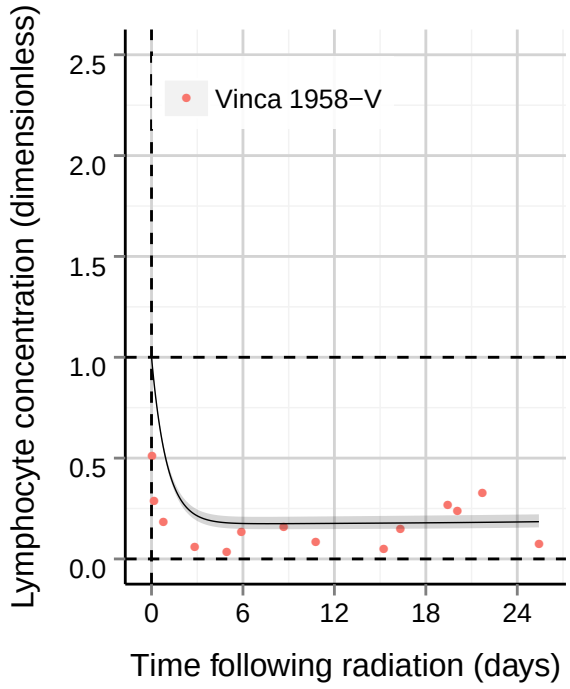

(l) Dose: 6.11 Gy ± 15%

Figure B.3: (3 of 3) Lymphopoiesis model compared to optimization data. Model output at the specified dose is delineated by a black line and, if a dose range is provided, a shaded region.

B.2 Other Model Validations and Comparisons

This section presents comparisons of the hematopoietic models to blood cell kinetic data obtained on radiation accident victims not shown in the main body of the report and not included in optimization. Some of these comparisons were used for validation, while others are shown to explore the effects of various factors on hematopoiesis. Again, details on each case study are given in Appendix A.

Model validation comparisons are shown in Figure B.4, Figure B.5, and Figure B.6 for thrombopoiesis, granulopoiesis, and lymphopoiesis, respectively. Studies presented in this figure were considered adequate for validation purposes. An exception to this is the Mol 1965 case study for thrombopoiesis and granulopoiesis which was a highly non-uniform exposure. The Mol exposure is included in the validation figures to provide a comparison with the Sarov 1963 case study, which is intended for validation, who received the same estimated dose of 5.5 Gy. Below we describe and present other comparisons not used for validation.

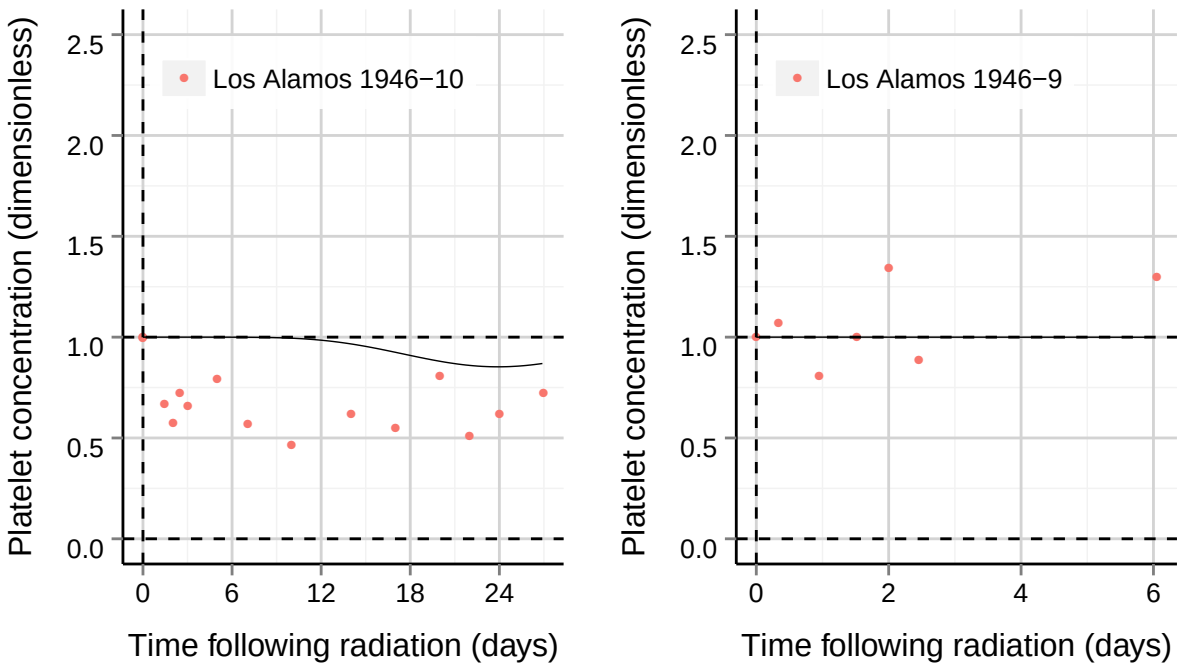

(a) Dose: 0.37 Gy

(b) Dose: 0.47 Gy

Figure B.4: (1 of 3) Thrombopoiesis model compared to validation data. Model output at the specified dose is delineated by a black line and, if a dose range is provided, a shaded region.

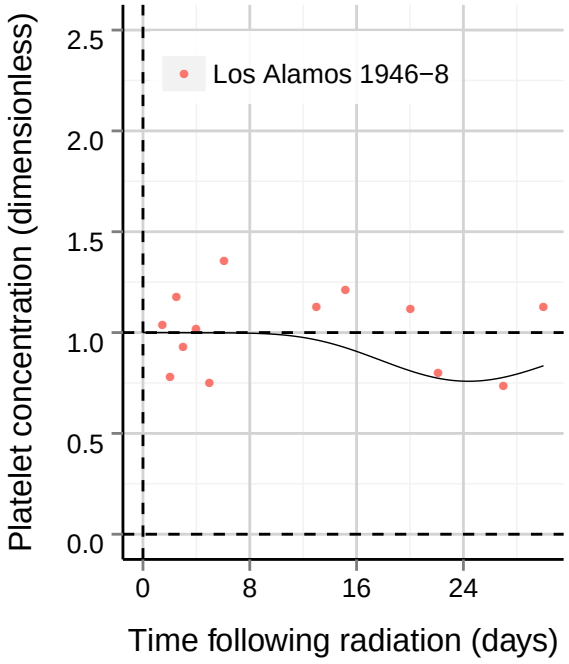

(c) Dose: 0.65 Gy

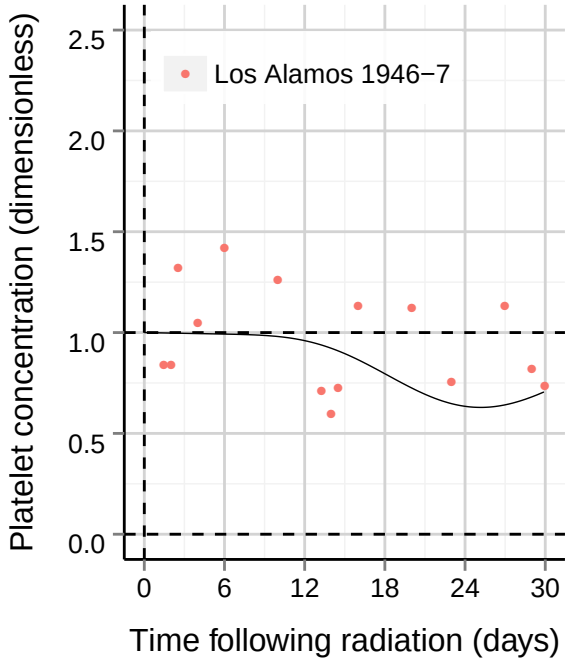

(d) Dose: 1.1 Gy

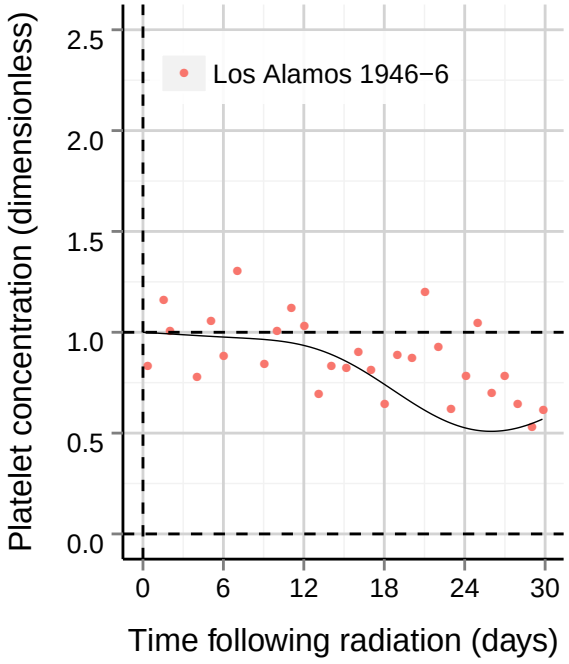

(e) Dose: 1.6 Gy

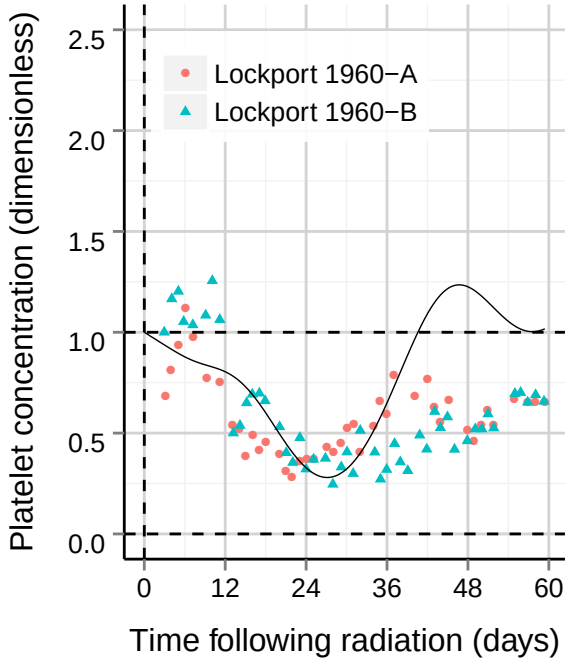

(f) Dose: 3.0 Gy

Figure B.4: (2 of 3) Thrombopoiesis model compared to validation data. Model output at the specified dose is delineated by a black line and, if a dose range is provided, a shaded region.

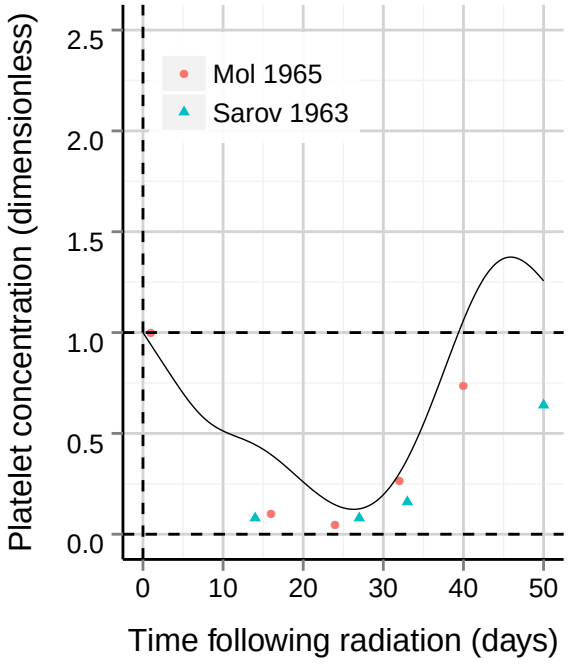

(g) Dose: 5.5 Gy

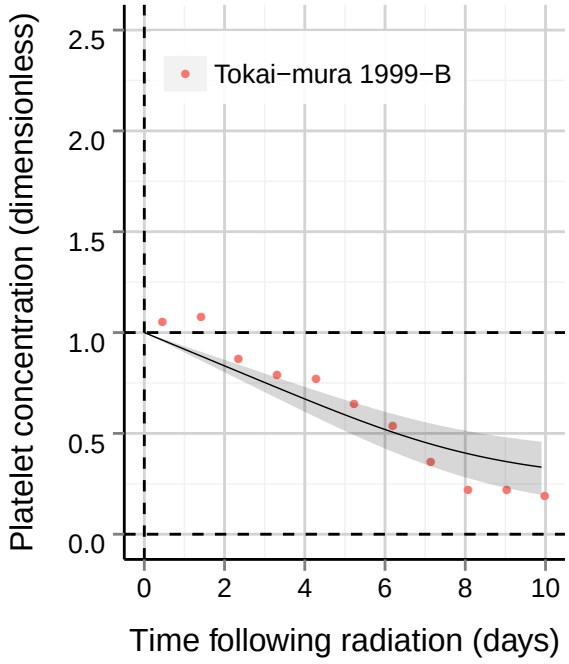

(h) Dose: 7.4 Gy (6-10 Gy)

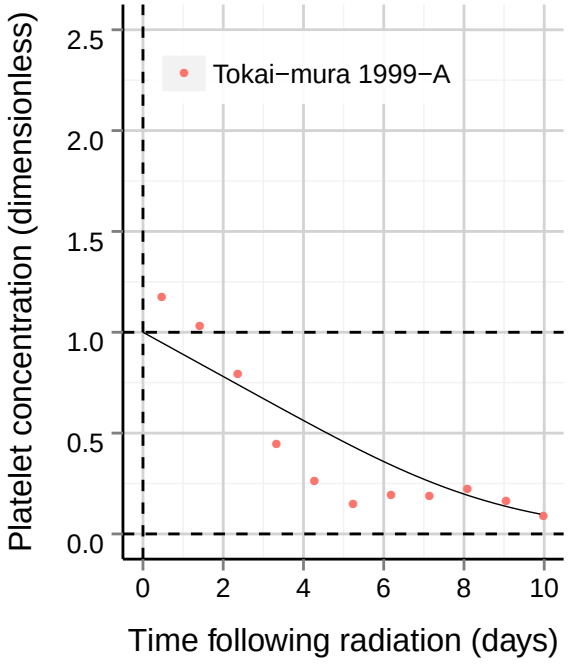

(i) Dose: 20.0 Gy

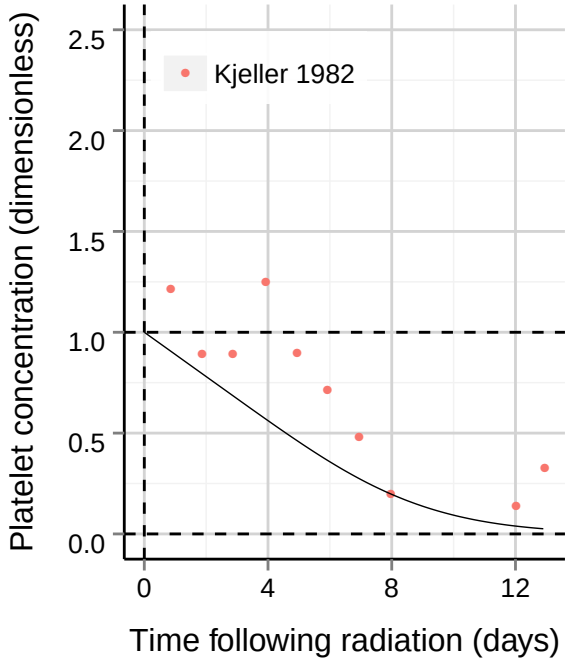

(j) Dose: 22.5 Gy

Figure B.4: (3 of 3) Thrombopoiesis model compared to validation data. Model output at the specified dose is delineated by a black line and, if a dose range is provided, a shaded region.

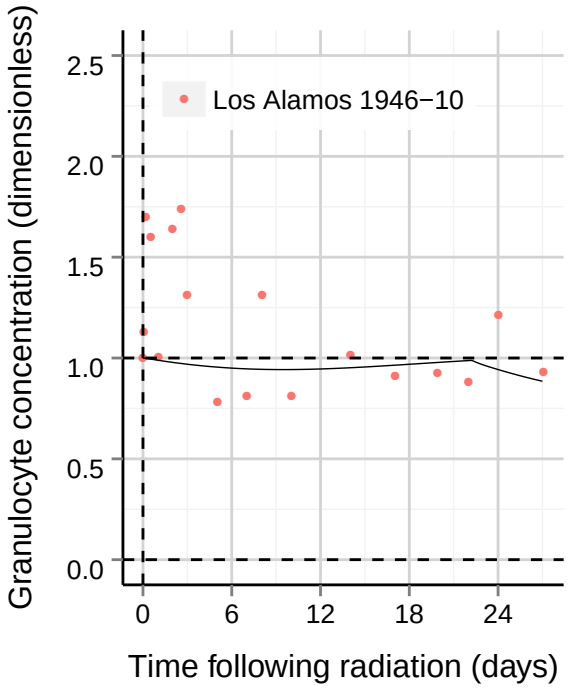

(a) Dose: 0.37 Gy

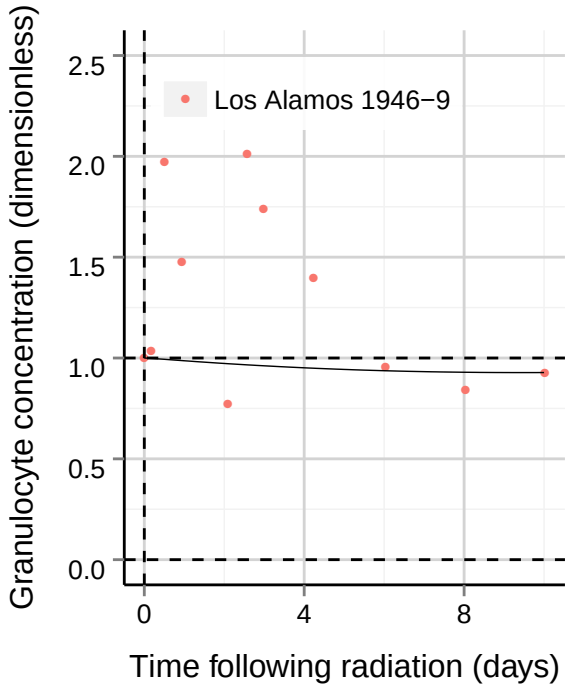

(b) Dose: 0.47 Gy

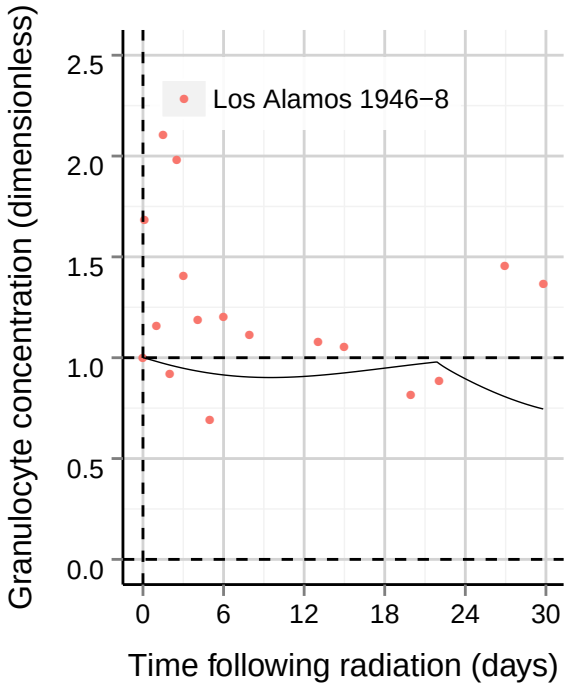

(c) Dose: 0.65 Gy

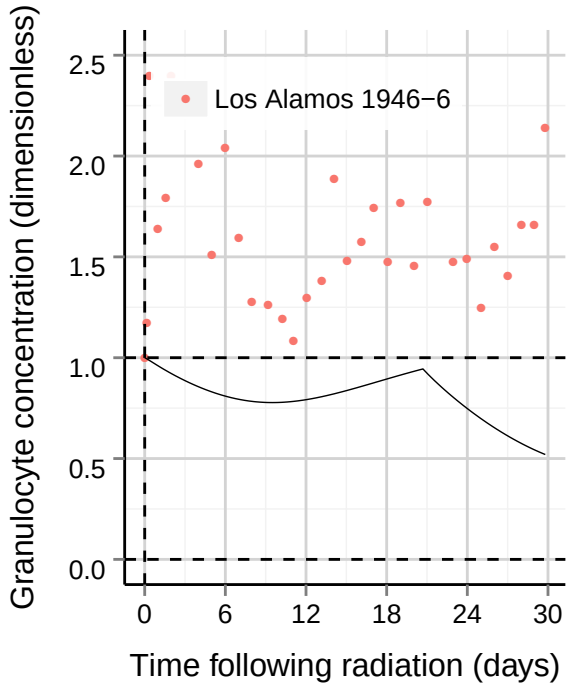

(d) Dose: 1.6 Gy

Figure B.5: (1 of 3) Granulopoiesis model compared to validation data. Output at the specified dose is delineated by a black line and, if a dose range is provided, a shaded region. If a generic baseline value was used, output initialized at the upper and lower end of the healthy granulocyte range is shown by dotted lines.

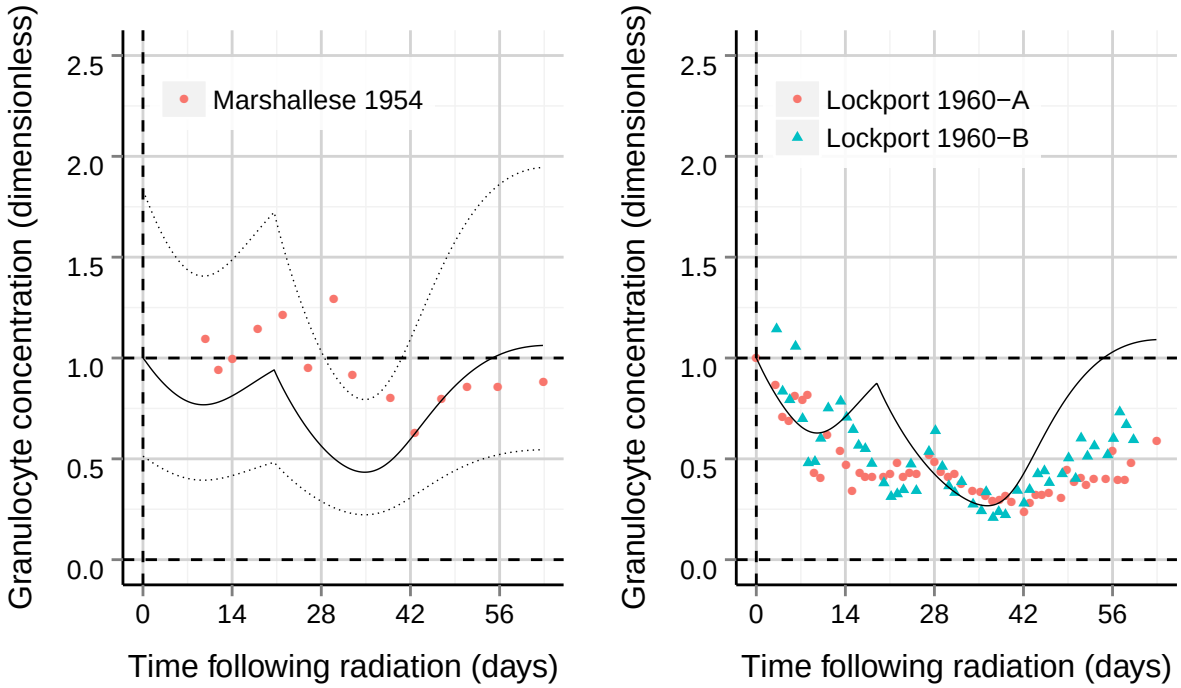

(e) Dose: 1.68 Gy

(f) Dose: 3.0 Gy

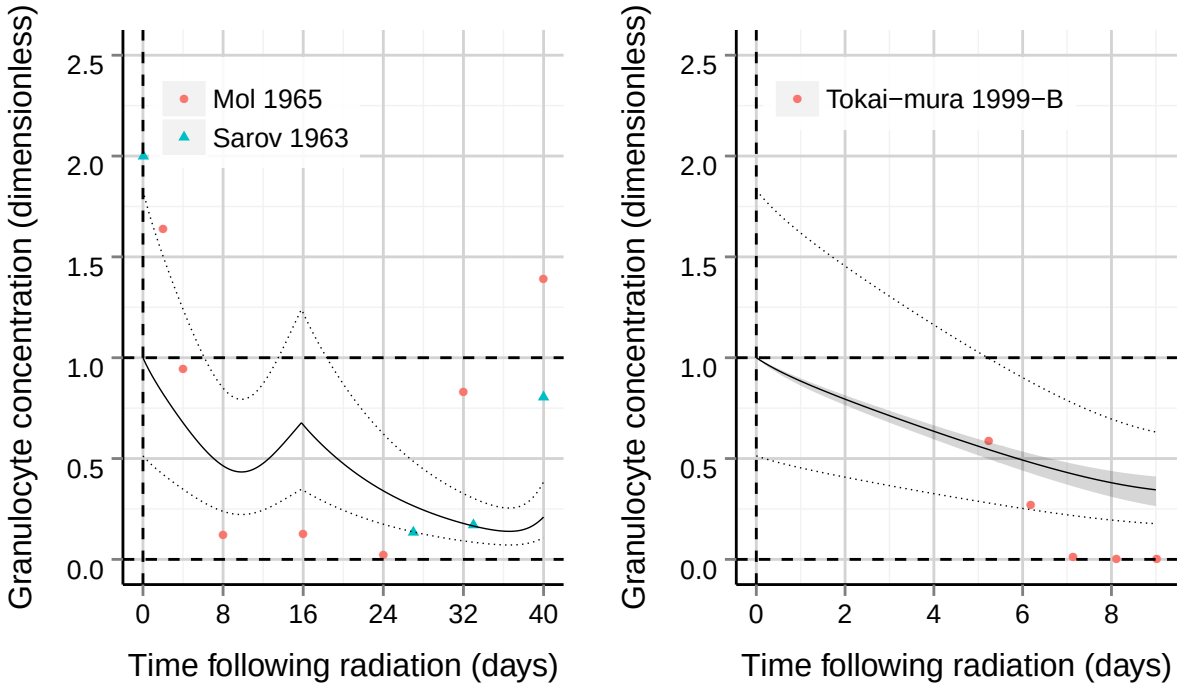

(g) Dose: 5.5 Gy

(h) Dose: 7.4 Gy

Figure B.5: (2 of 3) Granulopoiesis model compared to validation data. Output at the specified dose is delineated by a black line and, if a dose range is provided, a shaded region. If a generic baseline value was used, output initialized at the upper and lower end of the healthy granulocyte range is shown by dotted lines.

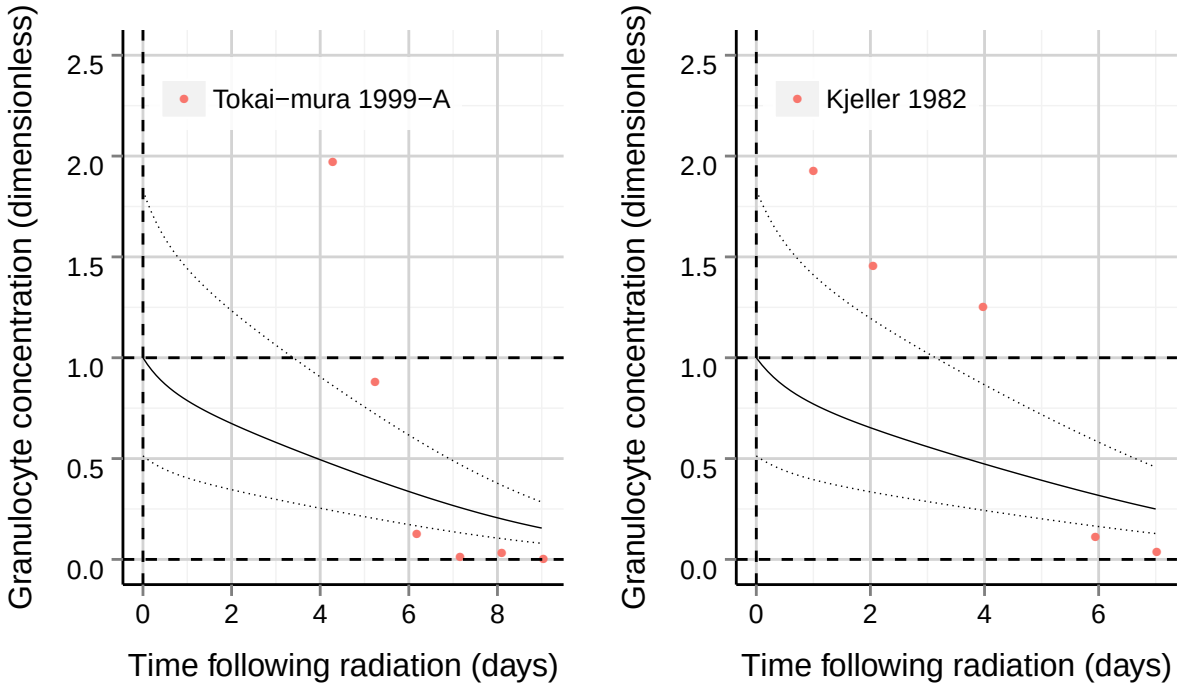

(i) Dose: 20 Gy (j) Dose: 22.5 Gy

Figure B.5: (3 of 3) Granulopoiesis model compared to validation data. Output at the specified dose is delineated by a black line and, if a dose range is provided, a shaded region. If a generic baseline value was used, output initialized at the upper and lower end of the healthy granulocyte range is shown by dotted lines.

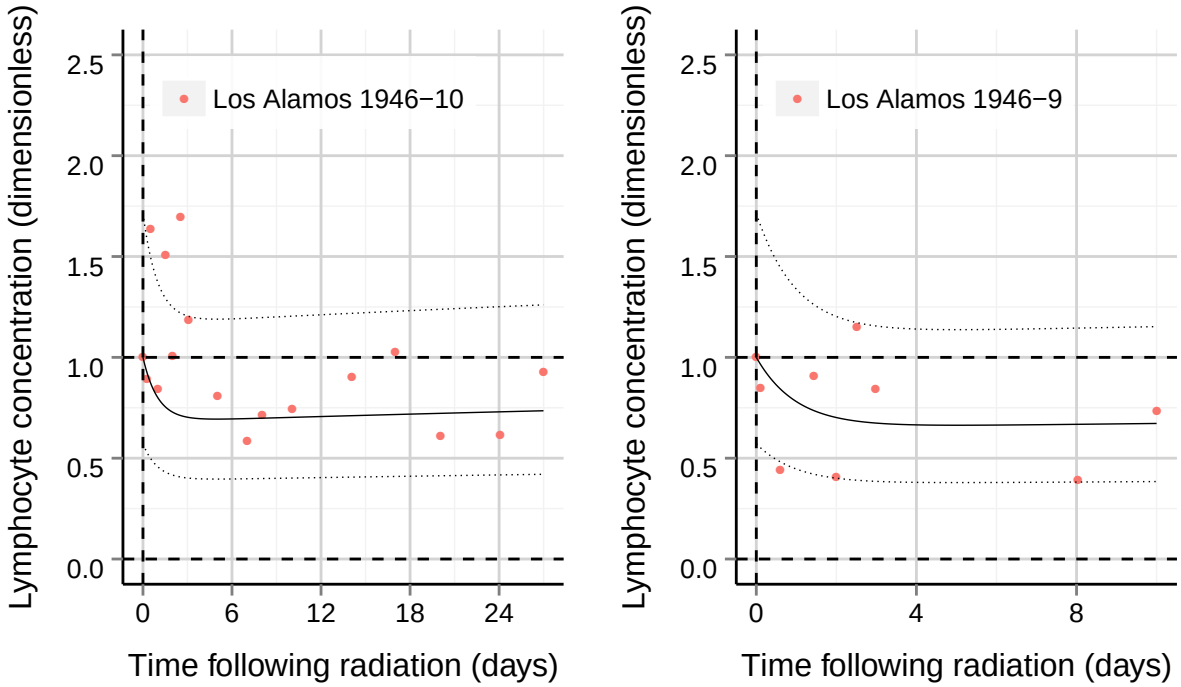

(a) Dose: 0.37 Gy (b) Dose: 0.47 Gy

Figure B.6: (1 of 3) Lymphopoiesis model compared to validation data. Output at the specified dose is delineated by a black line and, if a dose range is provided, a shaded region. Output initialized at the upper and lower end of the healthy lymphocyte range is shown by dotted lines.

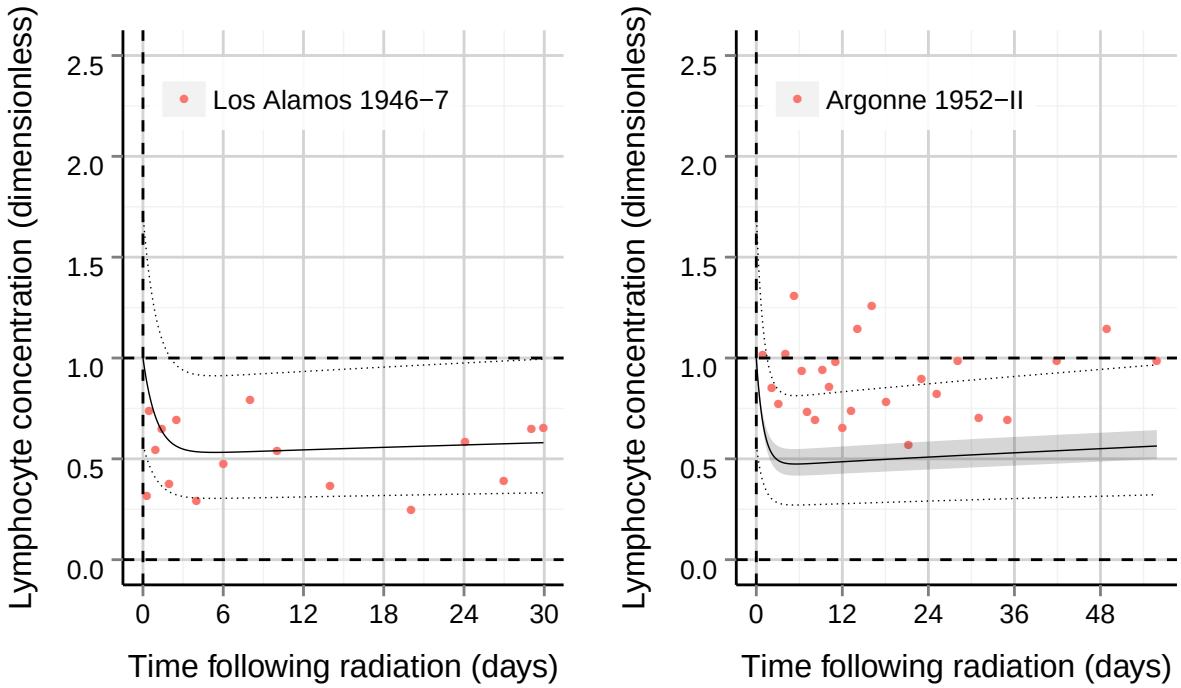

(c) Dose: 1.1 Gy

(d) Dose: 1.5 Gy (1-2 Gy)

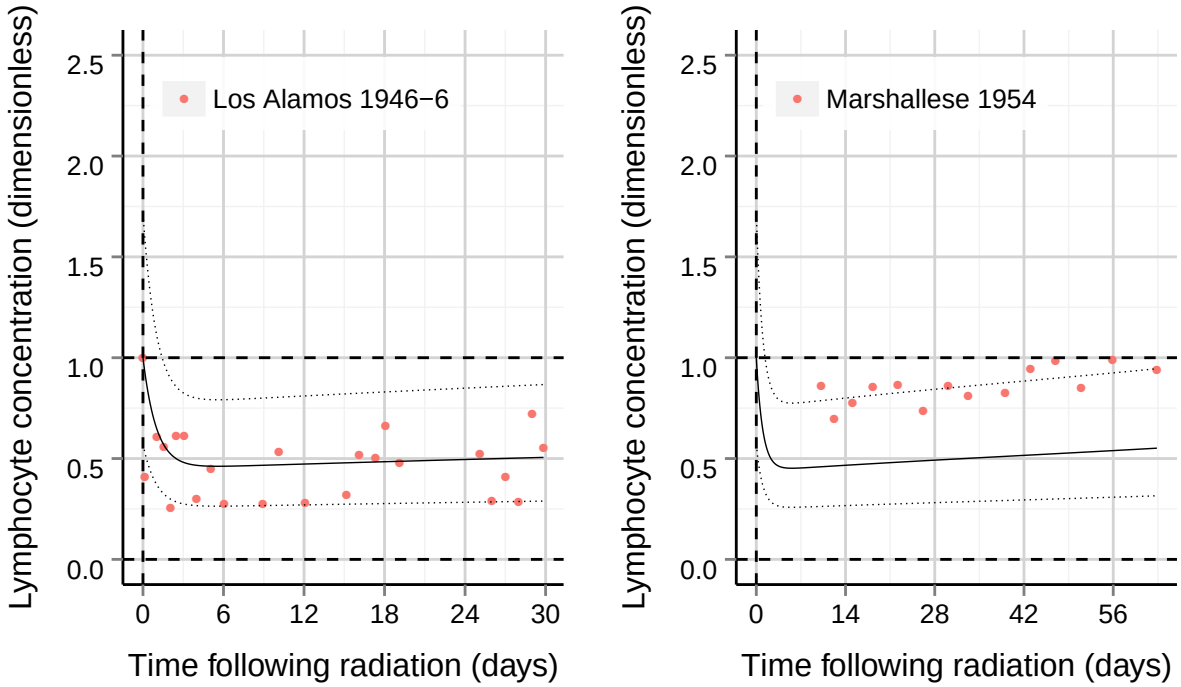

(e) Dose: 1.6 Gy

(f) Dose: 1.68 Gy

Figure B.6: (2 of 3) Lymphopoiesis model compared to validation data. Output at the specified dose is delineated by a black line and, if a dose range is provided, a shaded region. Output initialized at the upper and lower end of the healthy lymphocyte range is shown by dotted lines.

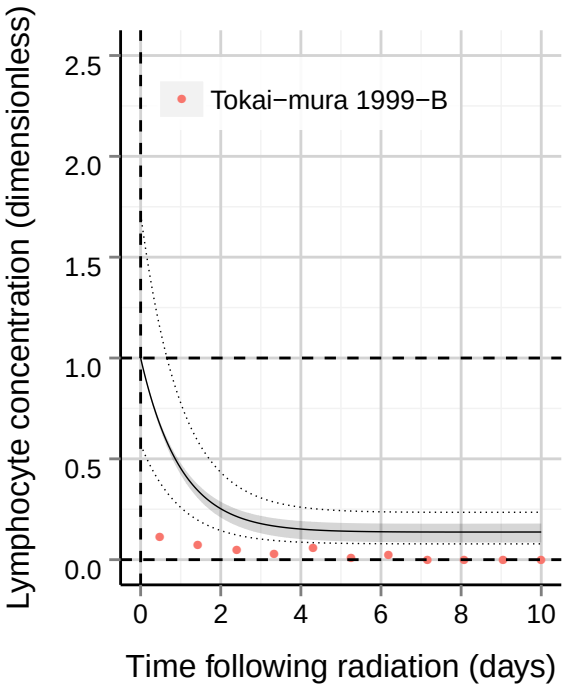

(g) Dose: 7.4 Gy

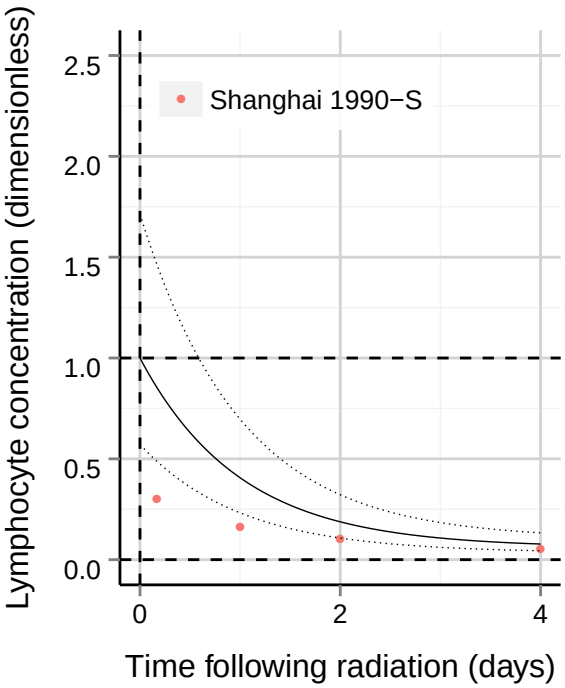

(h) Dose: 12.0 Gy

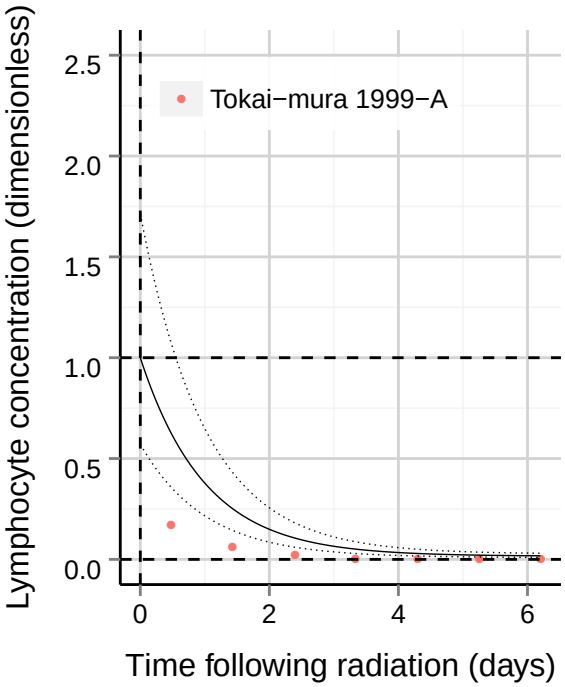

(i) Dose: 20 Gy

Figure B.6: (3 of 3) Lymphopoiesis model compared to validation data. Output at the specified dose is delineated by a black line and, if a dose range is provided, a shaded region. Output initialized at the upper and lower end of the healthy lymphocyte range is shown by dotted lines.

Skin and internal contamination and protracted exposure

The Chernobyl accident resulted in exposures that had both skin exposure, internal contamination and were protracted. Case studies from the Chernobyl accident demonstrate a much more severe hematopoietic response than what our models predict. Figure B.7 shows the mean platelet and granulocyte response of 11 subjects from the Chernobyl incident (Fliedner, Gräßle, et al. 2007) compared with the model output using the mean dose value of 4.85 Gy. Both the granulocytes and platelets show a faster drop and deeper nadir than the model predicts.

Figure B.8, Figure B.9, and Figure B.10 show individual responses of Chernobyl victims for the platelet, granulocyte, and lymphocyte response, respectively. Again, for both the platelets and granulocytes there is a stronger response in the data than in the model. However, for the lymphocytes the data is closer to what the model predicts. Radiation dose from skin contamination can result in cutaneous injury leading to systemic responses and may impact the observed hematopoietic response in the Chernobyl workers. Internal contamination could also contribute to blood cell depletion, and the protracted nature of these exposures further complicate the hematopoietic response.

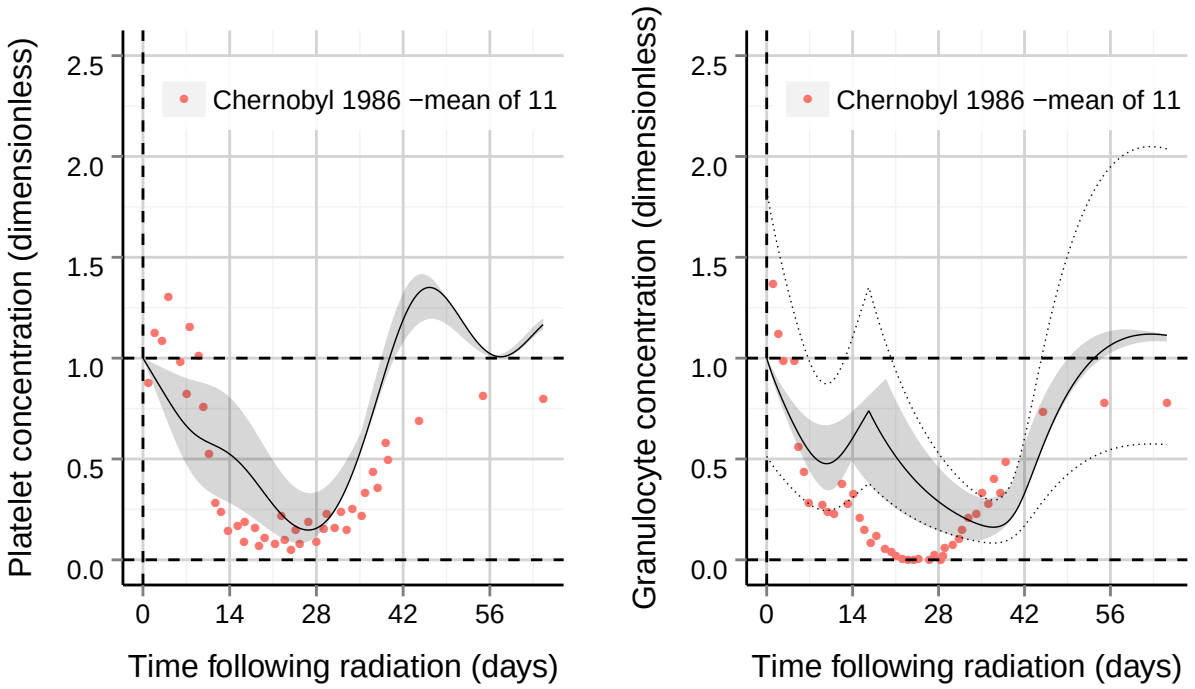

Figure B.7: Mean hematopoietic response of 11 subjects from Chernobyl 1986 who received a mean dose of 4.85 Gy (2.6-7.1 Gy). Model output at the dose (range) is delineated by a black line (shaded region). If a generic baseline value was used, output initialized at the upper and lower end of the healthy blood cell range is shown by dotted lines.

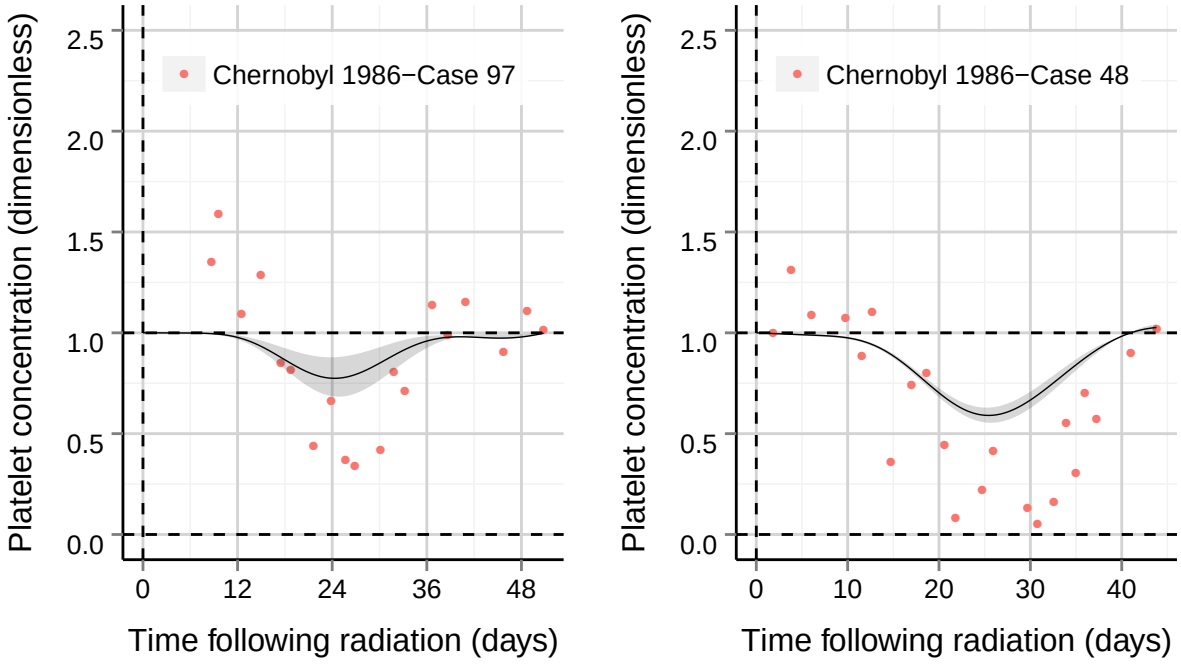

(a) Dose: 0.6 Gy (0.3-0.9 Gy)

(b) Dose: 1.25 Gy (1.1-1.4 Gy)

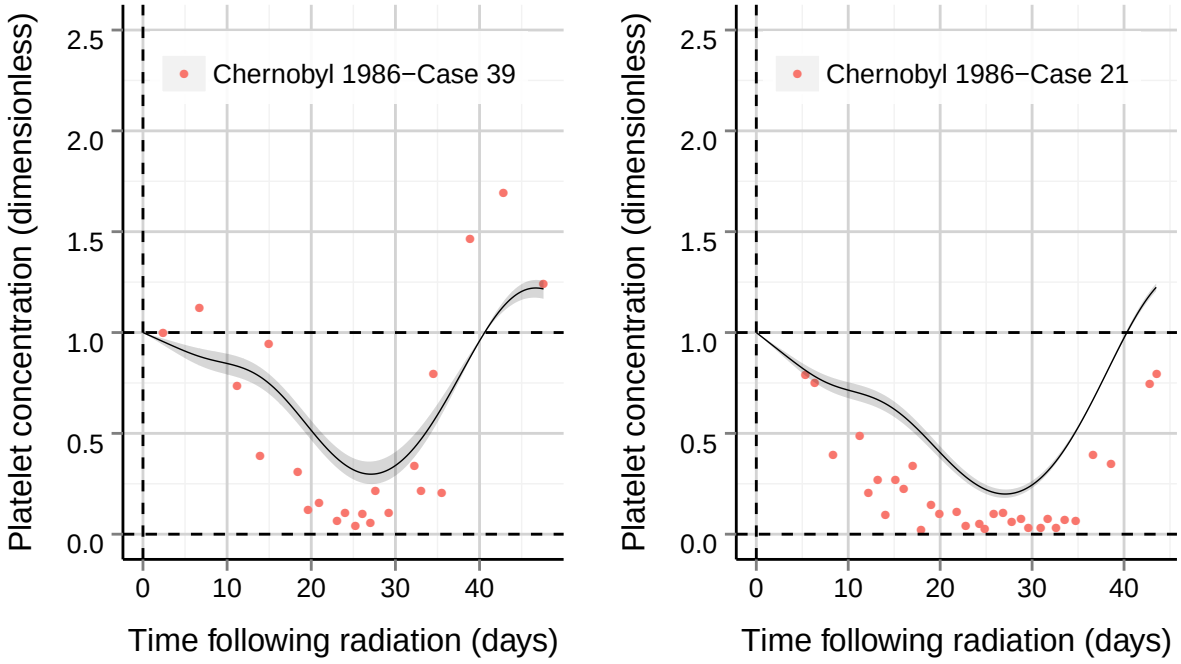

(c) Dose: 2.85 Gy (2.4-3.3 Gy)

(d) Dose: 3.9 Gy (3.6-4.2 Gy)

Figure B.8: Chernobyl case studies: Platelet data. Model output at the specified dose (range) is delineated by a black line (shaded region).

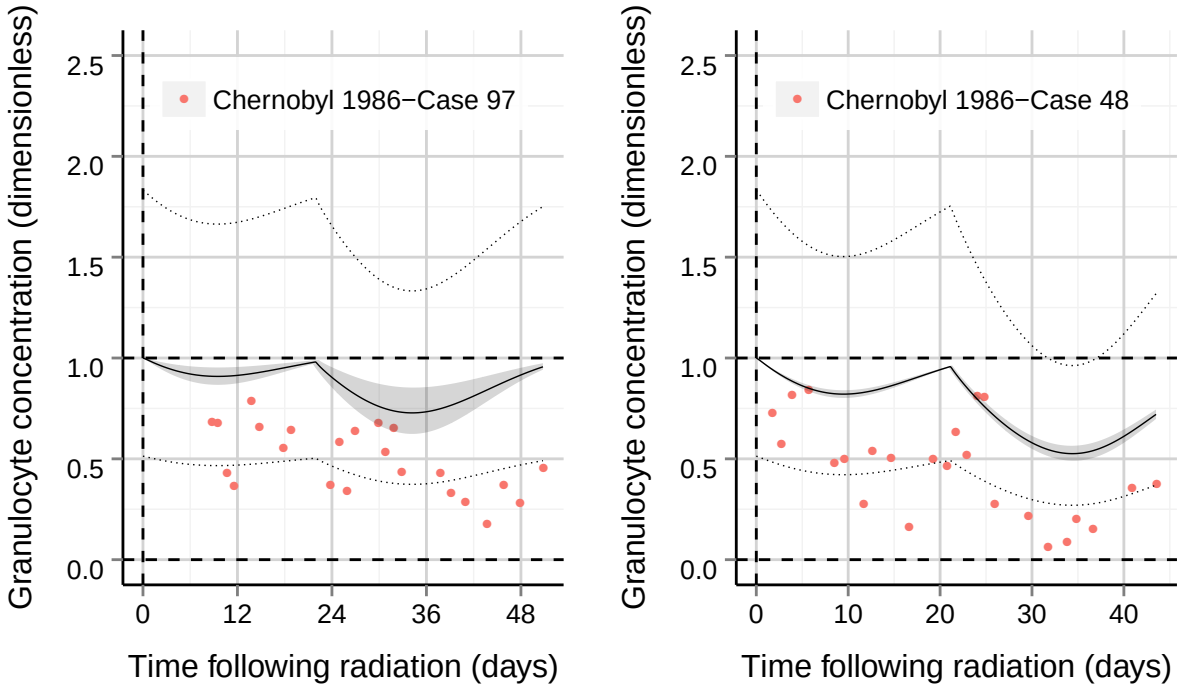

(a) Dose: 0.6 Gy (0.3-0.9 Gy)

(b) Dose: 1.25 Gy (1.1-1.4 Gy)

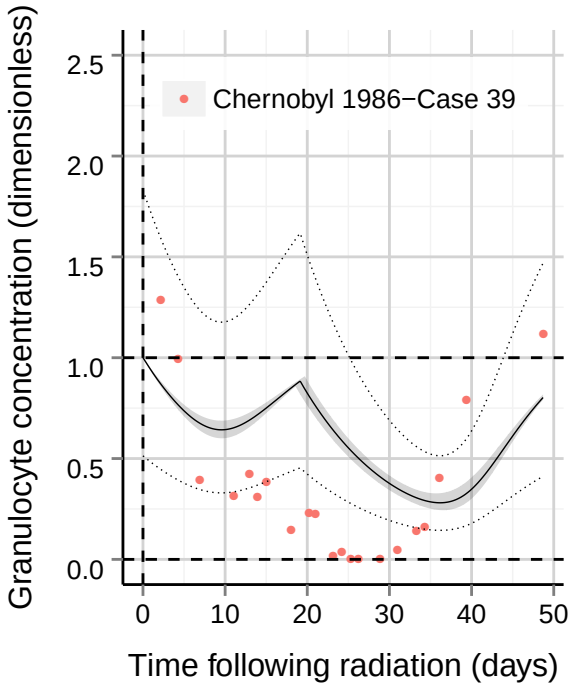

(c) Dose: 2.85 Gy (2.4-3.3 Gy)

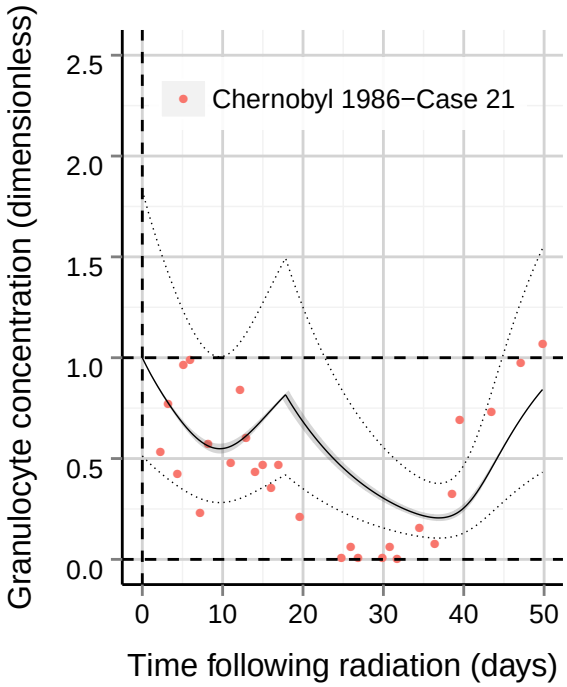

(d) Dose: 3.9 Gy (3.6-4.2 Gy)

Figure B.9: Chernobyl case studies: Granulocyte data. Model output at the specified dose (range) is delineated by a black line (shaded region). Output initialized at the upper and lower end of the healthy granulocyte range is shown by dotted lines.

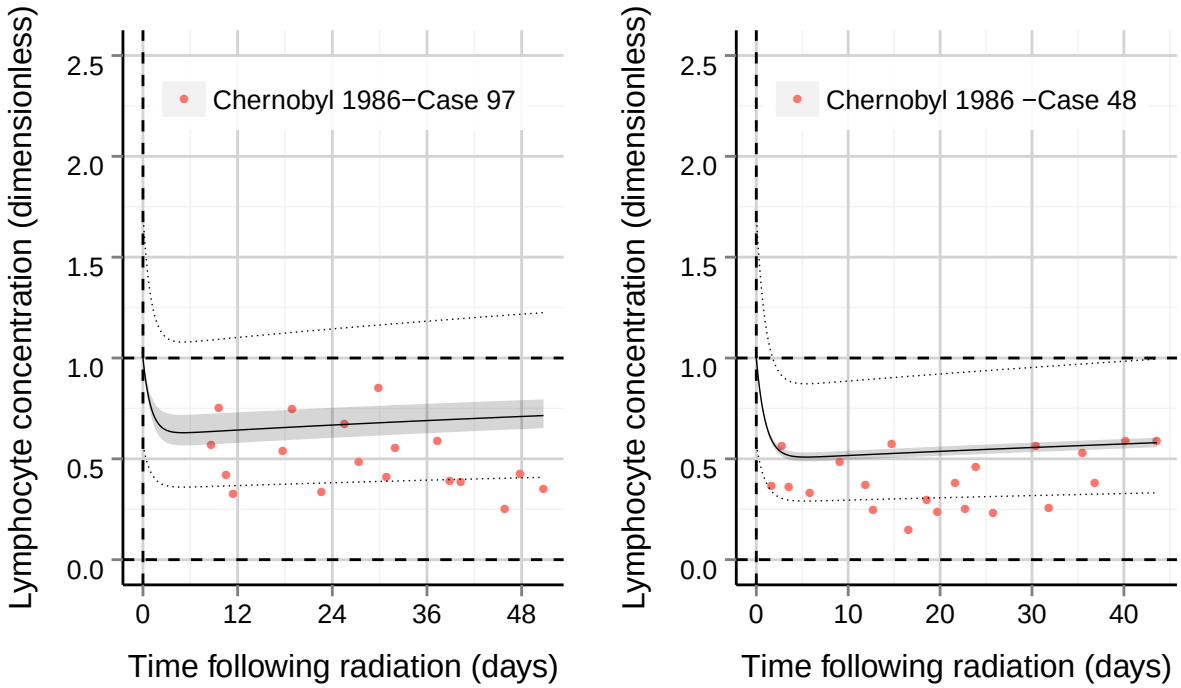

(a) Dose: 0.6 Gy (0.3-0.9 Gy)

(b) Dose: 1.25 Gy (1.1-1.4 Gy)

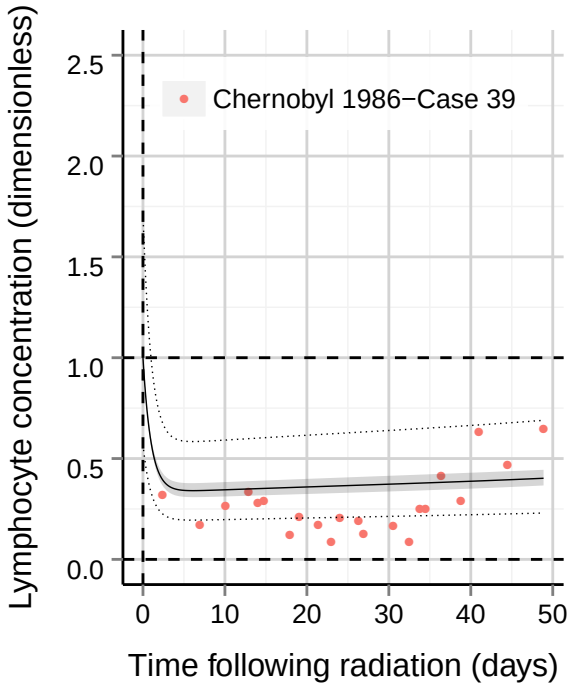

(c) Dose: 2.85 Gy (2.4-3.3 Gy)

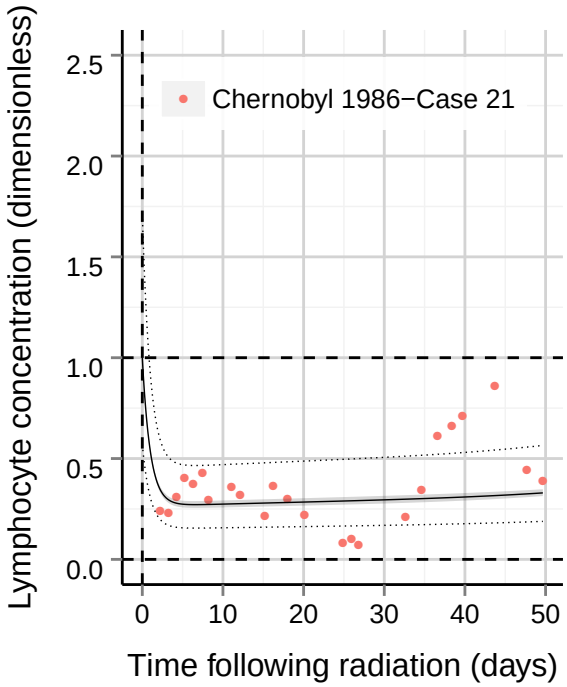

(d) Dose: 3.9 Gy (3.6-4.2 Gy)

Figure B.10: Chernobyl case studies: Lymphocyte data. Model output at the specified dose (range) is delineated by a black line (shaded region). Output initialized at the upper and lower end of the healthy lymphocyte range is shown by dotted lines.

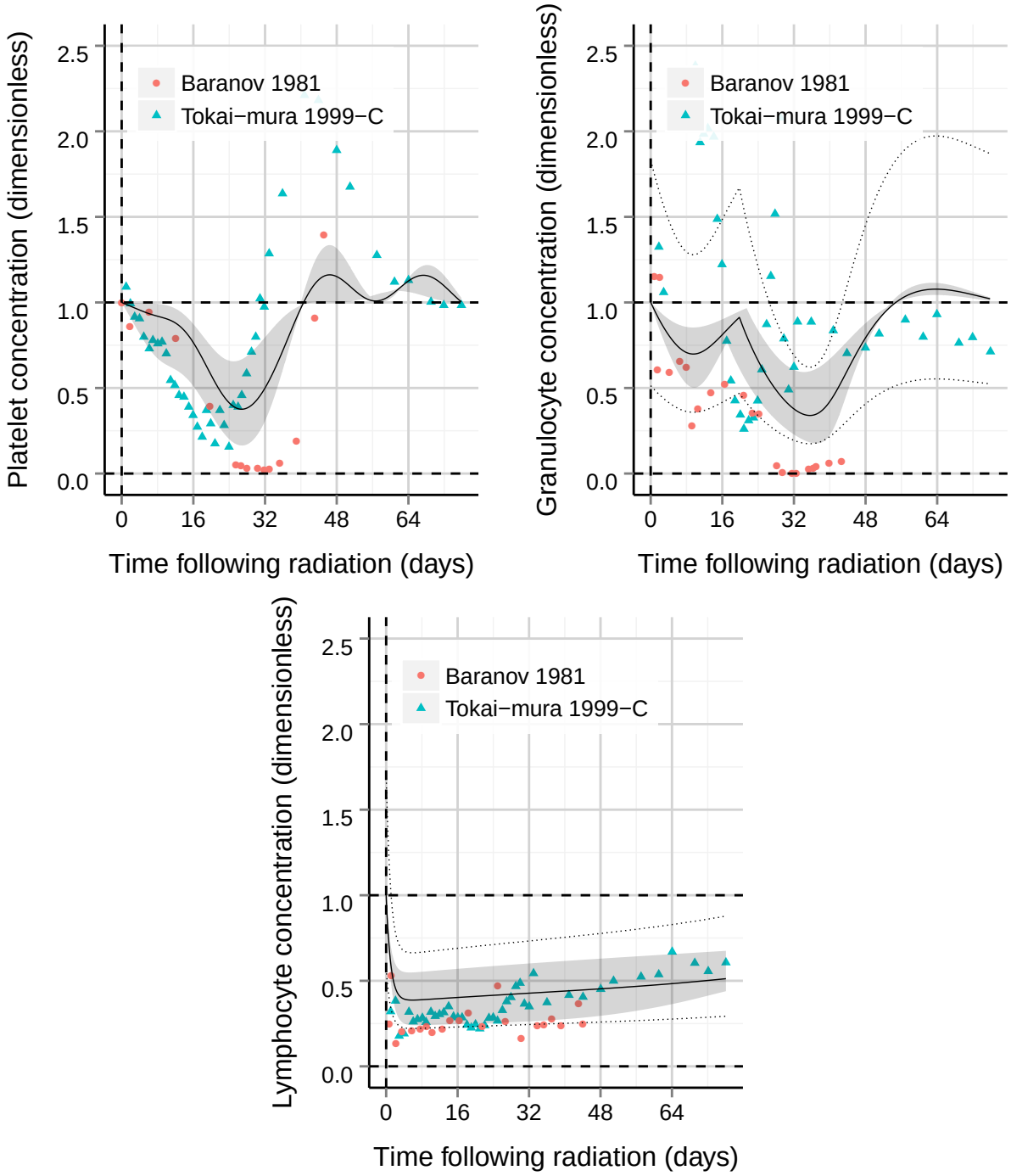

Figure B.11: Example of variability between the hematopoietic response of two radiation victims receiving 2.3 Gy (dose range shown for Tokai–mura C). Output at 2.3 Gy and between 1.0-4.5 Gy is delineated by a black line and shaded region. If a generic baseline value was used, output initialized at the upper and lower end of the healthy blood cell range is shown by dotted lines.

Dose and individual discrepancies

Here we compare two case studies, Baranov 1981 and Takai-mura 1999 C, that both received an estimated 2.3 Gy radiation dose. Figure B.11 shows the blood cell kinetics response for

these two subjects as well as the predicted model output for platelets, granulocytes, and lymphocytes. For all three blood cell types, the Baranov 1981 subject had a more severe hematopoietic response. This suggests that the differences in blood cell kinetics between these two studies is an issue with the calculated dose, but the discrepancies may also be due to treatment effects and individual variability. Few details are available on the exposure in the Baranov case study and the Tokai-mura 1999-C study was highly treated. The treatment may partially explain why the blood cell kinetic response of the Tokai-mura subject C is less severe than the Baranov case study.

Treatment

Figures B.12 and B.13 show blood cell kinetics from the kidney transplants study and the Shanghai 1990 W case study, respectively. Both of these subjects were highly treated. For the thrombopoiesis and granulopoiesis systems, the kidney transplant study has a faster hematopoietic recovery than the model predicts. The kidney transplant subjects received platelet transfusions which may have attributed to this faster recovery. The granulocyte nadir in the kidney transplant data is actually lower and earlier than the model predicts which is not what we would expect with treatment. On the other hand, the disease state of the individuals may impact the hematopoietic response.

The Shanghai W patient received whole blood, platelet, and bone marrow transfusions, however the effect of this treatment is not clear due to the limited blood cell data available. For thrombopoiesis, it appears as through the system takes longer to decline than the model

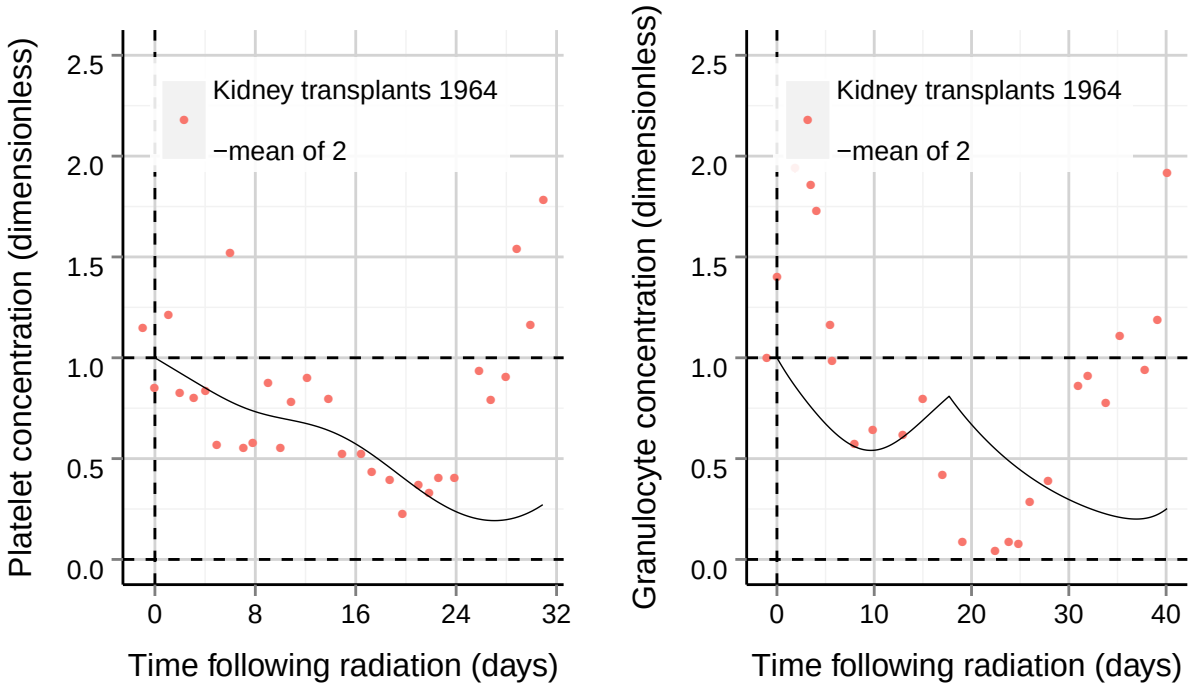

Figure B.12: Effects of treatment: 4.0 Gy case study. Model output at the specified dose is delineated by a black line.

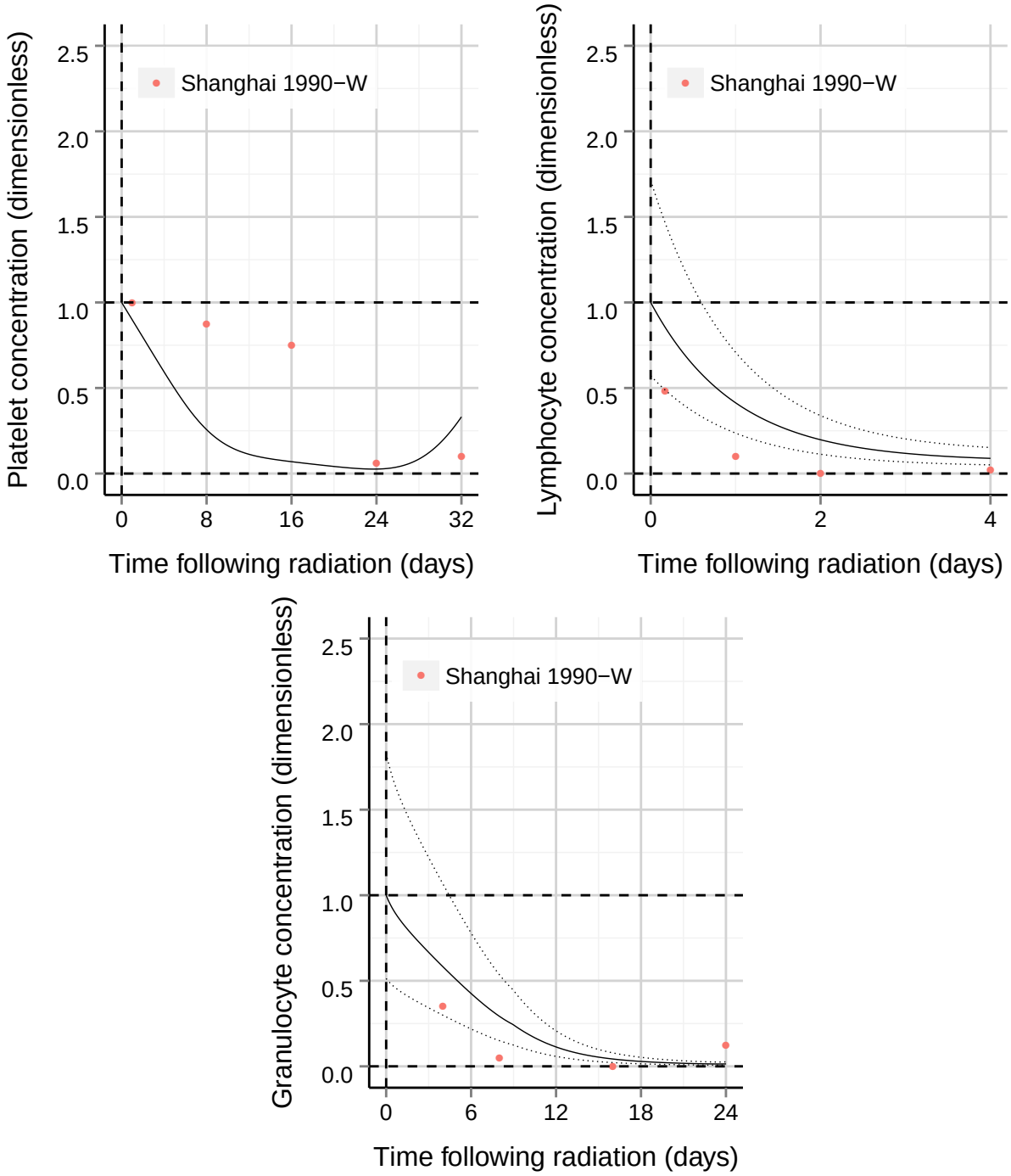

Figure B.13: Effects of treatment: 11.0 Gy case study. Model output at 11.0 Gy is delineated by a black line. If a generic baseline value was used, output initialized at the upper and lower end of the healthy blood cell range range is shown by dotted lines.

predicts. However, granulocyte and lymphocyte concentrations do not drastically differ from the model predictions. Again, these deviations may be due to both dose and individual variabilities.

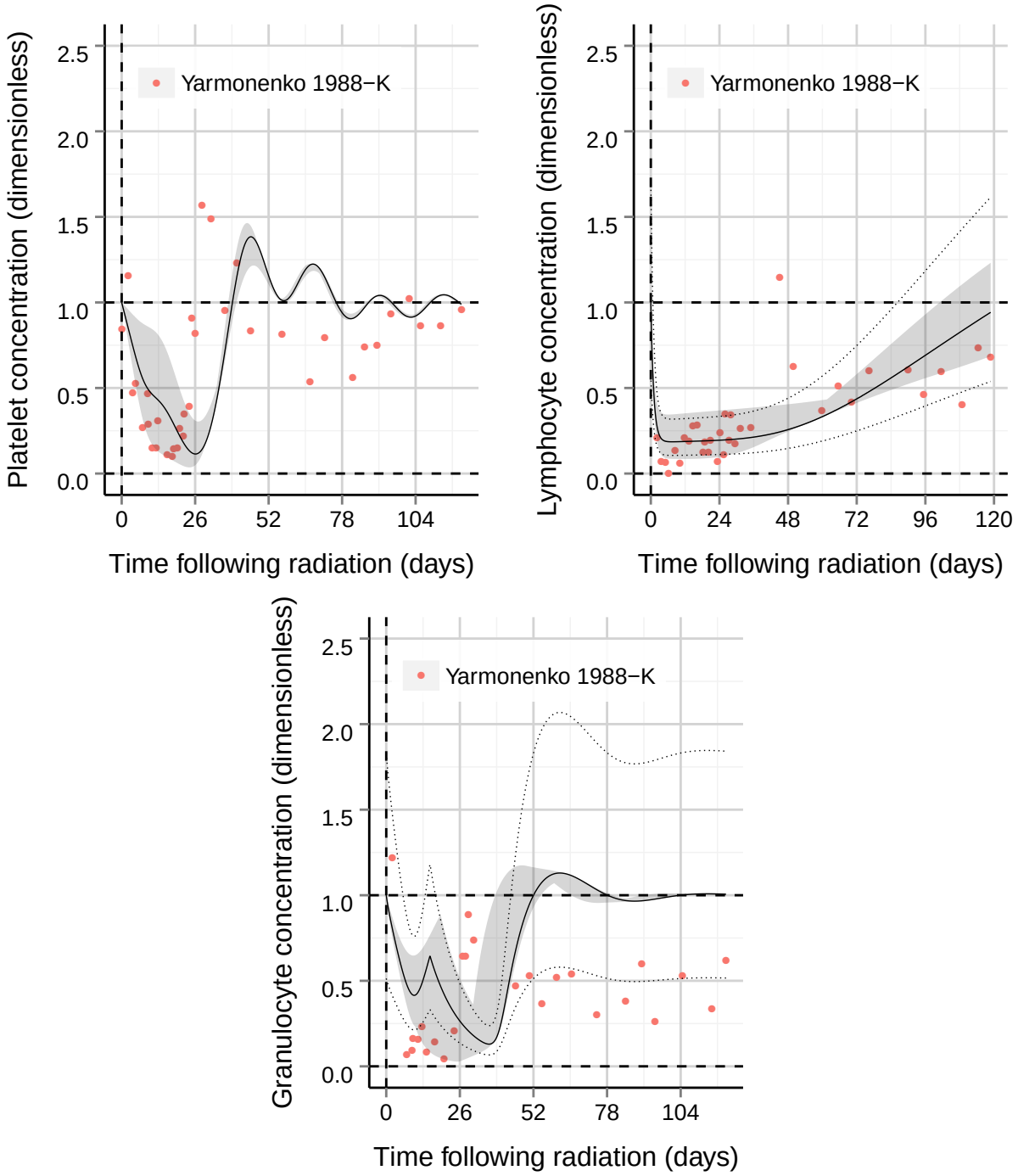

Figure B.14: Effects of non-uniform exposure: 5.8 Gy (2.8-10 Gy) case study. Model output at the specified dose and dose range is delineated by a black line and shaded region. If a generic baseline value was used, output initialized at the upper and lower end of the healthy blood cell range is shown by dotted lines.

Non-uniform exposures

Figure B.14 and B.15 show blood cell kinetics from non-uniform case studies, including subject K from Yarmonenko 1988 and Los Alamos 1946 subject 3. Subject K received 10 Gy to one side of the body and 2.8 Gy to the other side, and model output is shown across

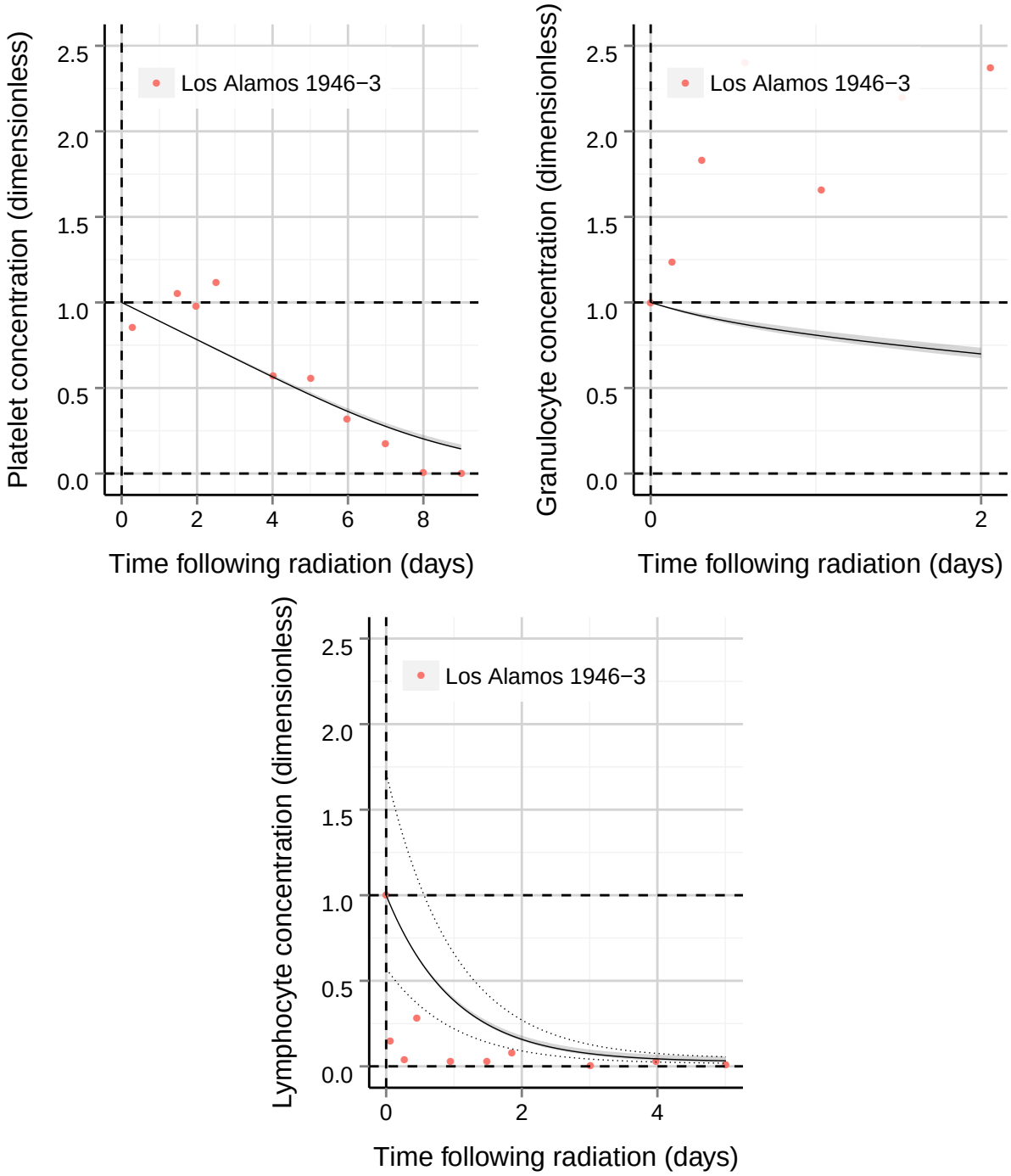

Figure B.15: Effects of non-uniform exposure: 17 Gy (13-20 Gy) case study. Model output at the specified dose and dose range is delineated by a black line and shaded region. If a generic baseline value was used, output initialized at the upper and lower end of the healthy blood cell range is shown by dotted lines.

this entire range; yet the data still does not match what the model predicts. This suggests other factors affect the response in this case. The Los Alamos subject 3 also suffered a very non-uniform exposure; however, due to the limited blood cell data available it is difficult to assess how this affected the blood cell kinetics. The platelets appear to plateau more prior to declining, while the lymphocytes decline sooner and further than the model predicts.

The implication is that non-uniform exposures may result in a more complex hematopoietic response than can be accounted for on the basis of radiation dose alone. This is due to more systemic responses from the acutely irradiated areas of the body complicating the overall hematopoietic response.

This page intentionally left blank.

Appendix C Markov Chain Monte Carlo and Identifiability Analysis

This section presents a more in-depth analysis of the Markov Chain Monte Carlo (MCMC) and identifiability analysis performed on the three optimized hematopoietic models. The goal of the MCMC analysis is to provide insight on parameter distributions and obtain parameter confidence intervals. This is done by testing different parameter combinations to see which combinations result in a satisfactory model output. An identifiability analysis provides insight into the quality of the optimization and whether the model is overparameterized. Although satisfactory visual results can be obtained with an overparameterized model, the lack of identifiability implies a lack of biological meaning behind the obtained parameter values. For a more complete description of this procedure see Section 2.

Following a MCMC analysis, the obtained parameter distributions are shown in Figures C.1, C.2, and C.3 for thrombopoiesis, granulopoiesis, and lymphopoiesis, respectively. Ideally these parameter distributions should be unimodal with a clear peak value. If the peak occurs at the upper or lower end of the bounding values, it implies that, if biologically reasonable, the boundary values should be changed.

Figures C.1, C.2, and C.3 also provide quantitative information on the correlation between parameters. Parameters are highly correlated if changing one parameter can make up for another changed parameter to obtain the same quality of optimization. High correlation exists when the correlation approaches -1 (negatively correlated) or 1 (positively correlated). When two parameters are highly correlated, obtaining a biologically meaningful optimization is nearly impossible. In the thrombopoiesis model, the optimized parameters γ and D_2^0 have the largest correlation which equals 0.79. In the granulopoiesis model optimization, the strongest correlation exists between ψ and l with a value of -0.82. In the lymphopoiesis model optimization, the strongest correlation was between γ and θ_2 with a value of -0.61.

This analysis can be extended by looking at the collinearity of all the parameters used in the optimization rather than simply comparing two at a time. The collinearity is a measure of linear dependencies between sets of parameters. As the collinearity value increases the parameters are more related. As a rule of thumb, models with a collinearity value less than about 20 are classified as identifiable (Soetaert and Petzoldt 2010). In the thrombopoiesis model, the collinearity of the optimized parameters is 36. In the granulopoiesis model, the collinearity of the optimized parameters is 7.73, and in the lymphopoiesis model, the collinearity of the optimized parameters is 7.80. Thus, the optimized values for the thrombopoiesis model should be interpreted cautiously because, while providing accurate predictions of radiation response, they may not provide biologically meaning values.

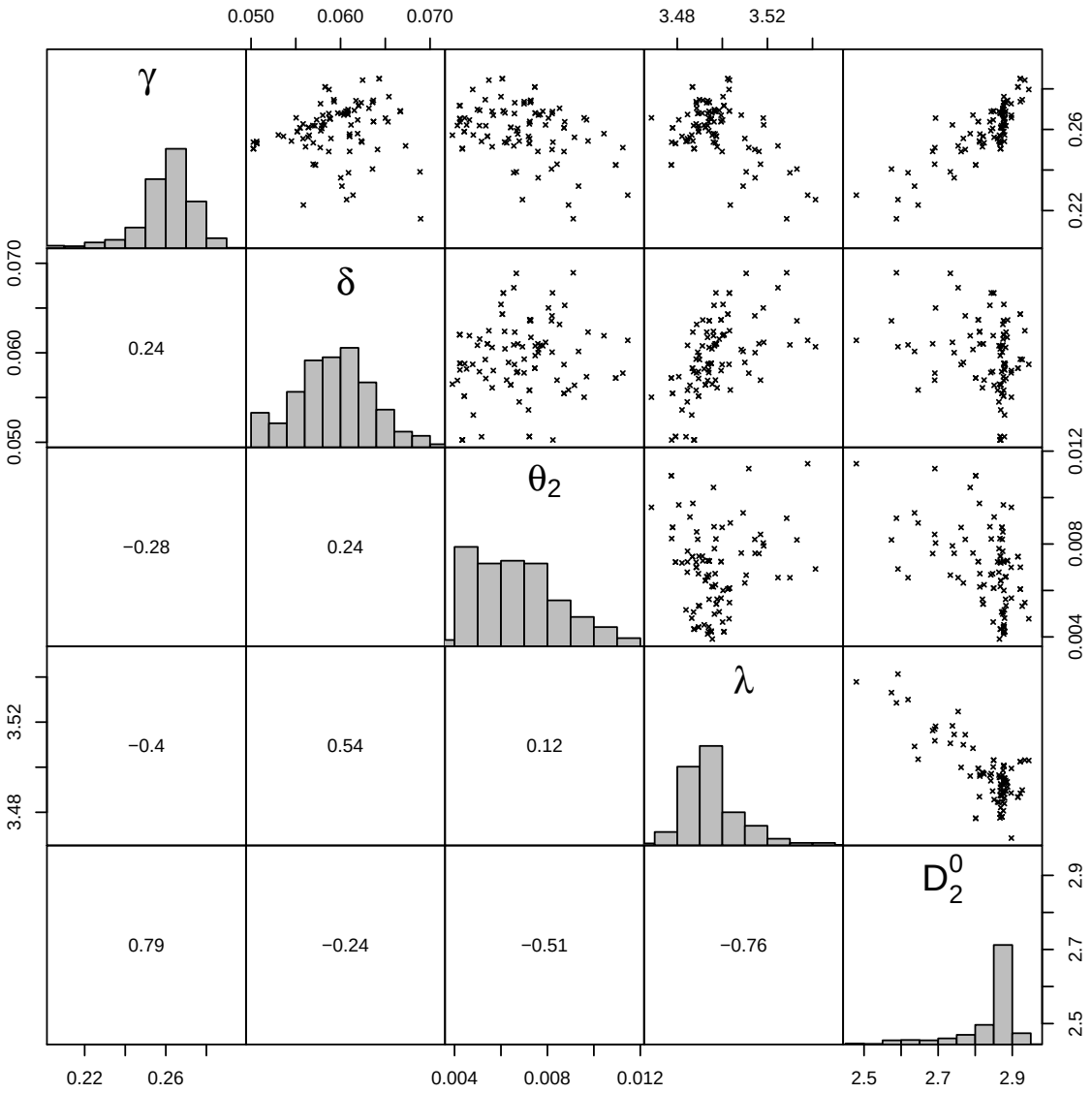

Figure C.1: Thrombopoiesis MCMC analysis results showing distributions of optimized parameters and correlations. The units for γ and δ are d^{-1}, and the units for D_2^0 are Gy. The other parameters, λ and θ_2, are unitless. The parameter frequency histograms show the relative likelihood of parameter values based on how often they occurred in the MCMC analysis.

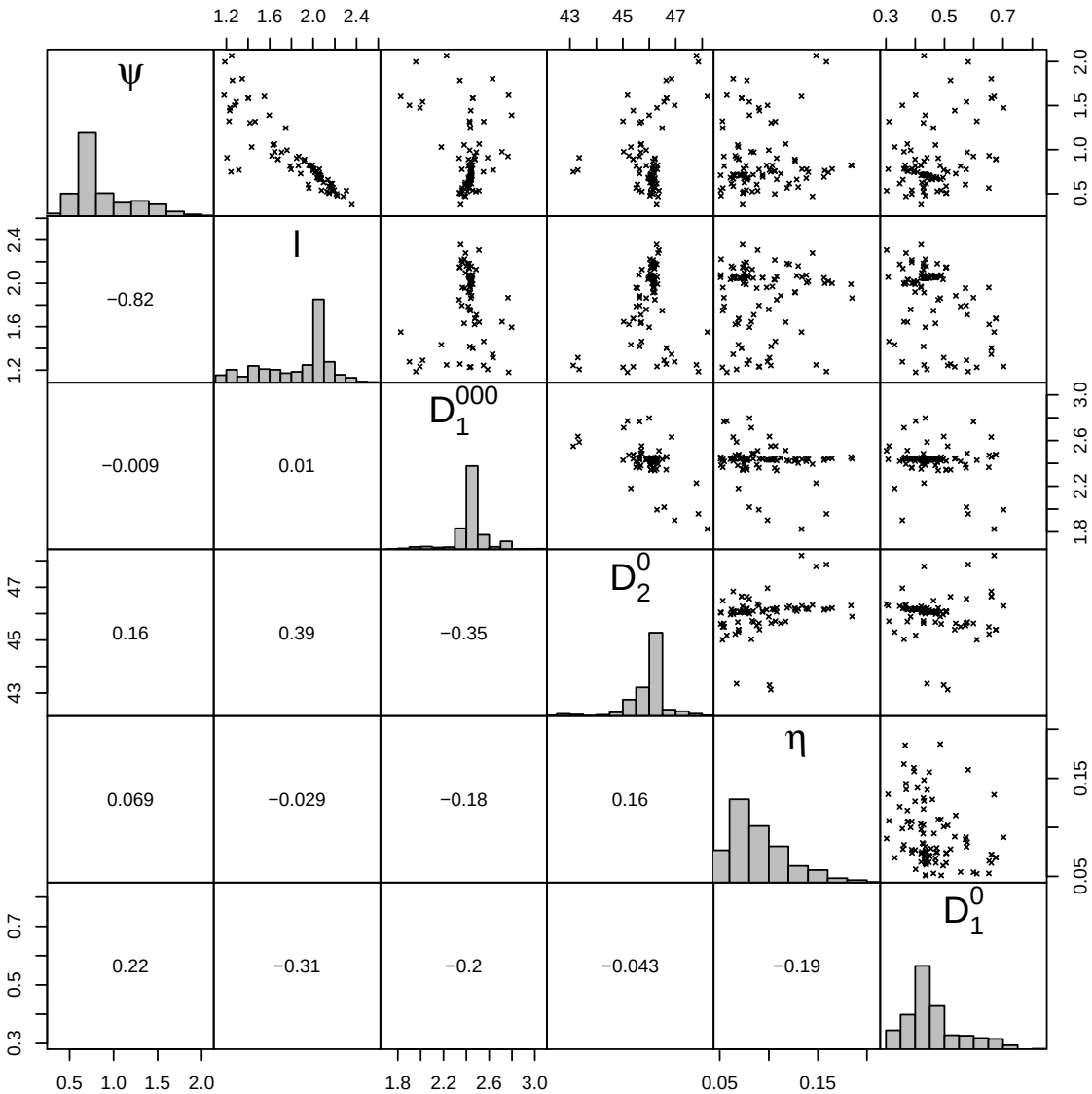

Figure C.2: Granulopoiesis MCMC analysis results showing distributions of optimized parameters and correlations. The units for ψ and η are d^{-1}. The units for D_1^0, D_1^{000}, and D_2^0 are Gy. The other parameter l is unitless. The parameter frequency histograms show the relative likelihood of parameter values based on how often they occurred in the MCMC analysis.

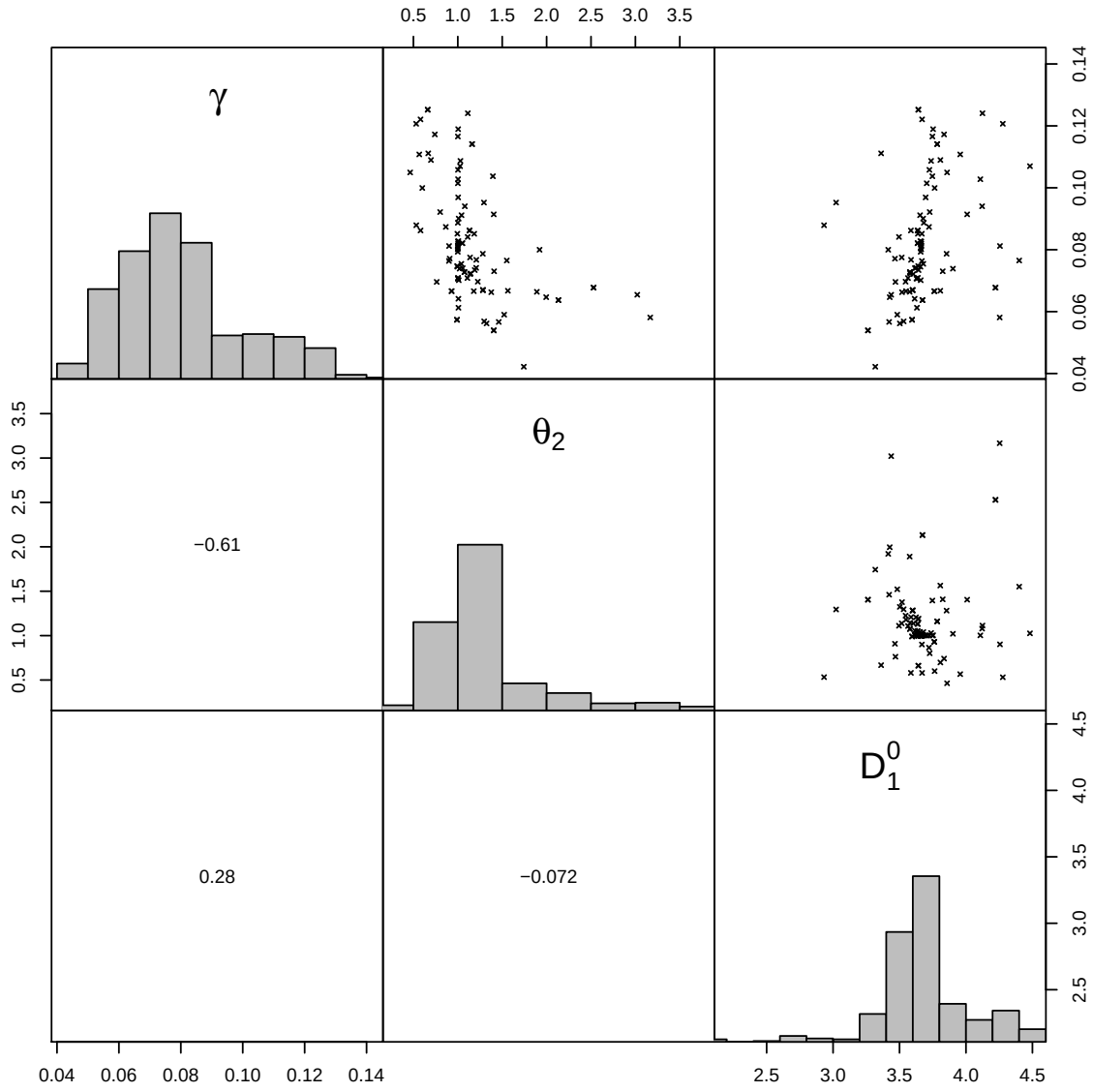

Figure C.3: Lymphopoiesis MCMC analysis: Parameter distributions and correlations. The units for γ are d^{-1}. The units for D_1^0 are Gy and θ_2 is unitless. The parameter frequency histograms show the relative likelihood of parameter values based on how often they occurred in the MCMC analysis.

Abbreviations, Acronyms, and Symbols

ARA	Applied Research Associates, Inc.
ARS	acute radiation sickness
β	beta dose
CFU-MK	megakaryocyte colony-forming unit
Co-60	Cobalt 60
d	day
DTRA	Defense Threat Reduction Agency
FDA	Food and Drug Administration
FIA	free-in-air
FME	flexible modeling environment for modeling, sensitivity, and Monte Carlo analysis (R plug-in)
G-CSF	granulocyte colony-stimulating factor
GM-CSF	granulocyte macrophage colony-stimulating factor
Gy	gray
GyEq	gray equivalent
γ	gamma dose
h	hour
HENRE	Health Effects from Nuclear and Radiation Environments
HSCs	hematopoietic stem cells
IAEA	International Atomic Energy Agency
IL-3	interleukin 3
IL-12	interleukin 12
kg	kilogram
MCMC	Markov Chain Monte Carlo
METREPOL	Medical Treatment Protocols for Radiation Accident Victims as a Basis for a Computerised Guidance System
MKs	megakaryocytes
MLT	midline tissue
L	microliter
n	neutron dose
NETs	neutrophil extracellular traps
NHP	non-human primate
NK	natural killer
ODE	ordinary differential equation

R	software programming language for statistical computing
RBE	relative biological effectiveness
RIPD	Radiation-Induced Performance Decrement
Sv	sievert
TPO	thrombopoietin
UNSCEAR	United Nations Scientific Committee on the Effects of Atomic Radiation
WMD	weapons of mass destruction